Testing the Pressure Transient Flow-Force for Spool-Type Two-Way Valves

A Dissertation

Present to

The Faculty of the Graduate School

At the University of Missouri-Columbia

In Partial Fulfillment

Of the Requirements for the Degree

Doctoral in Mechanical & Aerospace Engineering

By

Shusen Zhang

Dr. Noah D. Manring, Dissertation Supervisor

July, 2011

The undersigned, appointed by the dean of the Graduate School,

have examined the dissertation entitled

Testing the Pressure Transient Flow-Force for Spool-Type Two-way Valves

Presented by Shusen Zhang

A candidate for the degree of

Doctoral in Mechanical & Aerospace Engineering

And hereby certify that, in their opinion, it is worthy of acceptance.

Professor Noah D. Manring

Professor Roger Fales

Professor Craig Kluever

Professor Segert Jan

Professor Steven Borgelt

Acknowledgement

First I would like to thank my dissertation advisor, Dr. Noah D. Manring, for his time, his patience, his wisdom and his vision at every step of my doctoral program in University of Missouri-Columbia. I cannot overestimate how much I have learned from him. Being his student has given me much more than an in-depth training in hydraulic control system analysis and testing. His unwavering dedication to detail and relentless pursuit of the unknown continue to inspire me. He is an exceptional mentor and I feel extraordinary lucky to have the opportunity to be his student.

I would also like to extend my gratitude to people in the Mechanical & Aerospace Engineering department. Dr Roger Fales has taught me so much about hydraulic experiment. His student Richard Carpenter and Timothy Keim are willing to help me with the instrumentation, and we are happy to study the course together. I am also grateful to our technician Rex Gish, Brian Samuels and Richard Oberto. Without them I cannot make every design come into the real world. They are so patient for all the design and modification I have made.

I could not have finished this dissertation without love, support and patience fiancée. She believed me when I doubted myself, helped me stand when I lacked the strength, and kept me going when I have no compass.

The greatest sources of strength in my life have been my wonderful parents. Their unconditional support and love is the biggest blessing of my life. Everything I am and ever will be I owe to them.

Abstract

An analysis is presented of the flow force acting on a two-way valve using the equilibrium condition of the piston and the equilibrium condition of fluid in the control volume. Three types of flow forces are identified: pressure-difference-induced flow force, viscous-shear-induced flow force, and momentum-induced flow force. Nondimensional analysis shows that among all steady flow force the pressure-difference-induced flow force is largest with viscous-shear-induced flow force the second and momentum-induced flow force the smallest. However, the fluid inertial-induced flow force, which is a momentum-induced flow force, is very important while the pressure transient effect caused by the slight compressibility of the fluid is negligible.

A pressure-wave generation system has been designed and built with a novel square pressure-wave generator. By turning the square pressure wave generator sustained by the variable-displacement axial piston pump, a square wave can be generated to actuate the two-way valve with fixed piston. Simulation results shows that by taking the difference between the total flow force and steady flow force, the pressure transient effect can be observed.

The first experiment is conducted on a two-way valve with extremely low leakage. The trial test on a hydraulic circuit without pressure wave generator shows that the sound wave phenomenon is very strong and there is a pressure gradient in the vertical direction. In order to reduce the influence of the two characteristics mentioned above, the 100-points average technique and pressure profile factor is introduced, and the pressure transient effect is proved to be true.

The second experiment is conducted on a two-way valve with longer valve length, stepped housing and larger clearance. Those geometry modifications are made to reduce the energy that could be reflected at the ends and reduce the pressure gradient in the vertical direction. The usefulness of those modifications is proved experimentally. Furthermore, the influence of different damping length and non-metering length is tested and it is shown experimentally that the non metering length will have a impact on the transient flow force. The reason for this influence can be partially explained by Computational Fluid Dynamics (CFD) computation. The fluid in the non-metering section will be involved in the transient flow. And the birth of vortices will make the assumption that the fluid is moving as one chunk of fluid not valid.

TABLE OF CONTENTS

List of Figures

List of Tables

Nomenclature

A	generalized orifice area
A_1	supply orifice area
A_2	cross-sectional area of the control volume within the two-way spool valve
A_3	return orifice area
$A_{contact}$	generalized contact area
A_H	two-way valve housing surface area
A_h	orifice area connecting the high pressure chamber and the supply line of the two-way valve
A_{L1}	leakage passage cross-sectional on the right hand side
A_{L2}	leakage passage cross-sectional on the left hand side
A_l	orifice area connecting the low pressure chamber and the supply line of the two-way valve
A_o	nominal orifice area
A_{rec}	rectangular approximation for the circular orifice
A_s	two-way valve piston shaft area
A_{sta}	orifice area on the stator
A_v	cross-sectional area of the pressurized area of the two-way spool valve
C_d	generalized discharge coefficient
C_{d1}	discharge coefficient concerning the supply orifice
C_{d2}	equivalent discharge coefficient concerning the pressure drop across the valve chamber
C_{d3}	discharge coefficient concerning the return orifice

C_{de}	equivalent discharge coefficient pipe flow
C_{dh}	discharge coefficient concerning orifice area A_h
C_{dl}	discharge coefficient concerning orifice area A_l
C_{fxms}	pressure drop coefficient concerning the return orifice
C_{fxp}	pressure drop coefficient concerning the pressure drop across the valve chamber
$C_i \left(i = 1..3\right)$	smooth orifice coefficients
$C_{profile}$	pressure profile factor
C_{sta}	stator orifice coefficient
D_h	hydraulic diameter
De	denominator factor of the linearized pressure drop coefficients
d	valve orifice diameter
$\mathbf{F}_m$	vector fluid momentum force
$\mathbf{F}_{mr}$	momentum flow force caused return orifice flow
$\mathbf{F}_{ms}$	momentum flow force caused supply orifice flow
F	force needed to balance the valve piston
F_{shear}	generalized viscous shear force
F_{Pdiff}	force generated by the pressure difference between two ends of the piston
F_{xm}	momentum generated flow force in x direction
F_{xmL1}	momentum flow force caused by leakage flow on the right-hand side
F_{xmL2}	momentum flow force caused by leakage flow on the left-hand side
F_{xmt}	transient momentum generated flow force
F_{ym}	momentum generated flow force in y direction

$F_{\tau h}$	viscous shear force acting on the valve piston housing
$F_{\tau s}$	viscous shear force acting on the valve piston shaft
f	frictional force
f_p	frictional coefficient for fully developed turbulent flow
$\mathbf{i}$, $\mathbf{j}$	base vector for coordinate system used to define momentum generated flow force
K	linear leakage coefficient
K_L	coefficient used to account the leakage
K_Q	Coefficient in the parabolic velocity profile function to make the velocity profile to match the volumetric flow rate
L	valve damping length
$\mathbf{n}$	general outer normal vector for the control volume
$\mathbf{n}_1$	outer normal vector concerning the supply orifice
$\mathbf{n}_2$	outer normal vector concerning the return orifice
$\mathbf{n}_{L1}$	outer normal vector concerning the leakage flow on the right-hand side
$\mathbf{n}_{L2}$	outer normal vector concerning the leakage flow on the left-hand side
P_1	pressure at the right end of the valve piston
P_2	pressure at the left end of the valve piston
P_h	high pressure chamber pressure
P_l	low pressure chamber pressure
P_{no1}	pressure measured in port number 1
P_{no7}	pressure measured in port number 7
P_r	return pressure

P_s	supply pressure to the two-way valve
P_{s0}	nominal supply pressure
P_w	wetted perimeter
$\hat{P}_{send}$	nondimensionalized pressure at end of the piston near the supply orifice
$\hat{P}_{rend}$	nondimensionalized pressure at end of the piston near the return orifice
Q	generalized volumetric flow rate
Q_{dish}	volumetric flow rate from the discharge line of the pump to the high pressure chamber
Q_h	volumetric flow rate from the high pressure chamber to the supply line of the two-way valve
Q_{L1}	leakage volumetric flow rate on the right-hand side
Q_{L2}	leakage volumetric flow rate on the left-hand side
Q_l	volumetric flow rate from the low pressure chamber to the supply line of the two-way valve
Q_{lr}	volumetric flow rate from the low pressure chamber to the return line
Q_1	volumetric flow rate concerning the supply orifice of the two-way spool valve
Q_2	volumetric flow rate across the valve chamber
Q_3	volumetric flow rate concerning the return orifice of the two-way spool valve
Re	generalized Reynolds number
Re_c	critical Reynolds number
r	coordinate of the radial position
r_h	two-way valve housing radius
r_s	two-way valve piston shaft radius

$S_{P_{s0}}^{\hat{\lambda}_i}$	sensitivity coefficient of lambda family nondimensional group to nominal supply pressure
$S_{C_{dj}}^{\hat{\lambda}_i}$	sensitivity coefficient of lambda family nondimensional group to discharge coefficients
$S_{P_{s0}}^{\hat{\gamma}_i}$	sensitivity coefficient of gamma family nondimensional group to nominal supply pressure
$S_{C_{dj}}^{\hat{\gamma}_i}$	sensitivity coefficient of gamma family nondimensional group to discharge coefficients
$S_{\theta_j}^{\hat{\gamma}_i}$	sensitivity coefficient of gamma family nondimensional group to jet angles
t	time
$\mathbf{u}_{L1}$	leakage flow velocity vector on the right-hand side
$\mathbf{u}_{L2}$	leakage flow velocity vector on the left-hand side
$\mathbf{u}_1$	supply flow velocity for the spool valve
$\mathbf{u}_2$	supply flow velocity for the spool valve
u	generalized velocity
$\bar{u}$	generalized average velocity
u_{valve}	velocity profile on the valve cross-sectional area
V_1	half valve chamber volume
V_h	volume of high pressure chamber
V_l	volume of the flow pressure chamber
V_s	volume of the supply line to the two-way valve
x	valve piston displacement
y	coordinate normal to the flow direction
$\hat{y}$	nondimensionalized vertical position

ΔP	generalized pressure drop
ΔP_c	critical pressure drop
$\Delta P_{averaged}$	average pressure drop across the valve body
$\Delta P_{measured}$	measured pressure drop across the valve body
ρ	fluid density
μ	fluid viscosity
β	fluid bulk modulus
ϕ	coordinate of the angular position
θ_1	supply flow jet angle
θ_2	return flow jet angle
^	Indicate the variable is nondimensional
τ	characteristic time
$\hat{\lambda}_i \left(i = 1..5\right)$	lambda family nondimensional group
$\hat{\gamma}_i \left(i = 1..5\right)$	gamma family nondimensional group
$\hat{\delta}_i \left(i = 1..7\right)$	delta family nondimensional groups

Chapter 1: Introduction

1.1 Background

In industry, hydraulic and pneumatic systems are used extensively in transmitting fluid power. Because of the need to regulate fluid flow, valves are commonly used in fluid power systems. Different valves serve different roles. Some of them are used to provide power for direct actuation of an implement; some are employed to provide standby pressure for operating a control system; some valves are used as the pressure relieved valves. Although the applications are different, the motion of the moving part in the valve can only be maintained, when the actuation force, either active or passive, can overcome the flow force acting on the moving parts. Therefore, predicting the magnitude and direction of the flow force becomes a vital piece of information for fluid power engineers who design hydraulic valves.

Being unable to estimate the magnitude and direction of the flow force correctly can cause many problems. Underestimating the magnitude of the flow leads to an undersizing of the actuation device for the valve. Overestimating the magnitude of the flow force leads to an over-sizing of the actuation device and produces a large amount of energy and space waste. An opposite prediction of flow force can be disastrous, for the related stability problem. The forgoing situations provide a motivation for understanding fluid flow forces within hydraulic control valves in a precise way.

There are mainly two ways to consider the flow force in hydraulic valves: 1) the flow force is the force generated by the change of momentum of fluid flow across the valve based on the classical understanding of momentum conservation, which can capture

the general image of the flow; or 2) the flow force may be considered by assessing pressure distribution on the pressurized surface of the spool and viscous shear resulting from fluid momentum effects. In order to assess this pressure distribution and viscous shear force, we need to know detailed information about the flow field.

The first approach leads to the model including the classical orifice equation, which is very crude but effective for computation. The classical orifice equation is based on the steady incompressible Bernoulli equation, which is suitable for flow that is characterized by a large Reynolds number. The lumped coefficients need to be determined experimentally, otherwise the prediction may not be accurate. In addition to the inaccuracy that may be encountered when using the orifice equation, several assumptions have been added to make the modeling procedure easier and the model itself simpler. Some of them even violate our direct observation. For example, the pressure gradient inside the chamber is assumed not to exist, but no pressure gradient means zero velocity. The flow is also not ensured to have high Reynolds number characteristic and to be in steady state. Consequently, although the lumped model can approximately capture the general image, data generated using the lumped model may deviate from the experimental measurements for relatively low Reynolds-number and unsteady flow. However, because most control algorithms are developed based on ordinary differential equations, the lumped model is commonly used in hydraulic control system modeling and analysis and is justified based upon mathematical expediency.

The second approach motivates works using a numerical solution of partial differential equations that have been generated from the principles of fluid dynamics and numerical methods of computational fluid dynamics. Sometimes, these extra efforts,

compared with the lumped model approach, do not guarantee better results due to assumption in the numerical modeling, but computational fluid dynamics does have the potential to tell us more about the detail of the flow field. The Navier-Stokes equations can be extremely difficult to deal with when the flow is unsteady and three dimensional, and thus this numerical method does not lend itself to easy applications of control engineering.

The preference for selecting one of these two kinds of models is determined mainly by the purpose of the study. If the detailed information of the flow field is of interest, obviously a numerical solution to the partial differential equations will be preferred. If only the flow force is of interest and the computational resource is limited, the ordinary differential equation model will be preferred.

Although, these two modeling approaches can differ by way of complexity, both of them can be written to include the steady flow force and the transient flow force. The steady flow force is the flow force, which acts on the hydraulic valve during steady state operation, and depends on the valve displacement, operating pressure and the steady volumetric flow rate of the valve. In the steady flow situation, the steady flow force is the only force that needs to be overcome by valve actuation device. The transient flow force is the difference between the actual flow force and the steady flow force, when some of the states are changing with time. The difference can be small when the deviation from the steady state is small and slow, however, when some of the states change faster, the deviation from the steady state becomes large and, the difference can increase dramatically. As a result, under this kind of condition, the transient flow force must be

taken into consideration. The transient flow force will be of particular interest for this dissertation.

1.2 Literature Review

1.2.1 Review on the flow and flow forces

1.2.1.1 Ordinary Differential Equation (ODE) based research

In the past thirty years, only Manring [1] has studied the contribution of the pressure transient effect of the fluid flow force based on a linearized model of the flow force and a hypothesis that the first-order derivative of pressure with respect to time can be as important as input frequency of pressure transient increases. His work has been doubted by the contemporary scholars, mainly because of the lack of experimental support. Therefore this dissertation will be aimed at providing experimental results that will either support or refute Manring's claims.

One of the earliest works on the transient flow forces is the experimental work done by Nakada and Ikebe [2]. Their experiments showed that the magnitude of the transient flow force cannot be neglected in the high frequency region and the flow force will increase with an increasing damping length. Their model is neglected the pressure transient effect of the flow force and was linear, therefore the flow force was estimated using a transfer function. However, it should be noticed that when they were measuring the total flow force, the measurement would have included the pressure transient effect automatically, even though they did not include the pressure transient effect in their model. The agreement shown between their theoretical prediction and their experimental measurement only means that within the valid linearized region, the pressure transient

effect must not have been important. However, their experiments could not tell us whether the pressure transient effect can still be neglected when the linearized model is not valid anymore.

The perspective of Boswirth's work in reference [3] and [4] are different from all the other works concerning transient flow forces because Boswirth considers the difference between transient effects that are caused by both fluid compressibility and fluid inertia. Boswirth shows that due to the inertia of the fluid, the flow velocity change does not take place as soon as the pressure difference happens in a pneumatic valve. The volumetric flow rate has a certain lag. In addition to that, he shows that the geometric dimension has an influence on the transient flow response. These two papers challenge the classical orifice equation, because the classical orifice equation assumes an instant change of flow subject to an instant pressure difference. If Boswirth's work is true, the transient flow force will be much more complicated than a model based upon incompressible fluid flow. However, Boswirth's mathematical prediction lacks of proper experimental work to support his theory.

Based on the flow model proposed in [3-4], Boswirth [5] continued to investigate the non-steady flow in valves. He found out that in addition to the gas inertial effect, the work exchanged between flow and valve plate and gas spring effect should also be taken into consideration. This works together with his previous two papers adds extra terms to the quasi-static flow model.

In 1990, Shi, Li and Ge [6] proposed that the annular groove machined on the spool can reduce 56-59% of the steady flow force. Because, they only predicted the

influence of the annular groove theoretically, this paper might be the first paper concerning the geometric modification of the valve without using any numerical method.

Johnston [7] and his fellow scholars worked experimentally on the flow and force characteristics of poppet valves and disk valves after a brief analysis using the classical orifice equation. A comprehensive study on the influence of the changes to the geometric parameters of poppet and disc valves on the flow, pressure and force of these valves was carried out. Johnston's experimental results suggest that by setting certain geometric characteristics at small valve openings, undesired steady flow forces can be reduced. Johnston further shows that while the valve opening is large, modifying the same geometric parameters will induce instability.

It should be noticed that very similar to the two numerical solutions presented in reference [18], the experiments in [7] shows that under certain conditions, two different stable flow patterns can exist under exactly the same condition. It seems that although the objects investigated and the method used in [7] and [21] are different, the conclusions are closely connected as the flow behavior is stated in both papers as to be unpredictable. This phenomenon is possibly caused by the nonlinear nature of fluid flow. These two works were focused on the steady flow forces of the valve.

Similar to the method employed to analyze the flow force acting on the spool valve, the flow force acting on the flapper-nozzle valve has been estimated by Urata and Yamashina [8] using momentum conservation theory. In this work, it is theoretically shown that the flow force acting on the single flapper is a function of nozzle pressure and flapper nozzle gap. Further analysis of the double nozzle flapper reveals a quasi-linear

relationship between the force on the flapper, the flapper gap, and the flapper velocity. Furthermore, numerical simulation is used to test the limitation of the linear assumptions in this work. Based on an earlier work [9], a nonlinear numerical calculation of the flow force acting on the flapper shows that the quasi-linear relationship can only be obtained under certain parameter settings. Finally, the author arrived at the conclusion that flow force tends to counteract the control input of the armature torque. To verify the above theoretical predictions, an experiment was carried out. It can be seen that the opposing effect of this flow force acting on the flapper is very similar to the effect of the steady flow force acting on a spool valve.

Ruan [10] illustrates a special two-dimensional flow control valve to reduce the Bernoulli's forces and frictional forces, for the purpose of positioning the spool accurately. The proposed control valve, which combines rotary and linear motion to control the pressure in the spool chamber, can serve as a replacement for a nozzle-flapper valve. The necessity of balancing the static and dynamic performance by changing the parameters of the system and the speed of its response with a low pilot flow rate is demonstrated by both numerical simulation and experimental measurement. Like reference [24], the proof for reducing of Bernoulli flow force is indirect, because in the experiment, the forces are not measured. In addition to that, the Bernoulli forces are approximated as the function of valve displacement, therefore they should be categorized as steady flow forces only.

Perhaps Li and his students have contributed the most to the understanding and application of both transient and steady flow forces in recent years. The motivation for their work [11] in 2002 was the need to reduce the size of the solenoid actuators used to

actuate electro-hydraulic valves. According to his derivations, the transient part of the flow force is contributed by the velocity term of spool motion only as he neglects the time variation of the pressure. This is the same approach taken in the classic textbook written by Merritt [53]. The transient flow force, as modeled by Li and Merrit can serve as either negative or positive damping depending on the sign of the damping length, which is previously mentioned in reference [2]. Their work focuses mainly on how to improve the response of the system by manipulating the sign of the damping effect. Because the valve becomes open-loop unstable with a negative damping effect, the unstable valve must be stabilized using a close-loop feedback control.

Aiming at the same purpose, Li has shown that the agility of the valve can be improved differently than was previously shown in [11]. In 2005, after investigate the problem using momentum analysis, CFD and experiments, Li [12]-[13] pointed out that viscosity and non-metering momentum flux influences the magnitude of the steady flow force greatly. In order to reduce the steady flow force, a negative damping length is recommended and a properly designed non-metering flow force can be used to reduce the steady flow force also. Besides that, the port geometry can be modified to reduce the flow force. Li also designed an experimental setup that lends itself nicely to the type of work that is being proposed in the proposal for this dissertation.

Unlike reference [10] which presents a novel design of the pilot stage, Tang Wang [14] has focused on the optimal design of the control system for a nozzle-flapper type pneumatic servo valve. In reference [14], equation (1) and (2), verified by his earlier work [15], were used to compute the flow force acting on the flapper. It is obvious that the flow forces are nonlinear functions of displacement and pressure, and that no transient

effect is taken into consideration in this situation. The nonlinear dependence is quite different from conventional linear dependence shown in previous work. In order to facilitate the controller design, which is the main contribution of this paper, the nonlinear functions of the flow forces are linearized about the operating point. Based on the estimation of an applicable range of the linearized model in [15], the controller can only work within the range of about $\pm 30\%$ of the rated input current. Figure 7 in reference [15] showed that if the flow force is included in the model, the performance of the controller will be improved. A further study on the uncertain aspect of the model reveals that the model, which includes the flow force, exhibits better robustness while being controlled.

The experimental work [16] of Herakovic presents an alternative way to reduce the flow force within a spool valve. The author concentrated on how to change the jet angle by a proper design and shape of the valve piston. The valve piston is not perfectly cylindrical, instead it has many pressure compensation grooves on its outer surface. The difference between the grooves in [6] and [16] is that the annular groove is on the housing, while the so-called pressure compensation grooves shown in [16] are on the spool. The experimental results confirmed that these pressure compensation grooves are capable of changing the steady flow force greatly. It seems that his new design is very effective for reducing the steady flow force. Surely, the manufacturing cost will increase also, but compared with the energy saved on actuating the spool valve, the cost might be tolerable.

1.2.1.2 Partial Differential Equation (PDE) based research

In order to estimate the flow force, it is crucial to know the jet angle and the jet width of the flow out of the orifice. Ikeo and Hanya [17] used both potential flow theory

and numerical calculation to estimate the flow pattern. Although, the two methods involve fluid with and without considering fluid viscosity, the difference between the two studies was not large. In addition to the theoretical studies, experimental results verified the theoretical results. However, restricted by the ability of computers used in the year of 1986, their works only concern the steady flow field.

Although, the computation of the unsteady flow is difficult, there is some material addressing this particular problem. Early in the year from 1993-1995, Hayase, Cheng and Hayashi conducted numerical analysis on the time dependent orifice flow [18]-[20] subject to a suddenly imposed pressure gradient. Two distinct characteristic time constants are observed in the simulated transient flow. The first characteristic time is correspond to the volumetric flow rate change, while second one is claimed to be related to the variation of flow structure. The settling of volumetric flow rate agrees well with the commonly used simplified transient flow model. The complete settling of the flow field is established in the second characteristic time, which is about 10 times larger than the first characteristic time.

Hayase, Cheng and Hayashi then published a paper [21] on numerical analysis of the transient flow through the spool valve. This paper focused on steady laminar flow first and found that if the pressure difference between the upstream and downstream flow field exceeds some certain critical value, two solutions of different jet angles can be obtained. However, it is unclear whether the instability of the numerical method plays a part in generating two distinct solutions. It should be noticed that this phenomenon couldn't be predicted by a lumped parameter model, since this model used a preset jet angle. Then, a time dependent simulation was carried out. The numerical results coincide

well with the theoretical model with two time-constant that are significantly different. Unfortunately, this paper did not extend the numerical results to estimate the flow force acting on a spool valve. Only the flow field was investigated. Besides, their numerical results is based on laminar flow, as a result not applicable for turbulent flow.

One of the most interesting results in the previously mentioned work [21] is Figure 4, which shows that there is certain relationship between the value of discharge coefficient and the Reynolds number. If this figure is accurate, the discharge coefficient should be time dependent in a short period of time, when the spool valve starts to work. The relatively flat part of the high Reynolds number region indicates that when the Reynolds number reaches about 200, the discharge coefficient will not change much.

In order to reduce the amount of computation, some scholars have tried to numerically simulate the one-dimensional flow numerically. For instance, Sanada [22] and his fellow researchers proposed a finite element model with an interlacing grid to simulate the flow and pressure variation in the hydraulic pipelines with frequency related laminar friction. The grid was optimized to minimize the difference between theoretical natural frequency and the natural frequency of the numerical model. Later, Taylor and Johnston [23] extended the laminar friction to turbulent friction.

Later in 1998 Borghi and his research group [24] extended the work of Hayase [21] to include the flow force that was not considered. In this work the transient flow force on the pilot stage was considered, including both the velocity term of the spool and the pressure transient term, on the pilot stage of a hydraulic valve. Borghi concluded that as the time-rate-of change for the valve flow increases, the percentage of the transient

flow force increases too. He employed a Computational Fluid Dynamics (CFD) method for fully developed turbulent flow in the investigation rather than using the simpler two-dimensional momentum conservation theory. Due to the commonly existing difference between a CFD-generated numerical result and experimental measurements, the relative scale between the transient flow force, and the steady flow force may not have been so accurate. Furthermore that, Borghi did not compute the velocity term and pressure transient term separately, so there is no way to tell whether the pressure transient term is important or not in his experiment. And there is no experiment to support his numerical computation.

In 1998, Wang, Chen and Lu published their work [25] on the numerical prediction of steady flow forces acting on a spool valve. They use the k-ε two-equation model for the turbulent flow, and their work proves that modifying the relative position of the oil port and the "buckets" can remarkably reduce the steady flow force. In addition to the numerical results from CFD analysis, they also employed the particles velocimetry technology to visualize the flow field in experiment. The visualized flow field indicates that a vortex is born with in the valve chamber.

Other geometric modifications that help to reduce the flow force include recirculation lands. Jyh-Chyang Renn and Jiunn-Min Wu [26] first predicted the reduction of the flow force acting on a 4-way-3-position hydraulic directional valve due to the extra recirculation land using two-dimensional computational fluid dynamics, they then verified the result indirectly by performing a relevant experiment. One reason for choosing a 4-way-3-position valve as the subject of this study is the inherent canceling effect of the transient flow force term. This feature makes the numerical results more

plausible, because the computation is for steady flow. However, the authors of this paper did not measure the total flow force directly, which leaves the amount of the steady flow force reduction unconfirmed.

A group of Japanese researchers from the Toyota research and development center began to publish a series of work [23-25] on the flow force acting on a spool valve since 1999. In the first part of their report, they investigate comprehensively the three dimensional flow patterns and flow force for a spool valve, which has non-axial symmetrical flow paths with inlet and outlet ports. Important characteristics of the flow field such as jet angle and reattachment point of vortices were verified to be non-axial symmetric. The distribution of momentum flux, which is the main cause of flow force, was affected by the flow separation at the edge of the inlet port and the surface of the spool. Further analysis proves that the non-uniform distributed momentum flux was attenuated, when the spool stroke is reduced.

The non-axial symmetric spool valve is kept as the object of interest in the follow-up work done by Toyota, but this time, they focused on the lateral flow force, which is not a usual point of interest for the other scholars. From the result of their second report, it is shown that, in the case of both inflow jet and outflow jet, the magnitude of the lateral flow force depend on the jet impinging pattern including the jet angle and the jet impinging point. For the out flow jet situation, the magnitude depends also on the flow pattern near the outlet port. The total lateral flow force is small, mainly because the fluid forces acting in opposite directions tend to cancel this force out. This conclusion is different from the two-dimensional momentum flux analysis in Manring's textbook [52]. In the textbook, the lateral flow force can be very large, because no canceling effect

exists. The only reason to disregard the lateral flow force is that the actuation device only needs to overcome the axial flow force during operation, because the lateral flow force is in the perpendicular direction. Further study in their third report shows that a circumferential velocity component also has impact over the lateral flow force, therefore it was recommended that a larger axial spool length and the "bucket" depth are preferred to reduce the magnitude of the lateral flow force.

For a non-circular opening spool valve, which has axial symmetric located notches on the circumference of the spool piston, the shape of the restriction and the jet angle will change greatly with the motion of the spool piston; therefore, it becomes very difficult to estimate the flux of the flow momentum across the port. The flow force, estimated using traditional conservation of momentum theory, is not accurate for this kind of valve, so Ji [30] and his fellow researchers employed a CFD method to analyze and simulate the three-dimensional flow field inside the valve housing. Based on the foregoing computation, the steady flow force acting on the spool valve was obtained, and experimental results confirm the numerical prediction. According to his conclusion, the steady flow force tends to open the valve when the valve opening is within its middle range; however, the flow force serves as the effect to close the valve, when the valve opening is either smaller or larger. This feature might be unique for the non-circular opening spool valve, because, until now, this is the only paper showing this kind of conclusion.

Besides the machined geometric modification, a damping ring [31] can be added to reduce the flow force as well. It should also be noticed that the basic trend of the steady flow force is captured by both CFD method and experiments; however, the

absolute difference between numerical simulation and experimental measurements is not small.

Dempster and Lee [32] have studied the flow and force for safety relief valves, but the fluid inside the valve was gas instead of hydraulic oil. This difference made the flow to be fast enough to enter the sub-sonic and supersonic region. The method employed here included comparison between two-dimensional CFD work and experimental measurements. However, the flow model was compressible and turbulent compared with some of the previously stated research, which assumed laminar flow and incompressible conditions. The numerical and experimental results were of good correspondence to each other. However, just as much of the previous research has shown, the flow and force characteristics are related to the geometry of the valve port. Accordingly, sometimes, the results using CFD and the experimental measurements can differ significantly within certain regions, especially when turbulence is considered.

A group of scholars lead by Zhao [33] investigated the flow field inside the spool valve using CFD analysis. Although the method was well known, this article did verify some interesting things. First, under the condition of a small throttle with large flow and high speed, the transient flow force became so large that it could not be neglected. This transient effect included the fast movement of the spool valve. Because the work presented here is only computational, it is not convincing enough to persuade one that the transient flow force is mainly caused by the velocity term and that pressure transient effect does not exist. Second, this paper also pointed out that the normally neglected radial flow force can be thrown away under the same conditions that produce a large transient flow force in axial direction. Third, this paper questions the method of

calculating the discharge coefficient using the pressure of both the upstream and downstream flow field. The reason for this question is that the method does not account for the pressure loss from the inflow port to the outflow port. It was confirmed that the discharge coefficient decreased when the valve opening increased. Furthermore, when the valve opening was small, the motion of the spool would change the value of the discharge coefficient.

Many of the previously mentioned references performed numerical analysis on the flow and flow force acting on a spool valve. Some of them use two-dimensional model, while others use three-dimensional model. Vescovo and Lippolis published their work [34] on the comparison of different CFD models in 2003. This paper did computational work on a two-dimensional, axial-symmetric three-dimensional model and a full three-dimensional model. The computational results were steady state in nature. Although only steady state conditions were studied, this work did offer some important information. For instance, the difference of pressure drops across the restriction does not have much influence on the discharge coefficient and flow force coefficient. However, small change in valve opening will result in a considerable change in discharge coefficient and flow force coefficients. Furthermore different numerical results generated by models of different dimensions are different, even the results of the axial-symmetric three-dimensional model and the full three dimensional model differs significantly.

1.2.2 Review on the study of pressure wave generators

In order to test the pressure transient effect on the flow force exerted on a spool valve, it is necessary to use a pressure wave generator that can create a fast changing pressure wave. Among all the methods to generate a step pressure signal in gas, the

fastest method is the shock tube. A shock tube is a metal tube within which low-pressure gas and high-pressure gas are separated by a diaphragm. The diaphragm is made to burst under a critical condition to produce a shock wave, which travels down the low-pressure section of the tube. Because the velocity of the wave is so fast, the change of pressure at certain point happens in a short instant. Because of the rise time of the pressure step is about 2-3 μs, which is extremely short. The shock tube is used in testing pressure sensors [35]. However, due to strength limitations, the diaphragm cannot be used when the pressure difference across the diaphragm is large. Additionally, the shock tube structure can only create one step, and it is not capable of creating consecutive step wave forms.

Inspired by the shock tube, a very similar principle is used in the rotary square wave generator [36-39]. When the chamber of the spool valve is exposed to different pressurized ports, the high-pressure wave front will travel toward the low-pressure port, as long as the port pressure is kept constant. Kobata and Ooiwa [36] have presented a method to generate dynamic pressure at medium pressure level in 1999. This method is applicable to a lower frequency range compared to the shock-tube pressure wave generator. The rotating valve has two independent chambers, which are pressurized by two separate pressure sources. As the valve rotates, the port connected to the pressure sensor is switched between two different pressure levels, thus a square-wave pressure is created. Based on the experiment presented in their paper, the magnitude of the square wave can be up to 100 kPa, while the base frequency of the rotor can go up to 80 Hz. However, unfortunately, these authors have not offered a theoretical model for this square wave generator. The direct simulation of the wave propagation within a three dimensional container, which involves compressible unsteady flow, is difficult to perform.

Good pressure wave generators are always used to evaluate the pressure transducers. The foregoing rotary pressure wave generator has been used in testing pressure sensors one year later by the same group of scholars [37]. The advantage of the rotary square wave generator is beneficial because both magnitude and fundamental frequency can be varied easily in the testing procedure. Thus, quantitative calibration of the pressure transducers becomes possible. From the experiments carried out, we know that the amplitude spectrum of the square wave is proved to exhibit with good repeatability.

Ten years after the work of the Japanese scholars was done, Wang [39] and his fellow researchers proposed another type of rotary pressure wave generator. According to their experimental results, the square wave generated was very accurate, even smoother than the results in [36], except for exhibiting some overshoot, which is modeled by a second order system. The idea in this paper is very similar to the separated chambers and switching action in [36], but the design of the rotating valve is different. The new design has fewer parts for assembly. The good feature for this square-wave generator is that the fluid inside the chambers is hydraulic oil and the pressure can go up to 2 MPa. The rise time of the pressure transient is only 0.3 ms. Compared with the burst of the diaphragm, the opening and close of the rotating valve is slower.

Before the seemingly more basic paper in 2009 was published, the same group of Taiwan scholar did some experimental work [38] on the pressure square-wave generator with different tangent velocities. This work concluded that the larger the tangent velocity is the shorter the rise time. This kind of phenomenon is intuitively correct.

In fact the idea of generating a pressure wave by rotation dates back to the 1980s [40-41]. The original motivation for the design is not for the calibration of the sensors, but for the lateral pressure cutting device for ductile material. The phenomenon, which is able to create hydraulic pressure pulses of high frequency and high pressure, is called an oil hammer. A rotating valve, which controls the flow to be periodically on and off, just serves the same function as the rotor designed in [36-39]. From the first report, we know that the frequency of the pulse series or the square waveform can be increased by using a shorter pipe. One of the unique features of the design is that the pulse pressure is amplified through a booster piston. By controlling the amplifying ratio of the booster piston, the pulse pressure can be increased to about 140 MPa. The back-pressure applied to the low pressure side of the valve is used to keep the pressure at a more constant level. By doing this, the stability of the waveform is improved. In their second report, an additional intensifier was added to make the amplified pressure greater than 300 Mpa; and at last, the speed of the response makes this pressure generator capable of performing as a practical lateral cutting device requiring high repeated frequency.

Piezoelectric valves are an alternative way to generate pressure pulses and square pressure waves. Ouyang [42] and several scholars proved that piezoelectric on/off valve can do work for this application. They utilize the characteristic of the piezoelectric actuator, such as high frequency and high instant force, to actuate the poppet. In order to achieve the actuation objectives, the extremely small displacement of the piezoelectric component was amplified and the temperature effect was compensated. Finally, a maximum pressure of 20 MPa and a frequency of 200 Hz have been satisfied easily. As the first stage, this piezoelectric valve can provide us with high-precision control, which

can hardly be gain using conventional three-way spool valve with solenoid. Beside the good feature of the piezoelectric actuator, the fast response was also promoted by the smaller mass of the poppet. However, compared with the rotary square wave generator, this piezoelectric on/ off valve must is much more expensive to build.

There are also ways to generate extremely high pressures in the range of TPa [43]. The Korean and the Japanese scholars have successfully created such pressure impulses by using a colliding metal jet. These metal jets are generated by controlled detonation. The pressure level is not measured, but estimated by optical methods, because the pressure is too high for any pressure sensor to measure. However, it is crucial that the velocity of sound be surpassed. This condition can hardly be satisfied in liquid, because the speed of sound in liquid is much higher than in air.

In recent years, scholars in China [44] have tried to generate a high-speed sine pressure wave faster. Like the piezoelectric on and off valve, piezoelectric servo valves act much faster than conventional valves. The period of the sine wave is shortened to 40ms or even a smaller scale. The difficulty to achieve a sine pressure wave is caused by the nonlinearity of the system. Using conventional Proportional-Integral-Derivative (PID) control, it is impossible to track the desired sine wave. Thus, the authors proposed a bidirectional piecewise gearshift integral PID control in the paper. Experimental results confirmed the validity of the new PID controller.

1.2.3 Review on the application of artificial neural networks in fluid power systems

Due to the imperfection and the difficulty of using lumped parameter models and CFD methods, scholars have endeavored to find alternative techniques for studying the

flow characteristics within the fluid power systems. One such method is the application of Artificial Neural Networks (ANN).

Lead by Xu [45], a group of scholars in University of Sakatchewan did one of the earliest experimental studies on the application of ANN in fluid power systems. This group chose the simplest component for study: a flow orifice. In order to train the neural network, the conjugate gradient method was successfully employed. Figure 2 in reference[45] shows that the volumetric flow rate of the orifice does not increase linearly with respect to valve opening. When the valve opening surpasses a certain critical value, the linear relationship is destroyed. This nonlinear behavior is said to be caused by the internal structure of the valve. Thus, the classical orifice equation cannot be used to describe this nonlinear behavior relative to a large valve opening. The final prediction of the flow rate's change with respect to pressure drop and valve opening is quite satisfactory.

Later, Watton and Xue [46] investigated the capacity of prediction for neural networks on the behavior for hydraulic components, including an axial piston pump and filter, a pressure relief valve, a lumped volume, and a hydraulic subsystem. Biased Autoregressive Moving Average Model with Exogenous Input Model (BARMAX) and Group Method of Data Handling (GMDH) networks were proved to be effective in training and testing, while the Multilayer Perceptron (MLP) networks were not successful. Later, they [47] combined the before mentioned hydraulic components into a motor speed control system. In the investigation of the identification of the system's initial condition, MLP networks, instead of the BARMAX and the GMDH networks, proved to be the best network to use. However, when they tried to study the system out of the range of the

training data, their success was only limited. This indicates that although the artificial networks can predict the system's behavior within the range of the test data, it is not capable of making accurate predictions outside of this range.

Then, Xue and Watton [48] tried another kind of network, which is called the Radial Basis Function network to predict the dynamic behavior of a hydraulic pump and a proportional valve-controlled motor system. In order to make the network successfully converge to the desired target, a method involving a global error decent algorithm, a genetic algorithm and a least squares method was proposed. This method was proved to be efficient.

Motivated by the need to deal with asymmetric flow characteristics of the spool valves in an automatic transmission hydraulic control system, Wang [49] and his fellow scholars proposed a new hydraulic valve fluid model based on Non-dimensional Artificial Neural Network (NDANN) to predict the dynamics of an automatic transmission system. They confirmed that due to the nondimensional characteristics of the network used, the NDANN model was able to make accurate estimate of the fluid force and flow rate even when the operating condition and the design geometric parameters were not within the training data. This advantage can be preserved as long as the non-dimensional values of the operating condition and geometric parameters are within the nondimensional training sets.

1.2.4 Summary

A current understanding about the steady state flow force acting on spool valves is well developed, mainly because it is easy to understand. Theoretically, the steady flow

force can be computed by the static pressure distribution or conservation of momentum. Many theoretical, experimental and computational studies have been devoted to determine the magnitude and direction of the steady flow force. The works proves that the magnitude increases with increasing pressure difference and valve displacement, while the direction of the steady flow force always seeks to close the valve. The influence of the geometry and relative position of the spool and housing is also verified by various numerical simulation and experimental measurements. The current understanding of steady flow force has been proved sufficient in the past for systems that operate at relative slow speeds.

At the same time, the understanding of the transient flow force acting on spool valves is also growing. Some scholars have found that the transient flow force increases as the time rate of flow changes. After linearization, the transient flow force falls into two categories: the flow force related with the velocity of the spool and the flow force related with the time-rate-of-change of the pressure. Some investigators have discovered that the transient flow force can be manipulated to counteract the steady state flow force, where the flow force related with velocity serves as a kind of negative damping. In this case, the negative damping effect helps to accelerate the response of the valve. However, these researchers either only consider the transient term relative to the velocity of the spool, or the transient effect of velocity and the changing rate of pressure is mixed together in a single result. The researchers who have done this work believe that the influence of the changing rate of pressure does not have a great influence over the total flow force. In fact, in the past thirty years, the pressure transient effect is neglected in almost every paper and research report. Consequently, it can be seen that there is no direct proof about how much

the changing rate of pressure contributes to the transient flow force. To enhance the body of literature on this topic, experiments should to be carried out to verify the existence and importance of the pressure transient effect.

There are many researchers working on the attenuation of flow force acting on the spool valve. Their works and contributions are listed in Table 1 and Table 2. Theoretical, experimental and numerical results are all involved in their research. It should be noticed that except for Li's work, all the others are related with geometry modifications.

Table 1 Method of attenuation of the steady flow force

Researcher	Results	Approach
Shi, Li and Ge	Modified annular groove on valve housing based on linear model	Theoretical
Johnston	Geometric modification at small valve opening and induced stability problem (two competing flow pattern) on steady flow force	Theoretical and experimental
Ruan	Rotary and linear motion are both involved in controlling the valve to reduce the steady flow force	Numerical and experimental
Li.	Using transient flow force to reduce the total flow force and the stability problem	Theoretical
Li.	Manipulating viscosity, non-metering steady flow force and part geometry	Theoretical, numerical and experimental
Herakovic	Change the jet angle by proper design of the valve piston: pressure compensation groove	Experimental

Table 2 Method of attenuation of the steady flow force (continue)

Researcher	Results	Approach
Wang, Chen and Lu	• k-ε two-equation model for the turbulent flow • Modifying the relative position of the oil port and the bucket can reduce the steady flow force	Numerical
Jyh-Chyang Renn	Extra recirculation land can reduce steady flow force	Numerical
Ji	Influence of notches, on the circumference of the spool piston, will change the direction of the flow force	Numerical experimental
S Zhou	Damping rings can reduce the steady state flow force	Numerical
Dempster	• Flow and force on a safety relief valves based on compressible and turbulent flow • Geometry sensitivity: change in radii and chamfering	Numerical

It should also be noticed that although the hydraulic system utilizing a spool valves should be a nonlinear a system, most of the works done in the past were focused on linearized models. Only a few of them mentioned the characteristics of nonlinearity based on numerical solutions or experimental observation. As a result, none of them have analyzed the nonlinear system carefully or tried to find any nonlinear behavior based on the theoretically derived model. Currently, we do not know much about the nonlinearity of the spool valve.

The works concerning the pressure wave generator are limited. The rotary pressure wave generator, which attracts our attention, should be suitable to meet the requirement of testing the pressure transient effect in our research, and it is relatively inexpensive to build. Although several experiments have been carried out to prove the

effectiveness of the square pressure wave generator, none of them has proposed any theoretically derived model for the pressure wave generator. Therefore, finding a mathematical description of the pressure wave generator will be required.

1.3 Dissertation Outline

This remaining dissertation is organized into seven chapters in following order. Chapter 2 describes the analytical solution of the flow force in piston equilibrium condition and equilibrium condition for fluid in the control volume. It familiarizes the reader with basic geometry of the two-way valve and nomenclatures used in this work. This description is the very foundation for the nondimensional analysis, uncertainty sensitivity analysis and linearization presented in Chapter 3. The nondimensional analysis in Chapter 3 is helpful in directing the designing the pressure wave generator, which will be presented later in Chapter 4. Chapter 4 presents the description of the components in the pressure-wave generation system, which includes a variable axial piston pump, a rotary pressure wave generator, and an accumulator. Based on the description and function of the pressure wave generator, mathematical models are building for it and corresponding simulation results are presented. Chapter 5 present the steps to prove the existence of the pressure transient effect by processing the data acquired. First the sound wave phenomenon is identified as one dominant influence on the flow force. Second, the pressure profile at the two ends of the piston makes it difficult to estimate the steady flow force accurately. Third, 100 points average and pressure profile factor are introduced to reduce the influence of sound wave phenomenon and non-uniform pressure distribution. Chapter 6 presents the steps to prove the existence of pressure transient effect without involving manipulation on the data acquired. First the frictional force is required to be

small for all the experiments that will be conducted. Second, the validity of steady state pressure difference induced flow force and viscous shear force is proved experimentally. Third, by observing the difference between the total flow force and estimated steady state flow force, the pressure transient effect is proved. Chapter 7 is added after experimental validation and test in order to explain the reason for the inconsistency between the theoretical pressure transient flow force and the measured pressure transient flow force. Chapter 8 summarizes the important conclusions and limitation of this work and some ideas that could be explored to continue this project.

Chapter 2: Analysis of Flow Forces

2.1 General

The geometry of a two-way spool valve with damping length L is given in Figure 1. The damping length L is defined to be the distance between the supply orifice, which is connected to supply pressure P_s, and the return orifice, which is connected to return pressure P_r. In the analysis the valve damping length is close to the valve chamber length. The valve piston is held still by force F. Force F is the force, which is required to make the piston in equilibrium condition with the pressure difference $P_1 - P_2$ on two ends of the valve piston, the viscous shear force acting on the shaft and frictional force f. A force sensor will measure this force caused by fluid flow. Because the piston is not moving, there is no inertial and damping effect concerning the motion of the valve piston. The equilibrium condition of the valve piston can be represented as

$$\sum F = F + A_v\left(P_1 - P_2\right) - F_{\tau s} - f = 0, \tag{1}$$

where A_v is the pressurized area given in Figure 1 and $F_{\tau s}$ is viscous shear force caused by the fluid flow close to the valve piston shaft.

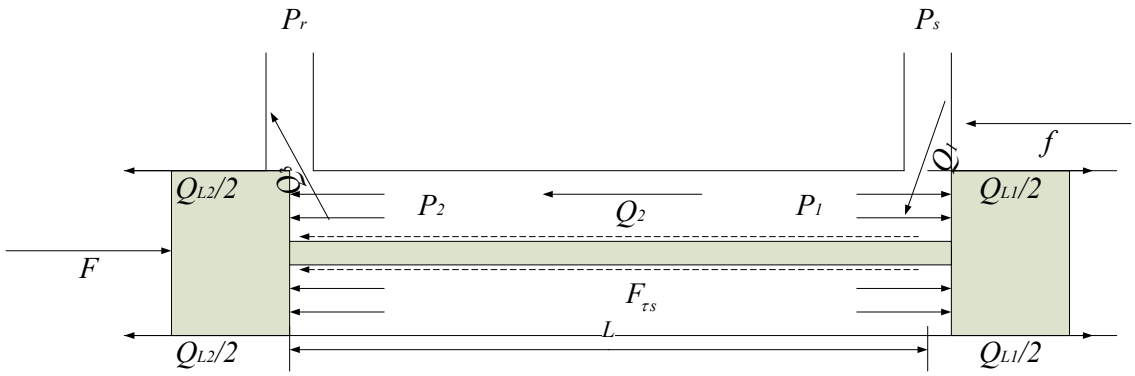

Figure 1 Geometry of a two-way spool valve

The coordinate system used to compute flow force is defined in Figure 2. The positive direction of x axis and y axis are denoted as two orthogonal base vectors **i** and **j** respectively. In Figure 2 there are two jet angles θ_1 and θ_2 which are related to supply volumetric flow rate Q_1 and return volumetric flow rate Q_3 respectively. These jet angles are defined to be the angle between the fluid flow direction and the positive direction of the x axis **i**. There are two possible causes for the pressure difference on two ends of the valve piston. First, because of the viscosity of the fluid, two viscous shear forces $F_{\tau h}$ and $F_{\tau s}$ are caused by fluid flow near the valve housing and piston respectively. These two viscous shear forces are tangential to the control volume boundary, and they are related to the velocity gradient on the boundary. As a result, they are classified as surface force. The second cause is the momentum change across the control volume denoted by dash line in Figure 2, which is called the momentum force. The momentum force is conventionally taken into consideration and is considered as the major component of the total flow force, while Li [13] has investigated the surface force recently using Hagen-Poiseuille flow model. Moreover, the Hagen-Poiseuille flow model is developed based on the low Reynolds number laminar incompressible flow assumption. To make the control

volume in equilibrium condition in x direction, the momentum-induced force should equal to the summation of external forces

$$F_{xm} = \sum_{external} F = F_{\tau h} + F_{\tau s} - A_v \left(P_1 - P_2 \right), \tag{2}$$

where F_{xm} is the x component of the momentum force in x direction that will be addressed in later sections. Eliminating pressure difference generated force $A_v \left(P_1 - P_2 \right)$ from Equation (2) and Equation (1) yields the second expression for the force F required to make the piston in equilibrium condition

$$F = F_{xm} - F_{\tau h} + f. \tag{3}$$

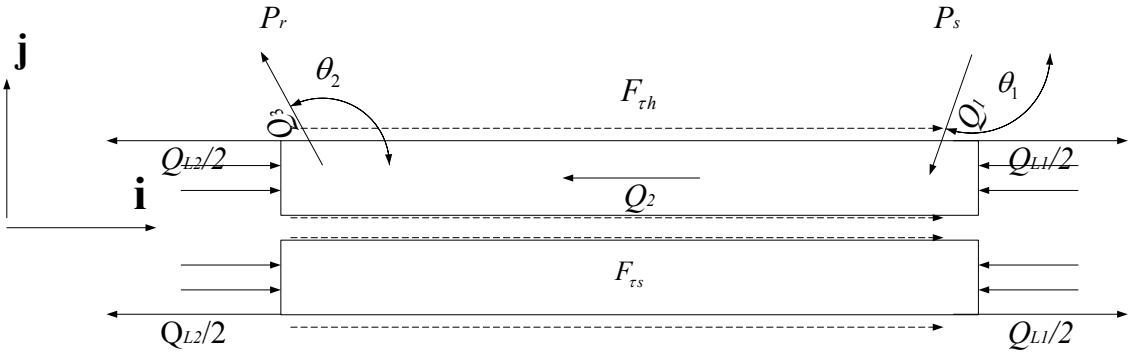

Figure 2 Control volume for calculating spool-valve flow force

To conclude the general analysis, there are two ways to estimate the flow force F on the valve. The first way is using the equilibrium condition of the valve piston in Equation (1). The second way is using the equilibrium condition of the fluid in the control volume in Equation (2) and eliminate the pressure difference term to get Equation (3). Using the first method, it is required to know the pressure difference $P_1 - P_2$ and the viscous shear force $F_{\tau s}$ acting on the piston shaft. In the second way, it is required to know

the viscous force $F_{\tau h}$ and momentum force F_{xm}. The following sections will address these problems step-by-step.

2.2 Orifice Equation and its Low Reynolds Number Limitation

Before running into the problem of how to find the analytical solution of the forces defined in the previous section, it is necessary to present the model for the fluid flow model. The reason for this organization is the strong interaction between volumetric flow rate and pressure.

Orifices are the fundamental element for the fluid power systems including the two-way spool valve that is being studied in this dissertation. An orifice is a sudden restriction of short length in a flow passage and may have a fixed or variable area. To model the fluid flow through an orifice, the classical orifice equation describes the general volumetric flow rate Q through an orifice with area A as

$$Q = AC_d\sqrt{\frac{2\Delta P}{\rho}}, \tag{4}$$

where C_d is the general discharge coefficient and ρ is fluid density.

Classical orifice equation is developed based on one-dimensional Bernoulli's equation. Therefore it can only be used to describe high Reynolds number flow. However, in the experiment that will be conducted in this research the pressure drop across the valve might be so low that the high Reynolds number flow assumption will no longer be valid. Thus, it is necessary to low Reynolds number volumetric flow rate

$$Q = K\Delta P. \tag{5}$$

Equation (5) shows that for low Reynolds number flow, the volumetric flow rate of the fluid can be a linear function of uniform pressure gradient ΔP. In order to connect the low Reynolds number flow with the high Reynolds number flow smoothly, it is proposed in reference [50] that the orifice equation should be a polynomial below certain critical Reynolds number Re_c

$$Q = \begin{cases} AC_d\sqrt{\dfrac{2}{\rho}}\left(C_1\Delta P + C_2\Delta P^2 + C_3\Delta P^3\right), \mathrm{Re} < \mathrm{Re}_c \\ AC_d\sqrt{\dfrac{2\Delta P}{\rho}}, \mathrm{Re} \geq \mathrm{Re}_c \end{cases}. \tag{6}$$

Equation (6) ensures the orifice flow follows the classical square root law for high Reynolds number flow and is close to the linear approximation for low Reynolds number flow. The Reynolds number is defined to be

$$\mathrm{Re} = \frac{\rho Q D_h}{\mu A} \tag{7}$$

where D_h is hydraulic diameter. The hydraulic diameter is defined as

$$D_h = \frac{4A}{P_w}, \tag{8}$$

where P_w is the wetted perimeter. For the fluid flow at the critical Reynolds number

$$\mathrm{Re} = C_d\sqrt{2\rho\Delta P_c}\,\frac{D_h}{\mu} = \mathrm{Re}_c. \tag{9}$$

Therefore, the corresponding critical pressure drop ΔP_c is

$$\Delta P_c = \frac{1}{2\rho}\left(\frac{\mu \mathrm{Re}_c}{C_d D_h}\right)^2. \tag{10}$$

A typical critical pressure drop is about 68 Pa. At the critical point, the polynomial model and the square-root law should be smoothly connected

$$\begin{aligned} &C_1\Delta P_c + C_2\Delta P_c^2 + C_3\Delta P_c^3 = \sqrt{\Delta P_c}, \\ &\frac{d}{d\Delta P_c}\left(C_1\Delta P_c + C_2\Delta P_c^2 + C_3\Delta P_c^3\right) = \frac{d}{d\Delta P_c}\left(\sqrt{\Delta P_c}\right), \\ &\frac{d^2}{d\Delta P_c^2}\left(C_1\Delta P_c + C_2\Delta P_c^2 + C_3\Delta P_c^3\right) = \frac{d^2}{d\Delta P_c^2}\left(\sqrt{\Delta P_c}\right). \end{aligned} \tag{11}$$

Three equations in Equation (11) stands for positional continuity, tangential continuity and curvature continuity respectively. Solve for coefficients C_1, C_2 and C_3 yields

$$C_1 = \frac{15}{8\Delta P_c^{1/2}},\ C_2 = -\frac{5}{4\Delta P_c^{3/2}},\ C_3 = \frac{3}{8\Delta P_c^{5/2}}. \tag{12}$$

The coefficients in Equation (12) ensures C^2 continuity between the polynomial model and the classical orifice equation as shown in Figure 3. The characteristic of continuity makes the newly developed orifice equation more computational efficient than the classic orifice equation around the origin. Because in most applications the pressure drop will be much greater than the estimated critical pressure drop ΔP_c, Equation (4) will be valid in these applications. For all the analysis and experiment that will be conducted in this paper, the pressure drop in most cases will be much larger than 68 Pa. Consequently, the classical orifice equation can be applied in current research.

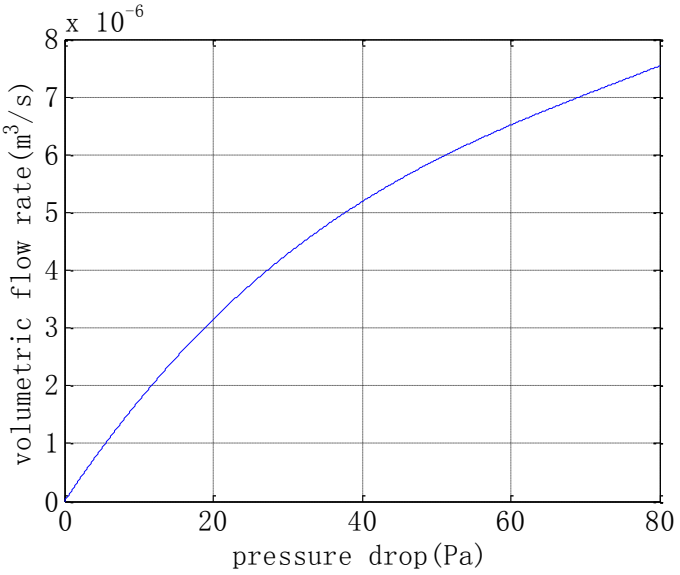

Figure 3 Modified orifice equation at low Reynolds number

2.3 Pressure Difference across the Valve

This section is devoted to the theoretical solution for the pressure difference term in Equation (1).There are three volumetric flow rates related to this valve: the volumetric flow rate in the supply line Q_1, the volumetric flow rate in the valve piston chamber Q_2, and the volumetric flow rate in the return line Q_3. If the fluid flow is incompressible and no leakage exists, all three volumetric flow rates should equal one another. However, on the two ends of the valve piston, leakage volumetric flow rates Q_{L1} and Q_{L2} exist. Therefore, all the volumetric flow rates should satisfy

$$\begin{aligned} Q_1 &= Q_2 + Q_{L1}, \\ Q_2 &= Q_3 + Q_{L2}. \end{aligned} \tag{13}$$

Because in the trial experiment the estimated Reynolds number is more than 100, so the flow is characterized as high-Reynolds number flow. In real application, the inner diameter of the hose, which connect the device in the upper stream to the downstream, is

larger than the diameter of the orifice. Consequently, restrictions exist for the fluid flow in and out of the control volume. The fluid flow from the right-hand side of the control volume to the left-hand side of the control volume can be considered as the fluid flow in a pipe, when the damping length L is much larger than the hydraulic diameter of the control volume cross section. In reference [53], the empirical equation for the pressure drop[1] for fully developed turbulent flow is

$$\Delta P = f_p \frac{L}{D_h} \frac{\rho \overline{u}^2}{2} = f_p \frac{L}{D_h} \frac{\rho Q^2}{2A^2}. \tag{14}$$

where f_p is pipe frictional factor which depends on Reynolds number and pipe roughness and $\overline{u}$ is the general average velocity of the fluid. The frictional factor can be estimated from experimental measurements. Manipulate the terms in Equation (14) so that volumetric flow rate is represented as the function of pressure drop ΔP yields

$$Q = A\sqrt{\frac{D_h}{f_p L}}\sqrt{\frac{2\Delta P}{\rho}}. \tag{15}$$

Noticing that by selection the equivalent discharge coefficient

$$C_{de} = \sqrt{\frac{D_h}{f_p L}}, \tag{16}$$

Equation (15) can be written in to the same form as the classic orifice Equation (4):

$$Q = AC_{de}\sqrt{\frac{2\Delta P}{\rho}}. \tag{17}$$

[1] Reference[12] page 36 Equation (3-21)

In other words, the turbulent flow in a pipe and the high-Reynolds number flow through a short restriction in a flow passage can be described using the same equation. The advantage of using Equation (17) is that the current formulation automatically takes the Reynolds number and surface roughness into consideration. Therefore, the pressure drop across the supply orifice, the pressure drop across the valve body and the pressure drop across the return orifice can be modeled based on classic orifice Equation (4), which is based on high-Reynolds number Bernoulli equation. As a result, all three volumetric flow rates can be described in the following expression

$$\begin{aligned} Q_1 &= C_{d1} A_1 \sqrt{\frac{2}{\rho}(P_s - P_1)}, \\ Q_2 &= C_{d2} A_2 \sqrt{\frac{2}{\rho}(P_1 - P_2)}, \\ Q_3 &= C_{d3} A_3 \sqrt{\frac{2}{\rho}(P_2 - P_r)}, \end{aligned} \tag{18}$$

where A_2 is the cross-sectional area in the center part of the control volume. This cross-sectional area is not necessary equal to pressurized A_v because of the manufacturing difficulty in the long valve piston bore with small diameter. By dividing the control volume into two equal parts in Figure 4, the pressure dynamics of P_1 and P_2 can be described using classical pressure rise rate equation for slightly compressible fluid

$$\begin{aligned} \frac{V_1}{\beta}\frac{dP_1}{dt} &= K_L Q_1 - Q_2, \\ \frac{V_1}{\beta}\frac{dP_2}{dt} &= K_L Q_2 - Q_3, \end{aligned} \tag{19}$$

where K_L is the coefficient used to account the leakage, β is fluid bulk modulus and half valve piston chamber volume is

$$V_1 = \frac{LA_2}{2}. \tag{20}$$

Coefficient K_L will be estimate later in experiment. The fluid bulk modulus β measures the compressibility of the fluid. Consequently, the pressure rise-rate equation describes the average pressure change for a slightly compressible fluid in certain control volume. When the fluid flows into the control volume is more than the fluid flows out of the control volume, the average pressure will rise. On the contrary, the pressure will fall. Whether the pressure-rise rate equation can be used to describe the pressure dynamics within the valve can be disputable for several reasons. First the orifice equation is essentially steady. Second, the pressure-rise rate equation is assuming that the fluid is under uniform compression, which is not necessarily the case in real application.

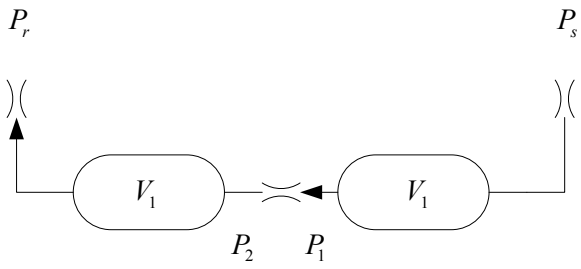

Figure 4 Three-orifice model for pressure difference

All three discharge coefficients should be estimated by the measuring volumetric flow rate, corresponding pressure drop and cross-sectional area using flow meter and pressure sensors. All the pressure drops can be measured directly using pressure sensors, but not all the volumetric flow rates can be measured. Restricted by the size of the piston bore diameter, the flow meter can only be placed in the supply line and return line to measure Q_1 and Q_3. The volumetric flow rate Q_2 in the middle can be estimated by

collecting the fluid leaking out from the valve piston chamber using a flask. In a trial experiment, the measured leakage volumetric flow rate is about 1.26% of the supply flow rate and the corresponding Reynolds number for the leakage passage is about 1.95. For this level of Reynolds number the flow cannot be characterized as either high-Reynolds number flow or low-Reynolds number flow. This characteristic makes it difficult to model the fluid flow in the leakage passage. More trial experiments show that the leakage on the high-pressure side is higher than the leakage on the low-pressure side. As a result, the pressure does have an influence on leakage. For the sake of convenience, it is assumed that steady state volumetric flow rate in downstream is certain percentage of the volumetric flow rate in the upper stream

$$\begin{aligned} K_L Q_1 &= Q_2, \\ K_L Q_2 &= Q_3, \end{aligned} \tag{21}$$

where lose coefficient $K_L \in (0 \quad 1)$. Because $Q_1 > Q_2 > Q_3$ is always satisfied, the corresponding leakage volumetric flow rates in Equation (13) can be described as

$$Q_{L1} = (1 - K_L) Q_1 > (1 - K_L) Q_2 = Q_{L2}. \tag{22}$$

The measured supply volumetric flow rate Q_1 and return volumetric flow rate Q_2 can be used to estimated lose coefficient K_L

$$K_L = \sqrt{\left(\frac{Q_1}{Q_3} \right)_{measured}}. \tag{23}$$

Correspondingly, discharge coefficient C_{d2} can be estimated by

$$C_{d2} = \frac{K_L (Q_1)_{measured}}{A_2 \sqrt{\frac{2}{\rho}(P_1 - P_2)_{measured}}} \tag{24}$$

Provided that the supply pressure and return pressure in Equation (18) are known or can be measured, there are only two unknowns in Equation (21). Solve for pressure P_1 and P_2 from Equation (18) yields steady state result:

$$\begin{aligned} P_1 &= \frac{(C_{d1}A_1)^2 (C_{d2}A_2)^2 P_s K_L^4 + (C_{d1}A_1)^2 (C_{d3}A_3)^2 P_s K_L^2 + (C_{d2}A_2)^2 (C_{d3}A_3)^2 P_r}{(C_{d2}A_2)^2 (C_{d3}A_3)^2 + (C_{d1}A_1)^2 (C_{d2}A_2)^2 K_L^4 + (C_{d1}A_1)^2 (C_{d3}A_3)^2 K_L^2} \\ P_2 &= \frac{(C_{d2}A_2)^2 (C_{d3}A_3)^2 P_r + (C_{d1}A_1)^2 (C_{d3}A_3)^2 P_r K_L^2 + (C_{d1}A_1)^2 (C_{d2}A_2)^2 P_s K_L^4}{(C_{d2}A_2)^2 (C_{d3}A_3)^2 + (C_{d1}A_1)^2 (C_{d2}A_2)^2 K_L^4 + (C_{d1}A_1)^2 (C_{d3}A_3)^2 K_L^2}. \end{aligned} \tag{25}$$

As a result, the steady state pressure difference caused force can be represented as the function of supply pressure and return pressure instead of the pressure on the two ends of the valve piston in

$$F_{xp} = A_v (P_1 - P_2) = A_v C_{fxp} (P_s - P_r), \tag{26}$$

where coefficient

$$C_{fxp} = \frac{(C_{d1}A_1)^2 (C_{d3}A_3)^2 K_L^2}{(C_{d2}A_2)^2 (C_{d3}A_3)^2 + (C_{d1}A_1)^2 (C_{d2}A_2)^2 K_L^4 + (C_{d1}A_1)^2 (C_{d3}A_3)^2 K_L^2}. \tag{27}$$

will be called the pressure drop coefficient in the rest of the dissertation. From Equation (26) it can be known that when supply orifice or return orifice closes completely, there is no pressure-difference induced flow force. This situation is physically right, because the piston chamber will be filled with uniform pressure in steady state, and the pressure inside will cancel in every direction. It should be emphasized that because Equation (26)

is the result based on the assumption that the pressure dynamics caused by fluid compressibility can be neglected, pressure transient effect is not included in Equation (26). In other words, Equation (26) is a steady state solution. Similar to the definition of pressure drop $(P_1 - P_2)$, the other two pressure drops can also be represented as the function of supply and return pressure

$$\begin{aligned} P_s - P_1 &= C_{fxms}(P_s - P_r), \\ P_2 - P_r &= C_{fxmr}(P_s - P_r), \end{aligned} \tag{28}$$

where the pressure drop coefficients are

$$\begin{aligned} C_{fxms} &= \frac{(C_{d2}A_2)^2 (C_{d3}A_3)^2}{(C_{d2}A_2)^2 (C_{d3}A_3)^2 + (C_{d1}A_1)^2 (C_{d2}A_2)^2 K_L^4 + (C_{d1}A_1)^2 (C_{d3}A_3)^2 K_L^2}, \\ C_{fxmr} &= \frac{(C_{d1}A_1)^2 (C_{d2}A_2)^2 K_L^4}{(C_{d2}A_2)^2 (C_{d3}A_3)^2 + (C_{d1}A_1)^2 (C_{d2}A_2)^2 K_L^4 + (C_{d1}A_1)^2 (C_{d3}A_3)^2 K_L^2}. \end{aligned} \tag{29}$$

The summation of all three pressure drop coefficients must be equal, because the pressure drop across the valve is always $(P_s - P_r)$. Typical curves for these coefficients with partial blocked circular orifice area in Figure 5 of diameter d

$$A_3 = \frac{d^2\pi}{8} - x\sqrt{\frac{d^2}{4} - x^2} - \arcsin\left(\frac{2x}{d}\right)\frac{d^2}{4}, \tag{30}$$

are given in Figure 6. In this picture, the slope changes as the valve displacement changes. This characteristic will cause problems, when the pressure drop coefficients are linearized at the origin of zero valve displacement.

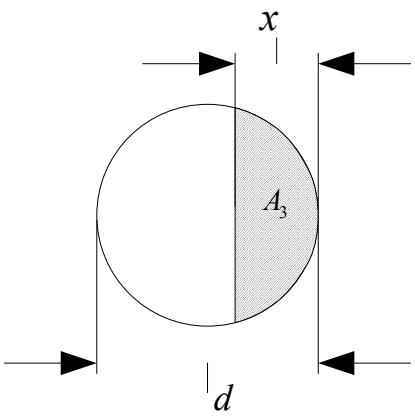

Figure 5 Geometry of partial blocked circular area

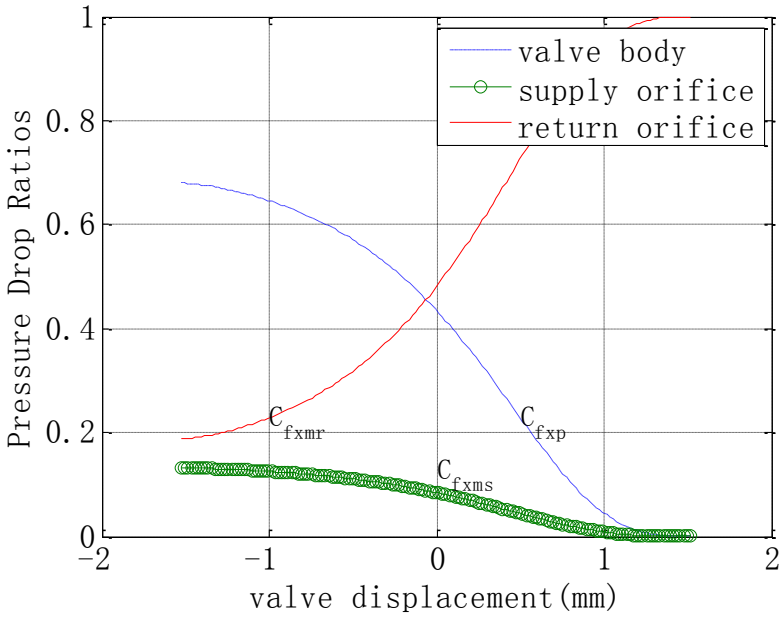

Figure 6 Pressure drop coefficients

2.4 Viscous Shear Force

This section is devoted to the theoretical solution of the viscous shear term in Equation (1) and (2). The flow field close to the wall is characterized as low-Reynolds number flow, despite the flow near the center can be high-Reynolds number flow. Therefore, the viscous shear force becomes dominant for the fluid flow near the wall. In

general, the viscous shear force between two parallel surfaces can be computed based on the velocity gradient on the surface using

$$F_{shear} = \mu A_{contact} \frac{\partial u}{\partial y}, \tag{31}$$

where $A_{contact}$ is the contact area between the fluid and the wall and u denotes the general fluid flow velocity.

Consequently, the two viscous shear force in Equation (1) and (3) can be computed using

$$F_{\tau s} = \mu A_s \left(\frac{\partial u_{valve}(r)}{\partial r} \right)_{r=r_s}, \; F_{\tau h} = -\mu A_H \left(\frac{\partial u_{valve}(r)}{\partial r} \right)_{r=r_h}, \tag{32}$$

where A_s and A_H are contact area of the shaft surface and housing surface respectively and their value can be computed as $A_s = 2\pi r_s L$ and $A_H = 2\pi r_h L$. Velocity profile $u_{valve}(r)$ is the axial symmetric velocity fields on the cross section of the control volume. The flow field should satisfy the following volumetric flow rate condition

$$\int_0^{2\pi} \int_{r_s}^{r_h} u_{valve}(r) r dr d\phi = Q_2, \tag{33}$$

and the boundary condition at the walls

$$u_{valve}(r)\big|_{r=r_s} = u_{valve}(r)\big|_{r=r_h} = 0. \tag{34}$$

In order to calculate the viscous shear force, the two velocity gradients at $r = r_s$ and $r = r_s$ are required. In Figure 7 the CFD result for steady-state velocity profile of the

annular flow is presented with corresponding Reynolds number shown in Figure 8, which confirms that the flow in the annular tube is characterized as high Reynolds number flow and the flow near the walls is low Reynolds number flow. It can be observed that because the flow between two circular tubes is different from the flow between two flat plates, the velocity profile is not perfectly symmetric about the centerline. The point of maximum velocity is biased to the inner diameter in the current axial symmetric model. Nevertheless, because the inner diameter is about 75% of the outer diameter the deviation is only about 0.025mm. Thus the velocity profile on the cross section can still be approximated using the following parabolic function

$$u_{valve}(r) = K_Q (r - r_s)(r - r_h). \tag{35}$$

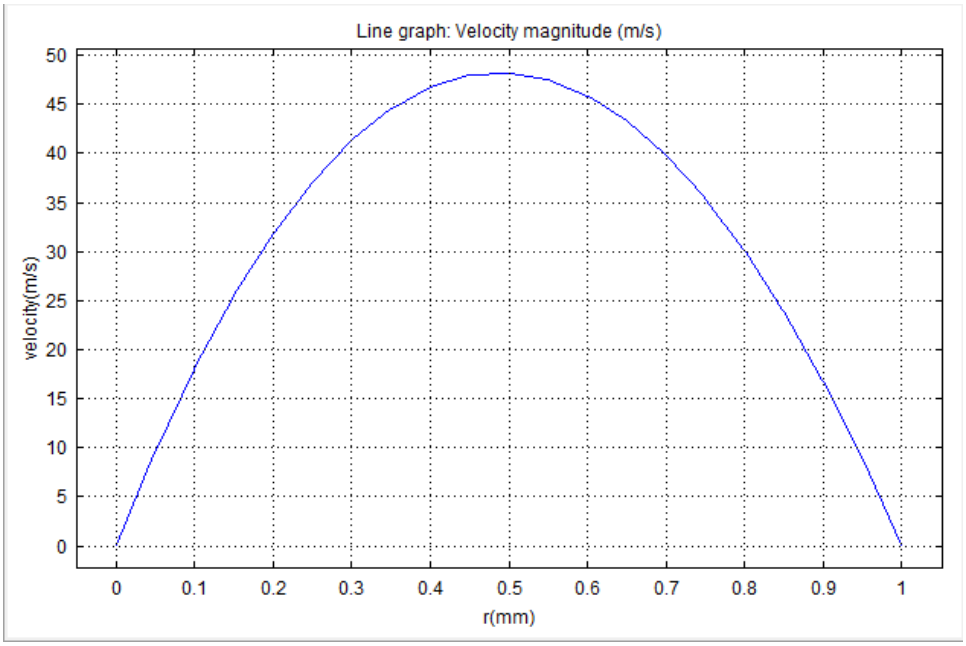

Figure 7 Annular-turbulence-flow-velocity profile: two-dimensional axial symmetric model

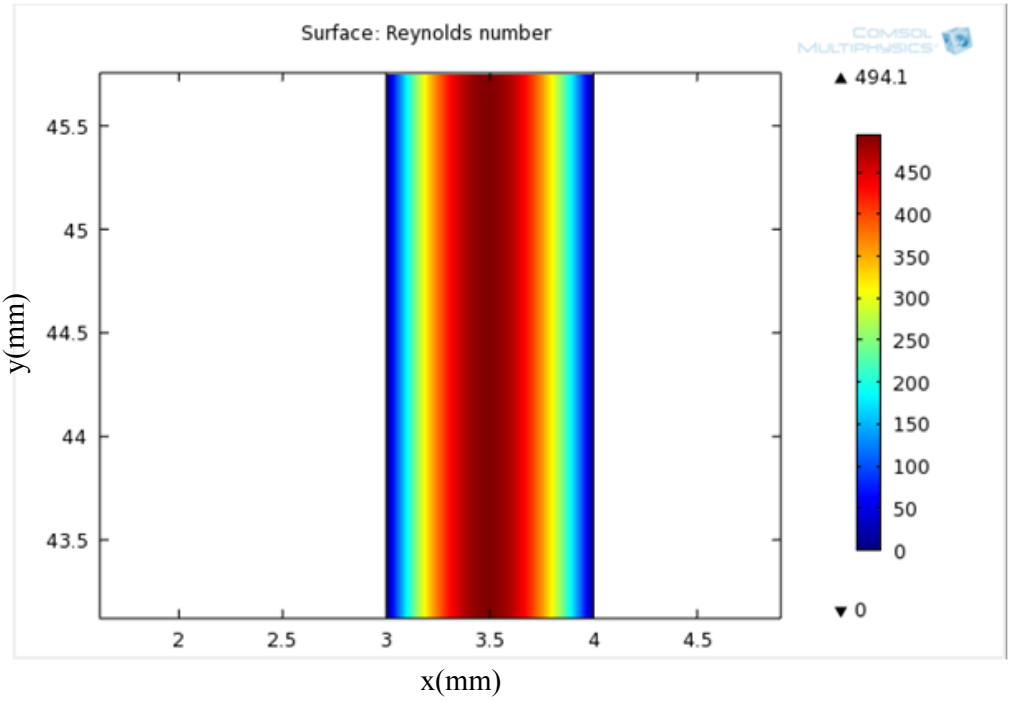

Figure 8 Reynolds number: two-dimensional axial symmetric model

Equation (35) automatically satisfies the boundary condition in Equation (34). To satisfy the volumetric flow rate condition in Equation (33), the coefficient can only be

$$K_Q = \frac{Q_2}{2\pi\left(\frac{1}{12}\left(r_s^4 - r_h^4\right) + \frac{1}{6} r_s r_h \left(r_h^2 - r_s^2\right)\right)}. \tag{36}$$

Corresponding velocity gradients on the contact surface are

$$\left(\frac{\partial u_{valve}(r)}{\partial r}\right)_{r=r_s} = K_Q\left(r_s - r_h\right), \left(\frac{\partial u_{valve}(r)}{\partial r}\right)_{r=r_h} = K_Q\left(r_h - r_s\right) \tag{37}$$

The velocity gradient will change with pressure boundary condition P_1 and P_2. For example, when the supply pressure and return pressure are the same, there is no pressure difference at the two ends of the valve piston chamber. Thus, there is no flow and velocity gradient. When there is pressure difference between the two boundary conditions,

then velocity gradient will be non-zero. Equation (37) can meet this requirement by adjusting K_Q and changing volumetric flow rate Q_2. Substitute Equation (36) and (37) into Equation (32) yields the viscous shear force as the function of the pressure difference

$$\begin{aligned} F_{\tau s} &= -\frac{\mu L r_s \left(r_h - r_s\right) C_{d2} A_2}{\left(\frac{1}{12}\left(r_s^4 - r_h^4\right) + \frac{1}{6} r_s r_h \left(r_h^2 - r_s^2\right)\right)} \sqrt{\frac{2}{\rho}\left(P_1 - P_2\right)}, \\ F_{\tau h} &= -\frac{\mu L r_h \left(r_h - r_s\right) C_{d2} A_2}{\left(\frac{1}{12}\left(r_s^4 - r_h^4\right) + \frac{1}{6} r_s r_h \left(r_h^2 - r_s^2\right)\right)} \sqrt{\frac{2}{\rho}\left(P_1 - P_2\right)}. \end{aligned} \tag{38}$$

Equation (38) shows that the steady viscous shear force can be influenced by fluid viscosity μ, pressure gradient, and valve geometry parameters such as damping length L, inner radius r_s and outer radius r_h. Substitute Equation (25) into Equation (38) yields the viscous shear force as the function of supply pressure, return pressure fluid properties and geometry parameters

$$\begin{aligned} F_{\tau s} &= -\frac{\mu L r_s \left(r_h - r_s\right) C_{d2} A_2}{\left(\frac{1}{12}\left(r_s^4 - r_h^4\right) + \frac{1}{6} r_s r_r \left(r_h^2 - r_s^2\right)\right)} \sqrt{\frac{2}{\rho} C_{fxp}\left(P_s - P_r\right)}, \\ F_{\tau h} &= -\frac{\mu L r_h \left(r_h - r_s\right) C_{d2} A_2}{\left(\frac{1}{12}\left(r_s^4 - r_h^4\right) + \frac{1}{6} r_s r_r \left(r_h^2 - r_s^2\right)\right)} \sqrt{\frac{2}{\rho} C_{fxp}\left(P_s - P_r\right)}. \end{aligned} \tag{39}$$

Some characteristics concerning Equation (39) should be emphasized. First, because Equation (39) is developed based on Equation (27), which is a steady state result, there is no pressure transient effect in this expression. Second, the coefficient C_{fxp} can be varied by the valve piston displacement as shown in Figure 6. Consequently, the viscous shear force in Equation (39) is also changing with valve displacement. When the metering orifice is fully open, the viscous shear force will be large. When the metering

orifice is completely closed, the viscous shear force will be zero, because no fluid flow exists. Third, the parabolic velocity profile function in Equation (35) can be a good approximation in steady flow, but its validity is not assured in transient flow. Besides, the real shear force between the fluid and the surface strongly depends on surface roughness. An uneven surface will induce extra drag besides the estimated value in Equation (39). The above characteristics make the application of Equation (39) restricted to steady state viscous shear force.

2.5 Momentum Force

This section is devoted to the theoretical solution of the momentum force in Equation (2). This momentum force is considered as the major contribution in classic flow force theory. From Reynolds transport theorem, the fluid momentum force is given by

$$\mathbf{F}_m = \frac{\partial}{\partial t}\int_{c.v.} \rho \mathbf{u} dv + \int_{c.s.} \rho \mathbf{u}(\mathbf{u}\cdot\mathbf{n}) dA \tag{40}$$

where $\mathbf{F}_m$ is the vector momentum force acting on the control volume, ρ is the fluid density $\mathbf{u}$ is the fluid velocity vector, and $\mathbf{n}$ is a unit vector that points normally outward from the control volume surface. The first term with derivative with respect to time is called transient term induced by inertial of the fluid. The second term, which describes the momentum flux across the control surface, is called the steady term. The fluid momentum force acting on the control volume may be written in

$$\mathbf{F}_m = F_{xm}\mathbf{i} + F_{ym}\mathbf{j}, \tag{41}$$

where F_{xm} and F_{ym} are the x component and y component of the fluid momentum force respectively. The flow force F_{ym} in y direction is balanced by the valve housing, and the flow force F_{xm} is in the direction that needs to be countered by force F as shown in Equation (3).

The transient momentum force is caused by the fluid velocity change within the valve piston chamber. Assuming that the clearance between the piston outer diameter and the piston bore only influence the fluid flow in an averaging way described by Equation (33) and the fluid in the valve piston chamber is moving as one chunk of fluid. Then the transient momentum force can be represented in the following from

$$F_{xmt} = \frac{\partial}{\partial t}\int_{c.v.} \rho u_{valve} dv = \frac{\partial}{\partial t}\int_0^L \int_0^{2\pi} \int_{r_s}^{r_h} \rho u_{valve}(r) r dr d\phi dx = \rho L \frac{\partial Q_2}{\partial t}. \tag{42}$$

The fluid momentum in and out from the control volume causes the steady momentum force. There are two categories of fluid flow in and out related to this control volume. The first category is through the leakage passage which is in the x direction, and the second category is the orifice flow Q_1 and Q_2 which are related to jet angles θ_1 and θ_2. In classic theory, those jet angles are treated as constants, but this assumption is not necessarily to be true. For the flow force generated by the leakage flow through the right-hand leakage passage, the induced flow force can be computed using

$$\begin{aligned} &\mathbf{u}_{L1} = \frac{Q_{L1}}{A_{L1}}\mathbf{i}, \mathbf{n}_{L1} = \mathbf{i} \\ &F_{xmL1} = \int_{c.s.} \rho \mathbf{u}_{L1}(\mathbf{u}_{L1} \cdot \mathbf{n}_{L1}) dA = \rho \frac{Q_{L1}^2}{A_{L1}}, \end{aligned} \tag{43}$$

where A_{L1} is the cross-sectional area of the leakage passage on the right-hand side and $\mathbf{n}_{L1}$ is the outer normal vector on the control volume. Similarly, for the left-hand leakage, the induced flow force can be computed using

$$\begin{aligned} &\mathbf{u}_{L2} = -\frac{Q_{L2}}{A_{L2}}\mathbf{i}, \mathbf{n}_{L2} = -\mathbf{i} \\ &F_{xmL2} = \int_{c.s.} \rho \mathbf{u}_{L2}\left(\mathbf{u}_{L2}\cdot\mathbf{n}_{L2}\right)dA = -\rho\frac{Q_{L2}^2}{A_{L2}} \end{aligned} \tag{44}$$

where $A_{L2} = A_{L1}$ for a symmetric spool valve. If the leakage on the right-hand equals the leakage on the left-hand, the two leakage-induced flow forces should cancel exactly. If they are not equal then certain net flow force can be contributed by the leakage flow.

The concept of jet angle is used to define the flow force induced by supply flow Q_1 and return flow Q_3. For the supply flow on the right-hand side, the induced momentum flow force can be computed using

$$\begin{aligned} &\mathbf{u}_1 = \frac{Q_1\cos(\theta_1)}{A_1}\mathbf{i} + \frac{Q_1\sin(\theta_1)}{A_1}\mathbf{j}, \mathbf{n}_1 = \mathbf{j} \\ &\mathbf{F}_{ms} = \int_{c.s.} \rho \mathbf{u}_1\left(\mathbf{u}_1\cdot\mathbf{n}_1\right)dA = \frac{\rho Q_1^2}{A_1}\left(\sin(\theta_1)\cos(\theta_1)\mathbf{i} + \sin^2(\theta_1)\mathbf{j}\right). \end{aligned} \tag{45}$$

where A_1 is the supply orifice cross-sectional area. Similarly, for the return flow on the left-hand side, the induced momentum flow force can be computed using

$$\begin{aligned} &\mathbf{u}_2 = \frac{Q_3\cos(\theta_2)}{A_3}\mathbf{i} + \frac{Q_3\sin(\theta_2)}{A_3}\mathbf{j}, \mathbf{n}_2 = \mathbf{j} \\ &\mathbf{F}_{mr} = \int_{c.s.} \rho \mathbf{u}_2\left(\mathbf{u}_2\cdot\mathbf{n}_2\right)dA = \frac{\rho Q_3^2}{A_3}\left(\sin(\theta_2)\cos(\theta_2)\mathbf{i} + \sin^2(\theta_2)\mathbf{j}\right). \end{aligned} \tag{46}$$

where A_3 is the return orifice cross-sectional area. It should be emphasized that the outer normal selection for both supply flow and return flow are the same. This analysis is different from conventional control volume analysis, which assumes that the control volume boundary is perpendicular to the flow direction. If the supply jet angle θ_1 and return jet angle θ_2 satisfy $\theta_2 = -\theta_1$, then $\sin(\theta_1)\cos(\theta_1) + \sin(\theta_2)\cos(\theta_2) = 0$. If there is no leakage $Q_1 = Q_3$. If all the above conditions are satisfied, then supply flow and return flow generated momentum flow force will cancel each other in the x direction. And there is no flow force caused by momentum flux through the supply orifice and return orifice. Substitute Equation for steady and transient flow forces in x direction into Equation (3) yields

$$F = \left(F_{xmL1} + F_{xmL2} + F_{xms} + F_{xmr} + F_{xmt}\right) - F_{rh} + f. \tag{47}$$

2.6 Summary of Analysis

In this section, the total flow force is described generally in two ways:

$$\begin{aligned} F &= -A_v\left(P_1 - P_2\right) + \frac{\mu L r_s \left(r_h - r_s\right) Q_2}{\left(\frac{1}{12}\left(r_s^4 - r_h^4\right) + \frac{1}{6} r_s r_h \left(r_h^2 - r_s^2\right)\right)} + f, \ or \\ F &= \left(\rho \frac{Q_{L1}^2}{A_{L1}} - \rho \frac{Q_{L2}^2}{A_{L2}} + \frac{\rho Q_1^2}{A_1}\sin(\theta_1)\cos(\theta_1) + \frac{\rho Q_3^2}{A_3}\sin(\theta_2)\cos(\theta_2) + \rho L \frac{\partial Q_2}{\partial t} \right) \\ &- \frac{\mu L r_h \left(r_h - r_s\right) Q_2}{\left(\frac{1}{12}\left(r_s^4 - r_h^4\right) + \frac{1}{6} r_s r_h \left(r_h^2 - r_s^2\right)\right)} + f. \end{aligned} \tag{48}$$

The first way is through the equilibrium condition of the valve piston; the second way is the through equilibrium condition of the fluid in the control volume. In the first description, only pressure difference term and viscous shear term acting on the valve

piston shaft exist in the description of the total flow force. The pressure transient effect caused by fluid compressibility is implicitly included by the pressure rise rate equations. To see the pressure transient effect, it is necessary to subtract the steady state pressure difference term in Equation (26) and viscous shear term in Equation (39) from the measured flow force. In the second description, the total flow force is decomposed into momentum force term and viscous shear term acting on the valve housing. The pressure transient effect caused by fluid inertial is explicitly shown as one component of the momentum induced flow force. To see the pressure transient effect, it is necessary to subtract the steady momentum flow force term and steady viscous shear from the measured flow force. Therefore, the analysis shows that whether the pressure transient effect can be isolated from the total flow force depends on the precision of the estimated steady forces.

There are several uncertainties concerning the analytical steady component of flow forces. First, the discharge coefficients can be uncertain, but their value can be estimated by measuring volumetric flow rates and pressure drops. Second, the viscous shear force can be uncertain, because the velocity profile function might not be a good estimator with the existing surface roughness. The error in viscous shear force can be reduced by better surface finish. In addition, it is very difficult to identify the velocity profile in transient flow. Third, the jet angles are uncertain and it is nearly impossible to measure them directly in experiment. At last, the frictional force f is not analyzed in this chapter, it will be treated in the experiment.

It can also be observed that in Equation (48) the description in valve piston equilibrium condition is not equivalent to the description in the equilibrium condition for

the fluid in the control volume in transient state, because they include different pressure transient effect. The first description only includes pressure transient effect caused by fluid compressibility, while the second description only include fluid inertial transient. The two types of transient effects can both exist. The two models are essentially not capable of including the both transient effect, but they must be equivalent in steady state. Otherwise, the equilibrium conditions in steady state will be violated.

Chapter 3: Modeling of Flow Forces

To understand the relative importance of all the terms in Equation (48) of Chapter 2 better, nondimensionalization is conducted in the current chapter. Both piston equilibrium and control volume equilibrium case are investigated.

3.1 Nondimensionalization of the Valve Orifice Opening

Select one-half of the orifice opening area as the scaling factor

$$A_i = A_o \hat{A}_i = \frac{\pi d^2}{8} \hat{A}_i, \quad x = \frac{d}{2} \hat{x}, \tag{49}$$

then the nondimensional partial blocked orifice opening described in Figure 5 can be represented as

$$\hat{A}_3 = 1 - \frac{2}{\pi} \hat{x} \sqrt{1 - \hat{x}^2} - \frac{2}{\pi} \arcsin(\hat{x}). \tag{50}$$

Using all the nondimensional areas $\hat{A}_i$ to replace all the dimensional areas in Equation (27) and (29), the pressure drop coefficients can be represented in a nondimensional way:

$$\begin{aligned}
C_{fxp} &= \frac{\left(C_{d1}\hat{A}_1\right)^2 \left(C_{d3}\hat{A}_3\right)^2 K_L^2}{\left(C_{d2}\hat{A}_2\right)^2 \left(C_{d3}\hat{A}_3\right)^2 + \left(C_{d1}\hat{A}_1\right)^2 \left(C_{d2}\hat{A}_2\right)^2 K_L^4 + \left(C_{d1}\hat{A}_1\right)^2 \left(C_{d3}\hat{A}_3\right)^2 K_L^2}, \\
C_{fxms} &= \frac{\left(C_{d2}\hat{A}_2\right)^2 \left(C_{d3}\hat{A}_3\right)^2}{\left(C_{d2}\hat{A}_2\right)^2 \left(C_{d3}\hat{A}_3\right)^2 + \left(C_{d1}\hat{A}_1\right)^2 \left(C_{d2}\hat{A}_2\right)^2 K_L^4 + \left(C_{d1}\hat{A}_1\right)^2 \left(C_{d3}\hat{A}_3\right)^2 K_L^2}, \\
C_{fxmr} &= \frac{\left(C_{d1}\hat{A}_1\right)^2 \left(C_{d2}\hat{A}_2\right)^2 K_L^4}{\left(C_{d2}\hat{A}_2\right)^2 \left(C_{d3}\hat{A}_3\right)^2 + \left(C_{d1}\hat{A}_1\right)^2 \left(C_{d2}\hat{A}_2\right)^2 K_L^4 + \left(C_{d1}\hat{A}_1\right)^2 \left(C_{d3}\hat{A}_3\right)^2 K_L^2}.
\end{aligned} \tag{51}$$

The relation between orifice displacement and orifice area corresponds to the partially blocked circular orifice area defined in Equation (50) is given by the blue curve in Figure 9. In the analysis of the previous works, the circular orifice is approximately by a rectangular area with constant area gradient, which is shown as the green line in Figure 9. This equivalent rectangular area has the same area as the circular area, when the valve is fully open. Therefore the rectangular area approximation can be described as the function of the valve displacement

$$A_{rec} = \frac{\pi d^2}{8} + \frac{\pi d}{4} x, \tag{52}$$

with corresponding nondimensionalized version

$$\hat{A}_{rec} = 1 - \hat{x}. \tag{53}$$

The comparison between the circular area and the rectangular area shows that they equal each other only at three points: the point with fully opened orifice, the point with half opened orifice and the point with completely closed orifice. The maximum error is about 5%. If the rectangular area is used, then additional uncertainty should be considered in the flow force model. To minimize the difference between the analytical solution and the measurement, it is obvious that the partial blocked circular orifice area is preferred.

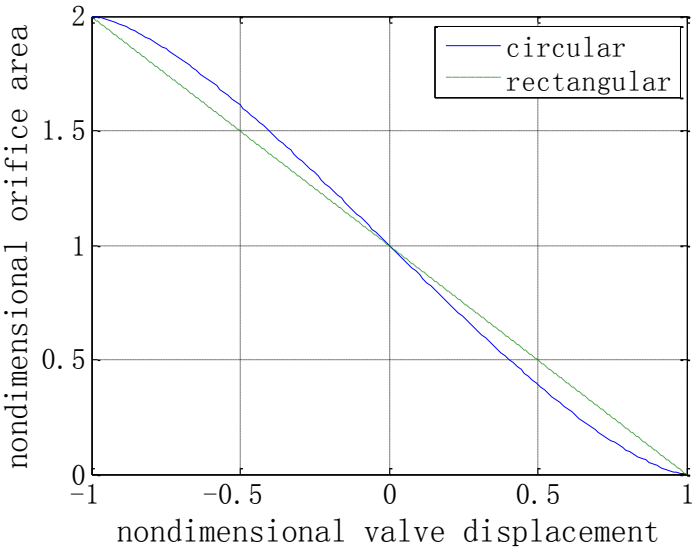

Figure 9 Valve displacement vs orifice area

3.2 Nondimensionalization of the Equations for Piston Equilibrium

Select the following scaling factors for pressure, time and force

$$P_i = \frac{P_{s0}}{2}\hat{P}_i, \quad t = \tau\hat{t}, \quad F = \left|C_{d3}^2 A_o P_{s0}\sin(\theta_2)\cos(\theta_2)\right|\cdot\hat{F}, \tag{54}$$

where P_{s0} is the nominal supply pressure and τ is the characteristic time. The scaling factor for force is selected to be related to the momentum flow force for the return orifice. Equation (19) and corresponding flow force exclude friction force f become

$$\begin{aligned}
\hat{\lambda}_1\frac{d\hat{P}_1}{d\hat{t}} &= K_L\hat{\lambda}_2\sqrt{\hat{P}_s-\hat{P}_1}-\sqrt{\hat{P}_1-\hat{P}_2},\\
\hat{\lambda}_1\frac{d\hat{P}_2}{d\hat{t}} &= K_L\sqrt{\hat{P}_1-\hat{P}_2}-\hat{\lambda}_3\hat{A}_3\sqrt{\hat{P}_2-\hat{P}_r},\\
\hat{F} &= -\hat{\lambda}_4\left(\hat{P}_1-\hat{P}_2\right)+\hat{\lambda}_5\sqrt{\hat{P}_1-\hat{P}_2}\\
&= -\hat{\lambda}_4 C_{fxp}\left(\hat{P}_s-\hat{P}_r\right)+\hat{\lambda}_5\sqrt{C_{fxp}\left(\hat{P}_s-\hat{P}_r\right)},
\end{aligned} \tag{55}$$

where the lambda nondimensional groups are

$$\hat{\lambda}_1 = \frac{V_1}{\beta}\frac{\sqrt{P_{s0}\rho}}{2C_{d2}A_2\tau} = \frac{L\sqrt{P_{s0}\rho}}{4\beta C_{d2}\tau},\ \hat{\lambda}_2 = \frac{C_{d1}A_1}{C_{d2}A_2},\ \hat{\lambda}_3 = \frac{C_{d3}A_o}{C_{d2}A_2},$$
$$\hat{\lambda}_4 = \frac{A_v}{2C_{d3}^2 A_o\left|\sin(\theta_2)\cos(\theta_2)\right|} \tag{56}$$
$$\hat{\lambda}_5 = -\frac{\mu L r_s\left(r_h - r_s\right)C_{d2}A_2}{\left(\frac{1}{12}\left(r_s^4 - r_h^4\right) + \frac{1}{6}r_s r_r\left(r_h^2 - r_s^2\right)\right)}\frac{1}{\sqrt{\rho P_{s0}}}\frac{1}{C_{d3}^2 A_o\left|\sin(\theta_2)\cos(\theta_2)\right|}.$$

From Equation (56), it can be observed that in order to make the pressure transient term in the pressure rise rate equation larger, nondimensional parameter group $\hat{\lambda}_1$ must be large. Despite fluid bulk modulus β and fluid density ρ which are not a parameter that can be designed in the following experiment, the damping length L and nominal supply pressure P_{s0} can be enlarged to make the pressure transient effect caused by compressibility easier to be observed. With characteristic time τ selected to make $\hat{\lambda}_1 = 0.01$ and the value of jet angle θ_2 that will be addressed in later sections, the values of the lambda family nondimensional parameters computed from certain parameters are given in Table 3. Except $\hat{\lambda}_1$ all the other nondimensional groups are not dependent on the selection of characteristic time τ, and all their values are above unity. Therefore, they are all important. The comparison between nondimensional groups $\hat{\lambda}_4$ and $\hat{\lambda}_5$ shows that the viscous shear force on the piston rod is about 11.3% of the pressure difference caused force. Therefore, the flow force is mainly caused by the pressure difference in current case of piston equilibrium condition.

Table 3 Lambda family nondimensional groups values $\tau = 1.5ms$

$\hat{\lambda}_1$	$\hat{\lambda}_2$	$\hat{\lambda}_3$	$\hat{\lambda}_4$	$\hat{\lambda}_5$
0.01	2.3241	0.9480	47.4048	5.3370

3.3 Nondimensionalization of the Equations for Fluid Control Volume Equilibrium

In order to nondimensionalize the force generated by fluid control-volume equilibrium condition, the amount of the leakage flow on both ends is required. From the trial experiment, the Reynolds number is about 1.95, which is not far from the CFD results in Figure 10.

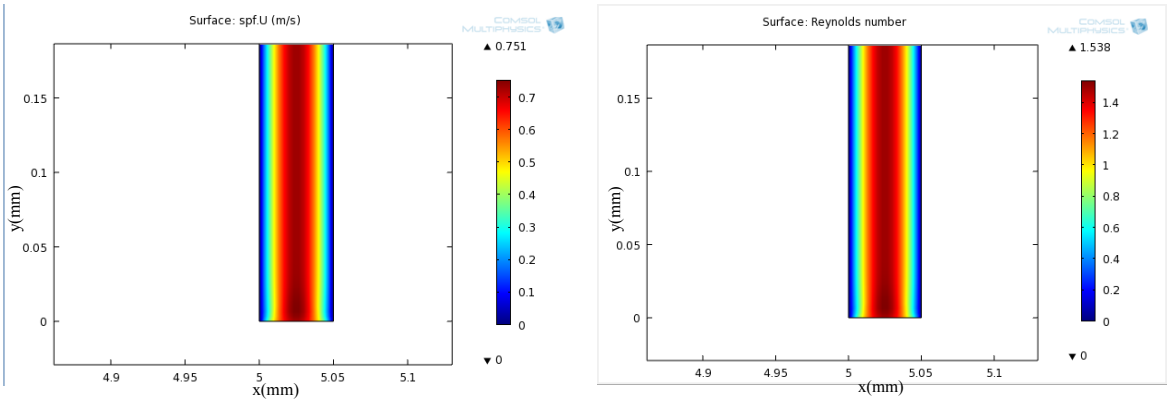

Figure 10 Velocity and Reynolds number in the leakage passage: axial symmetric model

However, for the fluid flow with Reynolds number around 2, no equation is proved to be valid in predicting the volumetric flow rate. The fluid flow can be characterized neither as high Reynolds number flow, nor low-Reynolds number flow. Therefore, trial experiment data is employed. From the measured leakage flow in the trial experiment, the estimated momentum force caused by leakage is in the order of $10^{-3} N$, but the measured total flow force is more than 30N. Therefore, the leakage caused momentum force can be neglected and the flow force becomes:

$$\begin{aligned}\hat{F} &= \hat{\gamma}_1 \frac{\partial\left(\sqrt{\hat{P}_1-\hat{P}_2}\right)}{\partial\hat{t}} + \hat{\gamma}_2\left(\hat{P}_s-\hat{P}_1\right) + \hat{\gamma}_3\hat{A}_3\left(\hat{P}_2-\hat{P}_r\right) - \hat{\gamma}_4\sqrt{\hat{P}_1-\hat{P}_2} \\ &= \frac{\hat{\gamma}_1}{2\sqrt{\hat{P}_1-\hat{P}_2}}\frac{\partial\left(\hat{P}_1-\hat{P}_2\right)}{\partial\hat{t}} + \hat{\gamma}_2\left(\hat{P}_s-\hat{P}_1\right) + \hat{\gamma}_3\hat{A}_3\left(\hat{P}_2-\hat{P}_r\right) - \hat{\gamma}_4\sqrt{\hat{P}_1-\hat{P}_2} \\ &= \frac{\hat{\gamma}_1\sqrt{C_{fxp}}}{2\sqrt{\hat{P}_s-\hat{P}_r}}\frac{\partial\left(\hat{P}_s-\hat{P}_r\right)}{\partial\hat{t}} + \hat{\gamma}_2 C_{fxms}\left(\hat{P}_s-\hat{P}_r\right) + \hat{\gamma}_3\hat{A}_3 C_{fxmr}\left(\hat{P}_s-\hat{P}_r\right) - \hat{\gamma}_4\sqrt{C_{fxp}}\sqrt{\hat{P}_s-\hat{P}_r}\end{aligned} \tag{57}$$

where the gamma family nondimensional group are

$$\begin{aligned}&\hat{\gamma}_1 = \frac{LC_{d2}A_2\sqrt{\rho}}{\tau C_{d3}^2 A_o\sqrt{P_{s0}}\left|\sin(\theta_2)\cos(\theta_2)\right|}, \quad \hat{\gamma}_2 = \frac{C_{d1}^2 A_1\sin(\theta_1)\cos(\theta_1)}{C_{d3}^2 A_o\left|\sin(\theta_2)\cos(\theta_2)\right|}, \\ &\hat{\gamma}_3 = \frac{\sin(\theta_2)\cos(\theta_2)}{\left|\sin(\theta_2)\cos(\theta_2)\right|} = \operatorname{sign}\left(\sin(\theta_2)\cos(\theta_2)\right), \\ &\hat{\gamma}_4 = -\frac{\mu L r_h\left(r_h-r_s\right)C_{d2}A_2}{\left(\frac{1}{12}\left(r_s^4-r_h^4\right)+\frac{1}{6}r_s r_r\left(r_h^2-r_s^2\right)\right)}\frac{1}{\sqrt{\rho P_{s0}}}\frac{1}{C_{d3}^2 A_o\left|\sin(\theta_2)\cos(\theta_2)\right|}.\end{aligned} \tag{58}$$

From Equation (58) it can be known that increasing damping length L and decreasing nominal supply pressure P_{s0} can increase the size of the pressure transient effect caused by the inertial of fluid by influence on nondimensional group $\hat{\gamma}_1$. This conclusion agrees with the conclusion from the valve-piston equilibrium condition on damping length L, but differs on the conclusion related to nominal supply pressure P_{s0}. This reason for this difference is the pressure transient effect in valve-piston equilibrium condition is caused by fluid compressibility, while the pressure transient effect in equilibrium condition for the fluid in the control volume is caused by fluid inertial. Increasing damping length L and decreasing nominal supply pressure P_{s0} will change the other terms too. Decreasing nominal supply pressure P_{s0} will cause the viscous shear force on the valve housing to increase. In addition, increasing L will make the pressure transient

term increases along with the viscous shear term. It can be inferred from this discussion that the pressure transient term and the viscous shear term are strongly related by valve chamber length L and nominal supply pressure P_{s0}. Thus, it is difficult to isolate one of them from the other.

In order to compute the value of the gamma family nondimensional groups, knowledge about supply jet angle θ_1 and return jet angle θ_2 is required. Since it is impossible to measure the jet angles directly in experiment with non-transparent metal valve housing, CFD analysis is employed here again to gain conceptual knowledge about jet angles. Different from the flow in the annular tube, which can be simplified to a two-dimensional axial symmetric problem, the flow from the supply orifice to the valve chamber and from the valve chamber to the return orifice is a three-dimensional problem. To reduce the computational effort, the three-dimensional flow problem into a two-dimensional flow problem similar to the flow in the elbow, it is required to know the proper equivalent diameter of the valve chamber. There are two possible choices of equivalent diameter. One is the hydraulic diameter defined in Chapter 2, the other is the diameter which makes the area equal to the annular area. Taking the algebraic mean of the two diameters, a diameter of 3.65mm is used. The computed two-dimensional results are given in Figure 11. The figure on the left shows that the inlet jet angle θ_1 is not -90 deg. Therefore the momentum through supply orifice will cause some flow force. This is completely difference from the classical theory, which uses the -90 deg as the default jet angle for the supply orifice. The value of the half-open return orifice jet angle θ_2 is about 113.9 deg, which is fairly close to the classic value 111deg[52]. However, the jet angle θ_2 for the return orifice will change with different valve displacement. When only one third

of the return orifice is open, the jet angle θ_2 is reduced to 106.05deg. When only one sixth of the return orifice is open, the jet angle θ_2 is reduced to 112.4deg. In addition, the streamline shows that it becomes much more difficult for the flow in the upper stream to influence of the fluid flow in the downstream, because the existence of a vortex. Although the computational results are useful to illustrate valve displacement's influence on jet angle, it is very difficult to make a conclusion on the mechanism of the influence of orifice opening on the jet angle.

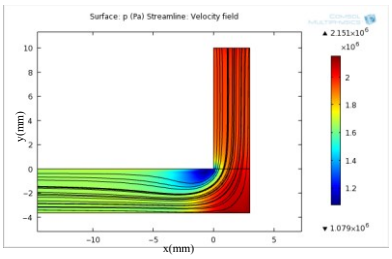

a) Supply orifice $\theta_1 = -102.7\,\text{deg}$

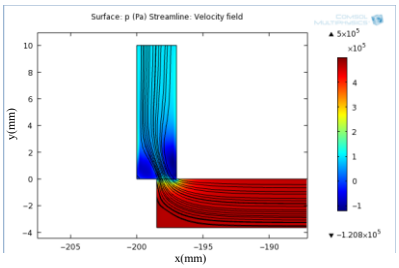

b) Return orifice ½ open $\theta_2 = 113.9\,\text{deg}$

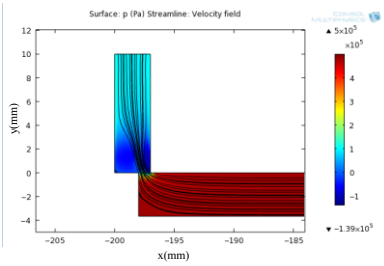

c) Return orifice 1/3 open $\theta_2 = 106.05\,\text{deg}$

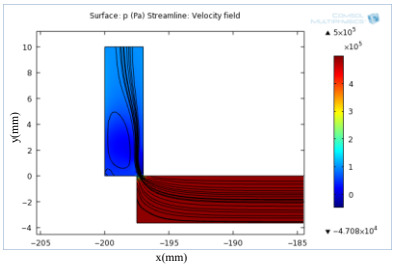

d) Return orifice 1/6 open $\theta_2 = 112.4\,\text{deg}$

Box is intentionally void

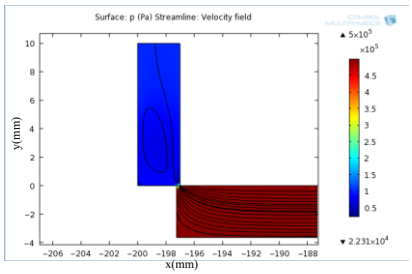

e) Return orifice 1/12 open

Figure 11 Inlet and outlet jet angles influence by orifice opening

The pressure drop will also change the jet angles. The CFD results with lower upper stream pressure are presented in Figure 12. Compared with the results in Figure 11, lower upper stream pressure will cause the jet angle to decrease, but the amount will be small. Similar to the influence of the orifice opening on the jet angle, the influence of the upper stream pressure is also ambiguous in the CFD analysis. Although it is certain that the upper stream pressure will change the jet angle, it is extremely difficult to estimate the value of jet angle accurately. Therefore, it is recommended to obtain the range of the jet angle based on the CFD analysis. Based on the observation, jet angle θ_1 falls between $[100,\ 110]$ deg, while θ_2 falls between $[105,\ 115]$ deg. The CFD analysis also shows that as the supply pressure and the orifice opening changes, the jet angle should be a time-varying variable instead of a constant. Fortunately, the definition of time-varying jet angle does not change the analysis and derivation in Chapter 2 and Chapter 3. Thus, all the results will still be valid and can be used in the following sections.

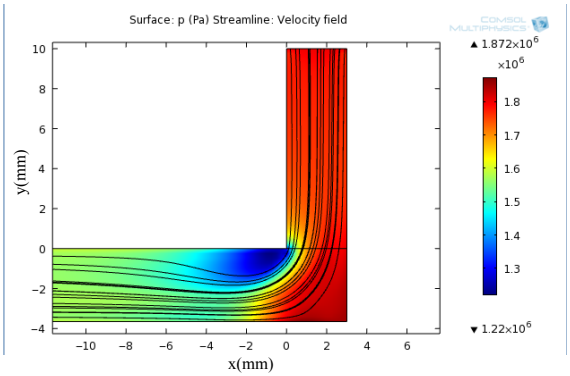

a) Supply orifice $\theta_1 = -107.4\,\text{deg}$

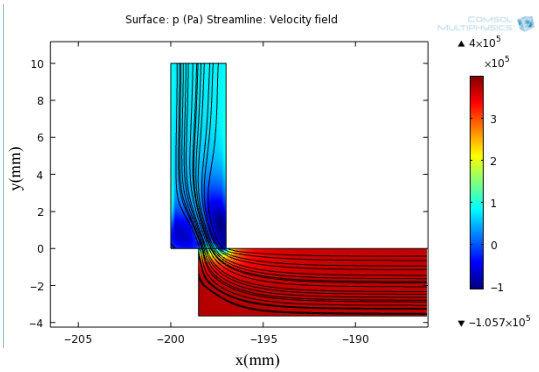

b) Return orifice ½ open $\theta_2 = 112.04\,\text{deg}$

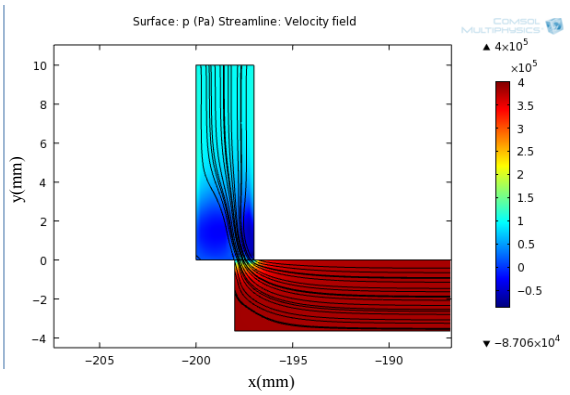

c) Return orifice 1/3 open $\theta_2 = 105.95\,\text{deg}$

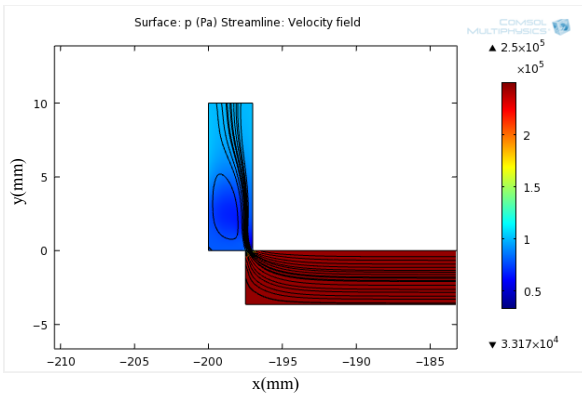

d) Return orifice 1/6 open $\theta_2 = 111.8\,\text{deg}$

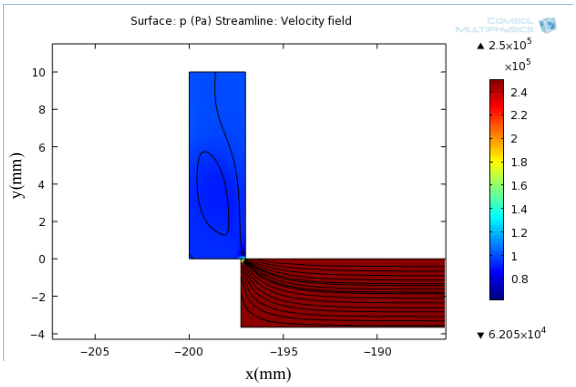

e) Return orifice 1/12 open

Box is intentionally void

Figure 12 Inlet and outlet jet angles influence by orifice opening with lower upper stream pressure

Based on the estimation of jet angles, the gamma family nondimensional group is given in Table 4. All the gamma family nondimensional groups are larger than unity, but because the sign of nondimensional group $\hat{\gamma}_2$ and $\hat{\gamma}_3$ are reversed, the steady state flow

force induced by the momentum into and out of the valve piston chamber will counter each other and the net contribution will be about 0.77, which is smaller than the magnitude of the value of $\hat{\gamma}_2$ and $\hat{\gamma}_3$. The nondimensional group $\hat{\gamma}_4$, which is related to viscous shear force on the valve housing is larger than $\hat{\lambda}_5$ defined in piston equilibrium condition because, the contact area is larger. The largest nondimensional group is $\hat{\gamma}_1$, which represents the contribution of the pressure transient effect. The value of $\hat{\gamma}_1$ is about 17 times of the value $\hat{\gamma}_2 + \hat{\gamma}_3$. Therefore, the transient momentum force is much more important than the steady momentum force.

Table 4 Gamma family nondimensional groups values $\tau = 1.5ms$

$\hat{\gamma}_1$	$\hat{\gamma}_2$	$\hat{\gamma}_3$	$\hat{\gamma}_4$
12.5177	1.7400	-1	6.9993

Nevertheless, Table 4 cannot reveal the true contribution of both steady momentum force concerning the metering orifice $\hat{A}_3$ and the pressure transient term concerning the selection of characteristic time τ. Because the valve displacement changes the pressure drop, it is necessary to consider the influence of gamma family nondimensional group $\hat{\gamma}_2$, the metering orifice area $\hat{A}_3$ and the pressure drop coefficients in Figure 6 all together to reveal the true contribution of the steady state momentum term of the metering orifice. The product of $\hat{\gamma}_2 \hat{A}_3 C_{fxmr}$ is shown in Figure 13. In this picture, the flow force will be zero when the valve is completely closed, but the maximum value of $\hat{\gamma}_2 \hat{A}_3 C_{fxmr}$ does not exist when the valve is fully open. The maximum steady state flow force exists near the point of half open. The reason for this is the nonlinear coupling

between orifice opening and pressure drop. This characteristic cannot be revealed by conventional linearized model, because in the conventional linearized model it is assumed that the valve displacement will not change the pressure drop across the metering orifice. However, this situation might not be true in real application.

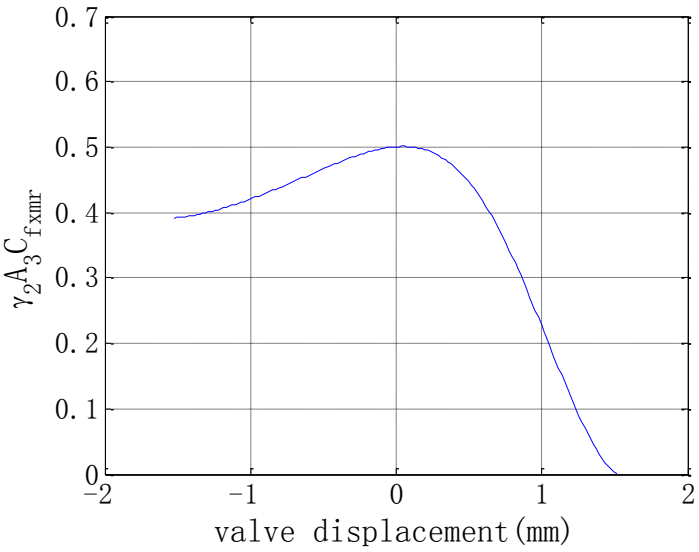

Figure 13 Contribution of return orifice on the steady state flow force

Because the size of nondimensional group $\hat{\gamma}_1$ which indicates the contribution of the transient momentum force term depends on the selection of characteristic time τ, it becomes necessary to see the influence of characteristic time on $\hat{\gamma}_1$ in Figure 14. When the state of the system changes faster or the characteristic time τ is smaller, the contribution of the pressure transient will be larger. Even when the characteristic time of the system is as slow as 10ms, the contribution of the transient momentum force term is still larger than the contribution of the steady state momentum force term.

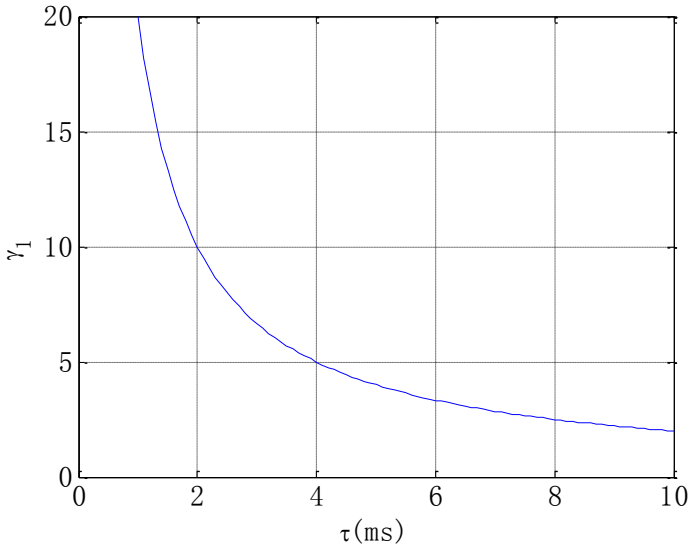

Figure 14 Characteristic time vs $\hat{\gamma}_1$

3.4 Sensitivity to Uncertainties

The discharge coefficients, jet angles and supply pressure are three major sources of uncertainty for the model of the flow force on the two-way spool valve. The following expression may be written to describe the change in lambda family nondimensional groups for small perturbations of these uncertain parameters

$$
\begin{aligned}
\frac{\delta\hat{\lambda}_1}{\hat{\lambda}_1} &= S_{P_{s0}}^{\hat{\lambda}_1}\frac{\delta P_{s0}}{P_{s0}} + S_{Cd2}^{\hat{\lambda}_1}\frac{\delta C_{d2}}{C_{d2}},\\
\frac{\delta\hat{\lambda}_2}{\hat{\lambda}_2} &= S_{Cd1}^{\hat{\lambda}_2}\frac{\delta C_{d1}}{C_{d1}} + S_{Cd2}^{\hat{\lambda}_1}\frac{\delta C_{d2}}{C_{d2}},\\
\frac{\delta\hat{\lambda}_3}{\hat{\lambda}_3} &= S_{Cd2}^{\hat{\lambda}_3}\frac{\delta C_{d2}}{C_{d2}} + S_{Cd3}^{\hat{\lambda}_3}\frac{\delta C_{d3}}{C_{d3}},\\
\frac{\delta\hat{\lambda}_4}{\hat{\lambda}_4} &= S_{Cd3}^{\hat{\lambda}_4}\frac{\delta C_{d3}}{C_{d3}} + S_{\theta_2}^{\hat{\lambda}_4}\frac{\delta\theta_2}{\theta_2},\\
\frac{\delta\hat{\lambda}_5}{\hat{\lambda}_5} &= S_{Cd2}^{\hat{\lambda}_5}\frac{\delta C_{d2}}{C_{d2}} + S_{P_{s0}}^{\hat{\lambda}_5}\frac{\delta P_{s0}}{P_{s0}} + S_{Cd2}^{\hat{\lambda}_5}\frac{\delta C_{d3}}{C_{d3}} + S_{\theta_2}^{\hat{\lambda}_5}\frac{\delta\theta_2}{\theta_2},
\end{aligned}
\tag{59}
$$

where the delta sign indicates small perturbations and the sensitivity coefficients are given by

$$
\begin{aligned}
&S_{P_{s0}}^{\hat{\lambda}_1} = \frac{P_{s0}}{\hat{\lambda}_1}\frac{\partial \hat{\lambda}_1}{\partial P_{s0}} = \frac{1}{2}, \quad S_{Cd2}^{\hat{\lambda}_1} = \frac{C_{d2}}{\hat{\lambda}_1}\frac{\partial \hat{\lambda}_1}{\partial C_{d2}} = -1, \\
&S_{Cd1}^{\hat{\lambda}_2} = \frac{C_{d1}}{\hat{\lambda}_2}\frac{\partial \hat{\lambda}_2}{\partial C_{d1}} = 1, \quad S_{Cd2}^{\hat{\lambda}_2} = \frac{C_{d2}}{\hat{\lambda}_2}\frac{\partial \hat{\lambda}_2}{\partial C_{d2}} = -1, \\
&S_{Cd2}^{\hat{\lambda}_3} = \frac{C_{d2}}{\hat{\lambda}_3}\frac{\partial \hat{\lambda}_3}{\partial C_{d2}} = -1, \quad S_{Cd3}^{\hat{\lambda}_3} = \frac{C_{d3}}{\hat{\lambda}_3}\frac{\partial \hat{\lambda}_3}{\partial C_{d3}} = 1, \\
&S_{C_{d3}}^{\hat{\lambda}_4} = \frac{C_{d3}}{\hat{\lambda}_4}\frac{\partial \hat{\lambda}_4}{\partial C_{d3}} = -2, \; S_{\theta_2}^{\hat{\lambda}_4} = \frac{\theta_2}{\hat{\lambda}_4}\frac{\partial \hat{\lambda}_4}{\partial \theta_2} = -\frac{\theta_2\left(2\cos\left(\theta_2\right)^2 - 1\right)}{\sin\left(\theta_2\right)\cos\left(\theta_2\right)} \\
&S_{Cd2}^{\hat{\lambda}_5} = \frac{C_{d2}}{\hat{\lambda}_5}\frac{\partial \hat{\lambda}_5}{\partial C_{d2}} = 1, \quad S_{P_{s0}}^{\hat{\lambda}_5} = \frac{P_{s0}}{\hat{\lambda}_5}\frac{\partial \hat{\lambda}_5}{\partial P_{s0}} = -\frac{1}{2}, \; S_{Cd3}^{\hat{\lambda}_5} = \frac{C_{d3}}{\hat{\lambda}_5}\frac{\partial \hat{\lambda}_5}{\partial C_{d3}} = -2 \\
&S_{\theta_2}^{\hat{\lambda}_5} = \frac{\theta_2}{\hat{\lambda}_5}\frac{\partial \hat{\lambda}_5}{\partial \theta_2} = -\frac{\theta_2\left(2\cos\left(\theta_2\right)^2 - 1\right)}{\sin\left(\theta_2\right)\cos\left(\theta_2\right)}
\end{aligned}
\tag{60}
$$

Similarly, the following expression may be written to describe the change in gamma family nondimensional groups for small perturbations of these uncertain parameters

$$
\begin{aligned}
\frac{\delta\hat{\gamma}_1}{\hat{\gamma}_1} &= S_{P_{s0}}^{\hat{\gamma}_1}\frac{\delta P_{s0}}{P_{s0}} + S_{Cd2}^{\hat{\gamma}_1}\frac{\delta C_{d2}}{C_{d2}} + S_{Cd3}^{\hat{\gamma}_1}\frac{\delta C_{d3}}{C_{d3}} + S_{\theta 2}^{\hat{\gamma}_1}\frac{\delta\theta_2}{\theta_2}, \\
\frac{\delta\hat{\gamma}_2}{\hat{\gamma}_2} &= S_{Cd1}^{\hat{\gamma}_2}\frac{\delta C_{d1}}{C_{d1}} + S_{\theta 1}^{\hat{\gamma}_2}\frac{\delta\theta_1}{\theta_1} + S_{Cd3}^{\hat{\gamma}_2}\frac{\delta C_{d3}}{C_{d3}} + S_{\theta 2}^{\hat{\gamma}_2}\frac{\delta\theta_2}{\theta_2}, \\
\frac{\delta\hat{\gamma}_4}{\hat{\gamma}_4} &= S_{P_{s0}}^{\hat{\gamma}_4}\frac{\delta P_{s0}}{P_{s0}} + S_{Cd2}^{\hat{\gamma}_4}\frac{\delta C_{d2}}{C_{d2}} + S_{Cd3}^{\hat{\gamma}_4}\frac{\delta C_{d3}}{C_{d3}} + S_{\theta 2}^{\hat{\gamma}_4}\frac{\delta\theta_2}{\theta_2},
\end{aligned}
\tag{61}
$$

Where the sensitivity coefficients are given by

$$
\begin{aligned}
&S_{P_{s0}}^{\hat{\gamma}_1}=\frac{P_{s0}}{\hat{\gamma}_1}\frac{\partial\hat{\gamma}_1}{\partial P_{s0}}=-\frac{1}{2},\quad S_{Cd2}^{\hat{\gamma}_1}=\frac{C_{d2}}{\hat{\gamma}_1}\frac{\partial\hat{\gamma}_1}{\partial C_{d2}}=1,\quad S_{Cd3}^{\hat{\gamma}_1}=\frac{C_{d3}}{\hat{\gamma}_1}\frac{\partial\hat{\gamma}_1}{\partial C_{d3}}=-2\\
&S_{\theta 2}^{\hat{\gamma}_1}=\frac{\theta_2}{\hat{\gamma}_1}\frac{\partial\hat{\gamma}_1}{\partial\theta_2}=-\frac{\theta_2\left(2\cos\left(\theta_2\right)^2-1\right)}{\sin\left(\theta_2\right)\cos\left(\theta_2\right)}\\
&S_{Cd1}^{\hat{\gamma}_2}=\frac{C_{d1}}{\hat{\gamma}_2}\frac{\partial\hat{\gamma}_2}{\partial C_{d1}}=2,\quad S_{\theta 1}^{\hat{\gamma}_2}=\frac{\theta_1}{\hat{\gamma}_2}\frac{\partial\hat{\gamma}_2}{\partial\theta_1}=2\theta_1\cot\left(2\theta_1\right),\\
&S_{Cd3}^{\hat{\gamma}_2}=\frac{C_{d3}}{\hat{\gamma}_2}\frac{\partial\hat{\gamma}_2}{\partial C_{d3}}=-2,\quad S_{\theta 2}^{\hat{\gamma}_2}=\frac{\theta_2}{\hat{\gamma}_2}\frac{\partial\hat{\gamma}_2}{\partial\theta_2}=-\frac{\theta_2\left(2\cos\left(\theta_2\right)^2-1\right)}{\sin\left(\theta_2\right)\cos\left(\theta_2\right)}\\
&S_{P_{s0}}^{\hat{\gamma}_4}=\frac{P_{s0}}{\hat{\gamma}_4}\frac{\partial\hat{\gamma}_4}{\partial P_{s0}}=-\frac{1}{2},\quad S_{Cd2}^{\hat{\gamma}_4}=\frac{C_{d2}}{\hat{\gamma}_4}\frac{\partial\hat{\gamma}_4}{\partial C_{d2}}=1,\\
&S_{Cd3}^{\hat{\gamma}_4}=\frac{C_{d3}}{\hat{\gamma}_4}\frac{\partial\hat{\gamma}_4}{\partial C_{d3}}=-2,\quad S_{\theta 2}^{\hat{\gamma}_4}=\frac{\theta_2}{\hat{\gamma}_4}\frac{\partial\hat{\gamma}_4}{\partial\theta_2}=-\frac{\theta_2\left(2\cos\left(\theta_2\right)^2-1\right)}{\sin\left(\theta_2\right)\cos\left(\theta_2\right)}
\end{aligned}
\tag{62}
$$

From Equation (60) and (62) it can be observed in general that the sensitivity coefficients of the nominal supply pressure and discharge coefficients are all constant, but the sensitivity coefficients of the jet angles are functions of jet angles. The values of the sensitivity coefficients indicate the percentage change in the nondimensional groups, when the uncertain parameters are certain percentage away from their nominal values. When the sign of the sensitivity coefficient is positive, higher values for the uncertain parameters will cause the nondimensional groups to increase. When the sign of the sensitivity coefficient is negative, higher values for the uncertain parameters will cause the nondimensional groups to decrease.

Take the sensitivity coefficient $S_{C_{d3}}^{\hat{\lambda}_4}$ of the nondimensional group $\hat{\lambda}_4$ for example. If the discharge coefficient C_{d3} is disturbed by $\pm 1\%$, $\delta C_{d3}/C_{d3}=\pm 0.01$, then nondimensional $\hat{\lambda}_4$ will be disturbed for about $\delta\hat{\lambda}_4/\hat{\lambda}_4=\mp 0.02$. Because the physical meaning of these sensitivity coefficients is related to percentage change, it should be

emphasized that the same percentage change in different nondimensional groups indicate different absolute amount of change. One percent of nondimensional group $\hat{\lambda}_4$ is about 0.474, while one percent of nondimensional group $\hat{\lambda}_5$ is about 0.0534. Therefore one percent disturbance in discharge coefficient C_{d3} will induced a disturbance of 0.9481 in nondimensional group $\hat{\lambda}_4$ and a disturbance of 0.1067 in nondimensional group $\hat{\lambda}_5$. The disturbance in pressure difference term is about 18 times the disturbances in viscous shear term. Consequently, it can be conclude that the uncertainty in discharge coefficient C_{d3} has a much stronger influence in the pressure difference term than the viscous shear term.

The sensitivity coefficients for nondimensional group $\hat{\gamma}_1$, which is related to the transient momentum force term, and nondimensional group $\hat{\gamma}_4$, which is related to the viscous shear term have exactly the same values. Thus, it can be inferred that they response similarly to the uncertainty in supply pressure and discharge coefficient. The sensitivity coefficients to jet angles, evaluated at the estimated jet angle θ_1 and θ_2, are 7.55 and -3.61 respectively. These two values indicate that the steady momentum force related to the supply orifice is more sensitive to the uncertainty in jet angle than any other nondimensional group that depends on jet angle. In addition, the sensitivity coefficients to jet angles is generally greater than the sensitivity coefficients to supply pressure and discharge coefficients. This observation indicates that the steady momentum flow force is more likely to be changed by the uncertainties in jet angle.

3.5 Linearization

As shown in Figure 6, the pressure drop coefficients are nonlinear functions of valve displacement. Therefore, From Equation (55) and (57), it can be observed that the valve displacement $\hat{x}$ and pressure drop across the valve $\hat{P}_s - \hat{P}_r$ are two variables that can change the size of the flow force $\hat{F}$. However, their influences on the flow force are nonlinear and complicated. In order to see the influences of valve displacement $\hat{x}$ and pressure drop across the valve $\hat{P}_s - \hat{P}_r$ independently, it is recommended to linearize the pressure drop coefficients and flow force. Apply Taylor expansion to the pressure drop coefficients in Equation (51) at nominal valve displacement where $\hat{x} = 0$ yields

$$\begin{aligned}
C_{fxp} &= \frac{\left(C_{d1}\hat{A}_1\right)^2 C_{d3}^2 K_L^2}{De} - \frac{8\left(C_{d1}\hat{A}_1\right)^4 \left(C_{d2}\hat{A}_2\right)^2 C_{d3}^2 K_L^6}{De^2\pi}\hat{x}, \\
C_{fxms} &= \frac{\left(C_{d2}\hat{A}_2\right)^2 C_{d3}^2}{De} - \frac{8\left(C_{d2}\hat{A}_2\right)^4 \left(C_{d1}\hat{A}_1\right)^2 C_{d3}^2 K_L^4}{De^2\pi}\hat{x}, \\
C_{fxmr} &= \frac{\left(C_{d1}\hat{A}_1\right)^2 \left(C_{d2}\hat{A}_2\right)^2 K_L^4}{De} + \frac{8\left(C_{d1}\hat{A}_1\right)^2 \left(C_{d2}\hat{A}_2\right)^2 K_L^4 C_{d3}^2 \left(\left(C_{d2}\hat{A}_2\right)^2 + \left(C_{d1}\hat{A}_1\right)^2 K_L^2\right)}{De^2\pi}\hat{x},
\end{aligned} \tag{63}$$

where the common denominator is

$$De = \left(C_{d2}\hat{A}_2\right)^2 C_{d3}^2 + \left(C_{d1}\hat{A}_1\right)^2 \left(C_{d2}\hat{A}_2\right)^2 K_L^4 + \left(C_{d1}\hat{A}_1\right)^2 C_{d3}^2 K_L^2. \tag{64}$$

Because every constant in Equation (63) is positive real, it can be conclude that when the valve displacement is positive the pressure drop across the supply orifice and valve momentum will decrease, but the pressure drop across the return orifice will increase. This linearization analysis coincide the shape of the curves in Figure 6.

However, the linear estimation of the slope will be far from the valve in the nonlinear model as the magnitude of the displacement becomes larger.

Similarly to the linearization of pressure drop coefficients, apply multi-Taylor series expansion to the steady state flow force described by the third equation in Equation (55) at nominal valve displacement $\hat{x}=0$, and nominal pressure drop $\Delta\hat{P}=\hat{P}_s-\hat{P}_r=\Delta\hat{P}_o$ yields its linearization

$$\begin{aligned}\hat{F}=&-\hat{\lambda}_4\frac{\left(C_{d1}\hat{A}_1\right)^2C_{d3}^2K_L^2\Delta\hat{P}_o}{De}+\hat{\lambda}_5\sqrt{\frac{\left(C_{d1}\hat{A}_1\right)^2C_{d3}^2K_L^2\Delta\hat{P}_o}{De}}\\&+\left(\begin{array}{l}\dfrac{8\hat{\lambda}_4\left(C_{d1}\hat{A}_1\right)^2C_{d3}^2K_L^2\Delta\hat{P}_o}{De}\dfrac{\left(C_{d1}\hat{A}_1\right)^2\left(C_{d2}\hat{A}_2\right)^2K_L^4}{\pi De}\\-4\hat{\lambda}_5\sqrt{\dfrac{\left(C_{d1}\hat{A}_1\right)^2C_{d3}^2K_L^2\Delta\hat{P}_o}{De}}\dfrac{\left(C_{d1}\hat{A}_1\right)^2\left(C_{d2}\hat{A}_2\right)^2K_L^4}{\pi De}\end{array}\right)\hat{x}\\&+\left(-\frac{\hat{\lambda}_4\left(C_{d1}\hat{A}_1\right)^2C_{d3}^2K_L^2}{De}+\frac{\hat{\lambda}_5}{2\Delta\hat{P}_o}\sqrt{\frac{\left(C_{d1}\hat{A}_1\right)^2C_{d3}^2K_L^2\Delta\hat{P}_o}{De}}\right)\left(\Delta\hat{P}-\Delta\hat{P}_o\right).\end{aligned}\tag{65}$$

The linearized flow force in Equation (65) share a similar form as the classic linearized steady flow force, because it has a displacement term, which is related to nondimensional valve displacement, $\hat{x}$ and a pressure term which is related to nondimensional pressure drop $\Delta\hat{P}$. However, the difference between the classic linearization and the linearization in (65) should be emphasized. First, the object that has been linearized is different. In the classic theory, it is the momentum change induced flow force that has been linearized, while Equation (65) is used to describe the linearized pressure difference term and viscous shear term. Second, the nominal point used to define the linearization is defined differently. In the classical theory, the linearized flow force is

defined based on the pressure drop across the metering orifice, but in the new linearized flow force model in Equation (65) is defined based on the pressure drop across the whole two-way spool valve.

Similarly, apply multi-Taylor series expansion to the steady state flow force described by Equation (57) at nominal valve displacement $\hat{x}=0$, nominal pressure drop $\Delta\hat{P}=\hat{P}_s-\hat{P}_r=\Delta\hat{P}_o$ and nominal pressure transient $d\Delta\hat{P}/d\hat{t}=0$ yields

$$\begin{aligned}\hat{F}=&\hat{\gamma}_2\frac{\left(C_{d2}\hat{A}_2\right)^2C_{d3}^2\Delta\hat{P}_o}{De}+\hat{\gamma}_3\frac{\left(C_{d1}\hat{A}_1\right)^2\left(C_{d2}\hat{A}_2\right)^2K_L^4\Delta\hat{P}_o}{De}-\hat{\gamma}_4\sqrt{\frac{\left(C_{d1}\hat{A}_1\right)^2C_{d3}^2K_L^2\Delta\hat{P}_o}{De}}\\&+\frac{\hat{\gamma}_1}{2\sqrt{\Delta\hat{P}_o}}\sqrt{\frac{\left(C_{d1}\hat{A}_1\right)^2C_{d3}^2K_L^2}{De}}\frac{d\Delta\hat{P}}{d\hat{t}}\\&+\left(\hat{\gamma}_2\frac{\left(C_{d2}\hat{A}_2\right)^2C_{d3}^2}{De}+\hat{\gamma}_3\frac{\left(C_{d1}\hat{A}_1\right)^2\left(C_{d2}\hat{A}_2\right)^2K_L^4}{De}-\hat{\gamma}_4\sqrt{\frac{\left(C_{d1}\hat{A}_1\right)^2C_{d3}^2K_L^2}{2De\Delta\hat{P}_o}}\right)\left(\Delta\hat{P}-\Delta\hat{P}_o\right)\\&+\left(\begin{array}{l}4\hat{\gamma}_4\sqrt{\frac{\left(C_{d1}\hat{A}_1\right)^2C_{d3}^2K_L^2\Delta\hat{P}_o}{De}}\frac{\left(C_{d1}\hat{A}_1\right)^2\left(C_{d2}\hat{A}_2\right)^2K_L^4}{\pi De}\\-\frac{8\hat{\gamma}_2\left(C_{d2}\hat{A}_2\right)^2C_{d3}^2\Delta\hat{P}_o}{\pi De}\frac{\left(C_{d1}\hat{A}_1\right)^2\left(C_{d2}\hat{A}_2\right)^2K_L^4}{De}\\+\frac{4\hat{\gamma}_3\left(C_{d1}\hat{A}_1\right)^2\left(C_{d2}\hat{A}_2\right)^2K_L^4\Delta\hat{P}_o}{\pi De}\left(-1+\frac{2\left(\left(C_{d2}\hat{A}_2\right)^2C_{d3}^2+\left(C_{d1}\hat{A}_1\right)^2C_{d3}^2K_L^2\right)}{De}\right)\end{array}\right)\hat{x}.\end{aligned}\tag{66}$$

It should be emphasized that the linearized flow force in Equation (66) does not have a velocity term, because the valve displacement is assumed to be fixed. Different from the linearized flow force in Equation (65), which is a steady state result, this linearized model includes the pressure transient term explicitly. Similar to the

linearization in Equation (65) the linearized flow force in (66) is different from the classic linearized flow force, although they share the same form.

In Equation (66), some of the terms have $\sqrt{\Delta\hat{P}_o}$ on the denominator. As a result, when the pressure drop is zero, those terms will go to infinity. However, the situation of infinite term is not physically possible. The zero-pressure drop situation is not the case that can be described by the equation, which is derived based on the high Reynolds number assumption. When the pressure drop across the valve is below some critical value, the fluid flow through the two-way valve should no longer be characterized as high Reynolds number flow. And the poly nominal model for the flow in Equation (6) should be used.

3.6 Summary of Modeling

In this chapter, nondimensional analysis is first conducted on both valve piston equilibrium condition generated flow force and fluid control volume equilibrium condition generated flow force. Although the two equilibrium conditions are on different objects, the nondimensional analysis in both cases shows that increasing damping length L can enlarge the pressure transient effect without changing the steady state momentum force term. However, pressure transient component is not the only force that can be changed by damping length L. The viscous shear force will also increase as the damping length increases. Therefore, longer damping length does not necessarily ensure the dominance of pressure transient effect, but longer damping length can largely reduce the contribution of the steady state momentum force, which is conventionally considered as the major source of flow force. The influence of characteristic time on the

nondimensional group size shows that the shorter the characteristic time is the larger the pressure transient effect will be. Therefore, it is recommended that fast pressure rise and fall should be created to excite the system represented in Equation (55). The comparison between nondimensional group $\hat{\lambda}_1$ and $\hat{\gamma}_1$ shows that the transient flow forces caused by fluid compressibility is much smaller than the transient flow force caused by fluid inertial.

Then the sensitivity analysis is conducted on the nondimensional groups derived in the first step. It is shown that the sensitivity coefficients to uncertainty in supply pressure and discharge coefficients are variable-independent constants. While the sensitivity coefficients to the uncertainty in jet angles are dependent on the value of the jet angles. Moreover, the pressure difference term is more sensitive to the uncertain in discharge coefficient than any other nondimensional groups, because the absolute value of pressure difference term is the largest. Therefore, discharge coefficient has to be estimate with high accuracy. The influence of uncertainty in jet angles are stronger than the uncertainty in supply pressure and discharge coefficients.

The linearized pressure drop coefficients shows that positive displacement will cause the pressure drop across the supply orifice and valve momentum to decrease, but the pressure drop across the return orifice will increase. The linearization of the flow force in Equation (65) is derived from the valve piston equilibrium condition based on the steady state assumption. It decomposes the nonlinear steady state flow force into the displacement term and the pressure term. The linearization of the flow force in Equation (66) is derived from fluid control volume equilibrium condition. It decomposes the nonlinear flow force with fixed valve piston into the displacement term, the pressure term

and the pressure transient term. This analytical study indicates that by subtracting the steady flow force from the total flow force, the pressure transient effect can be observed.

Chapter 4: Analysis of Pressure Wave Generation System

4.1 General

Based on the nondimensional analysis in Chapter 3, the pressure rise and fall should be fast enough to make the pressure transient effect the major component in the total flow force. Thus, the pressure-wave generation system should have the capability to generate pressure waves with sharp pressure change edges. In the proposal for the current dissertation, a rotary pressure wave generator is introduced to generate the pressure square wave. Moreover, this pressure wave generator will be driven by a variable axial-piston pump. The diagram of the pressure wave and generation system to be tested is shown in Figure 15. A very sensitive pressure relief valve and an accumulator are added to either smooth the pressure or to absorb the high frequency oscillation of the pressure. An induction motor and a DC motor are used to drive the variable axial-piston pump and the pressure wave generator respectively. As the DC motor rotates, the supply pressure to the two-way spool valve P_s will be switched between the high pressure P_h and low pressure P_l. Thus, a continuous fast pressure wave is generated to excite the two-way spool valve. A force sensor with very high stiffness is attached to the valve piston and fixed with respect to the valve housing. This force sensor is employed to measure the total flow force acting on the valve piston. The measurement from the force sensor can be decomposed into the terms in Equation (55) or the terms in Equation (57).

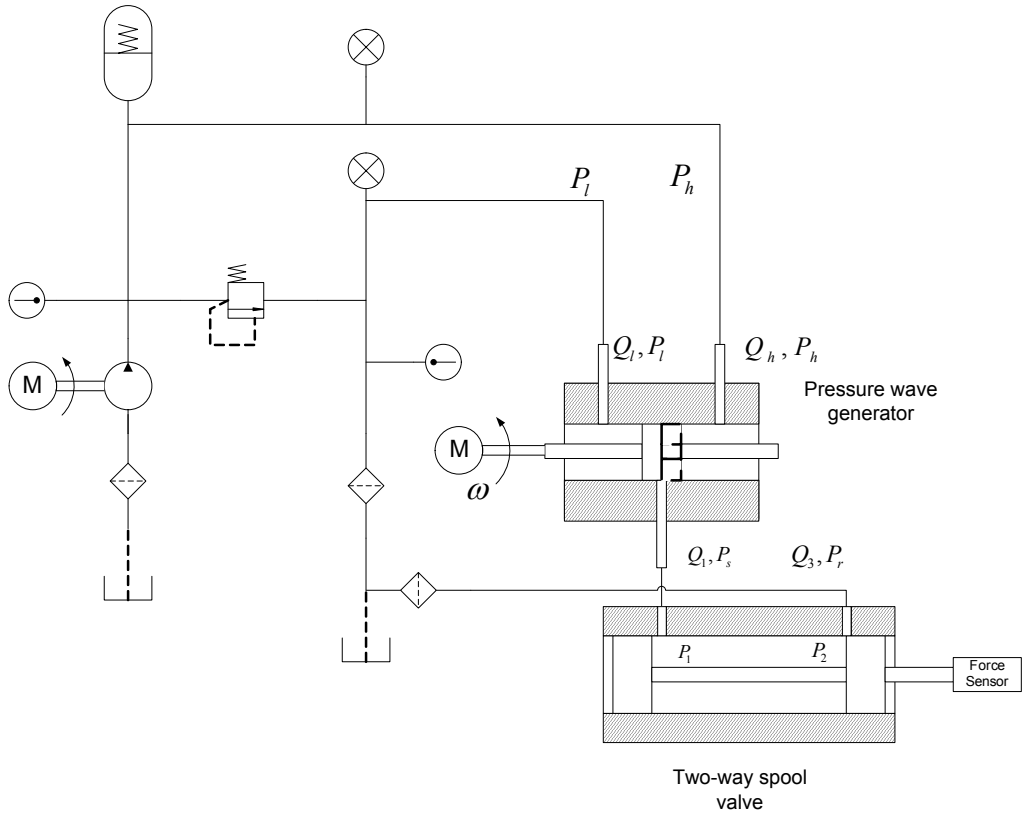

Figure 15 Pressure-wave generation system and the system to be tested

The pressure-wave generation system shown in Figure 15 is anticipated to generate a perfect square wave. However, this target can be very difficult to achieve, because of the internal dynamics of the variable axial-piston pump and the pressure wave generator itself. For example, the variable axial-piston pump acts according to the demanding volumetric flow rate. Moreover, as the square pressure wave generator is rotated by the DC motor, the demanding volumetric flow rate will be changing periodically. Thus, the swash plate of the axial piston pump will have to be repositioned to provide the corresponding volumetric flow rate. Therefore, it becomes important to analyze the dynamics of the components of the pressure-wave generation system and see their influences over the pressure wave generated.

4.2 Variable Axial-piston Pump

4.2.1 General description of the axial piston pump

Axial-piston pump has been used to provide fluid power in hydraulic system for a long time. In real applications, multiple applications may be driven by the same axial-piston pump and one device can have different working condition depends on the configuration. Therefore, the demanding load flow for the axial-piston pump can be different. Consequently, the variable displacement axial-piston pump came into existence in order to change the amount of flow that is delivered to the hydraulic circuitry by sensing the flow needs instantly.

In an axial piston pump of the in-line type, where the cylinders and the drive shaft are parallel, the pistons are nested in a circular array within a common cylindrical block at equal intervals about the x-axis. Here, the reciprocating motion is created by the swash plate rotation. The cylinder block is held tightly against a valve plate using the force of the compressed cylinder-block springs. A ball and socket joint connects the base of each piston to their respective slippers, which are kept in reasonable contact with the swash plate. While the valve plate is balanced by a rigid constrain, the input shaft is used to drive the cylinder block about the x-axis at a constant angular velocity ω. When the drive shaft is rotated, it rotates the pistons and the cylinder block with it. As the pistons reciprocate in the cylinder block, they pass over the intake and discharge ports in succession causing fluid to enter the piston chamber, compressed and discharged at the high-pressure side. This motion repeats itself for each pump revolution and the basic task of pumping fluid is then accomplished.

4.2.2 Variable axial piston pump control mechanism

The schematic drawing for the pump and control mechanism is shown in Figure 16. The hydraulic circuit to the right of the axial piston pump achieves the stabilization of the pump working condition. When the discharge pressure is more than the desired value, the control valve piston will be pushed upward until the orifice connecting the actuator chamber and discharge pressure is open. Then, the actuator pressure increases and the actuator piston is pushed upwards. As the actuator piston moving, the swash plate of the axial piston pump will rotate about its axis to make the swash plate angle smaller. Because smaller swash plat angle indicate smaller supply volumetric flow rate, the pressure in the discharge line will decreases if the demanding volumetric flow rate is constant. Thus the discharge pressure is stabilized.

This control mechanism can also reject the disturbance in demanding volumetric flow rate. When the demanding volumetric flow is rising, the pressure in the discharge line will decrease and the control valve piston is pushed downwards to have the orifice connecting the return line and the actuator chamber open. Then the actuator will be moving downwards by the spring force. As the actuator moving down, the swash plate will rotate so that the swash plate angle is increasing. The system will be driving to a new working condition by increasing the supply volumetric flow rate to the value close to the new demanding volumetric flow rate and then stabilized around this new working condition. From this section on the discharge pressure of the variable axial piston pump is denoted as P_{dis} .

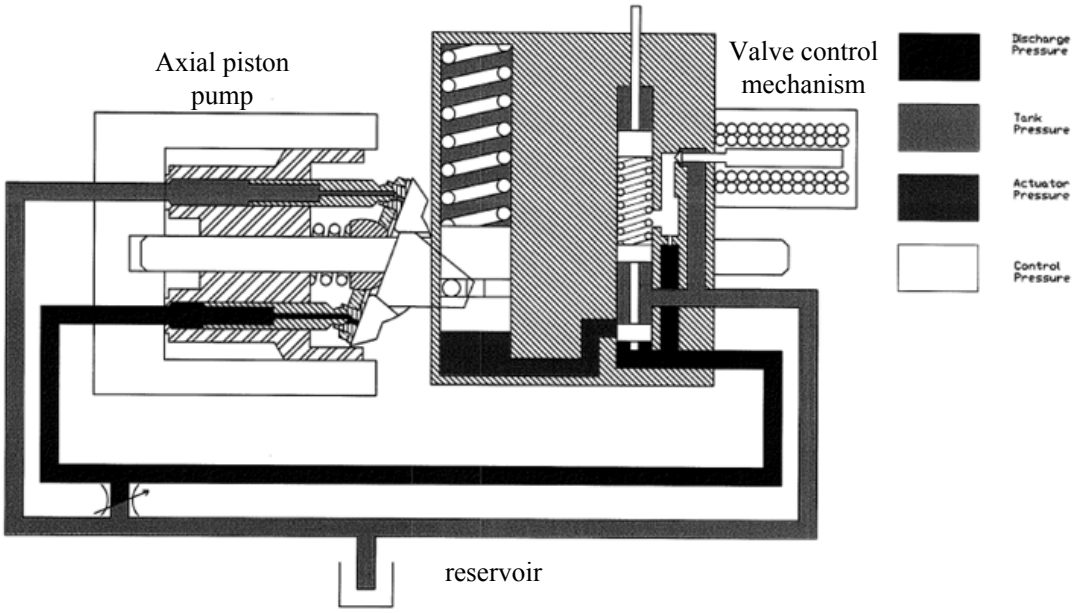

Figure 16 Variable axial-piston pump control mechanism

4.3 Square Pressure Wave Generator

4.3.1 General description of the pressure wave generator

The proposed rotary pressure wave generator consists of a rotor and a stator, which is the same as the one, presented in reference [36]. Figure 17 illustrates the three dimensional structure of the assembly presented in reference [36]. The rotor, which is separate into two chambers by a pass-partition plate, rotates in the stator. As the rotor rotates, the transducer port will be switching between the high-pressure chamber and the low-pressure chamber. Thus the square pressure wave is created. The experiment done by the author of [36] shows that this kind of device can generated very good square wave.

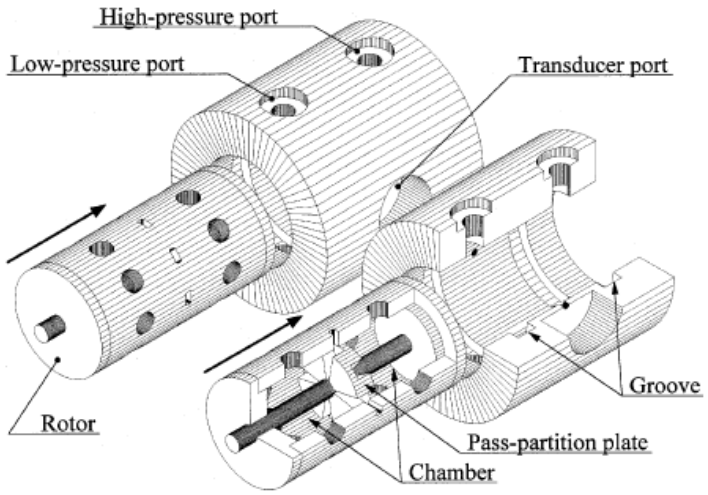

Figure 17 External view and internal structure of the rotor [36]

4.3.2 Analyze the pressure wave generator

Based on the description in reference [36], the square wave generator can be essentially seen as a control volume in the downstream exposed to a high-pressure chamber and a low-pressure chamber intermittently. The discharge pressure P_{dis} from the variable axial piston pump sustains the pressure in the high-pressure chamber P_h. The reservoir pressure P_r sustains the pressure in the low-pressure chamber P_l. When the control volume in the downstream of the pressure wave generator is connected to the high-pressure chamber, it is obvious that the flow will be high Reynolds number flow, because the pressure in the upper stream is high. However, when the control volume is connected to the low-pressure chamber, the fluid flow will be characterized as low Reynolds number flow. Because this dissertation is focused on flow forces, which will be zero when there is no flow, the volumetric flow rates through the pressure wave generator can be modeled using the orifice equation.

In a trial experiment with the original rotor design in Figure 17, leakage is detected to flow from the high-pressure chamber to the transducer port and from the transducer port to the low-pressure chamber. The observation to prove this is that the pressure sensed in the transducer port to rise and fall when it is not suppose to be connected to either high-pressure chamber or low-pressure chamber. The leakage can flow in three ways. The first way is from the clearance between the shaft and the pass-partition plate. The second way is from the clearance between the rotor and the stator. The volumetric flow rate in the first leakage passage can be largely reduced by installing a high-pressure seal ring, which is indicate by a seal ring groove in Figure 18. However, it is very difficult to reduce the volumetric flow rate in the second leakage passage. The reason is the large outer diameter of the rotor and the competing effect between good sealing and small friction, which will facilitate the rotational motion of the rotor. If a high-pressure seal ring is installed, the pressure between the seal ring and the stator should be large enough to prevent the leakage. This pressure will increase the friction that has to be overcome by the motor that is driving the pressure wave generator. To maintain small friction and overcome the influence of volumetric flow in the second leakage passage, the rotor is modified to have extended groove on the outer surface as shown in Figure 18. This extended groove helps to maintain a much more constant pressure in the transducer port by utilizing the feature of the variable axial-piston pump. The third leakage passage is from the high-pressure chamber and the low pressure chamber to atmosphere pressure.

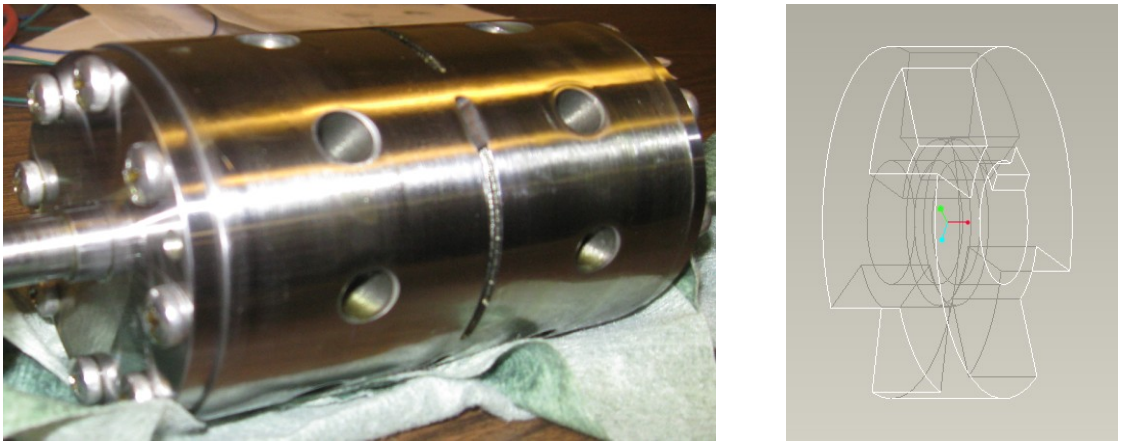

Figure 18 Modified rotor and pass-partition plate design

To summarize the above description on the flows in the pressure wave generator, the pressure dynamics for the pressures mentioned in Figure 15 can be described by

$$\begin{aligned}
\frac{V_h}{\beta}\frac{dP_h}{dt} &= Q_{dish} - Q_h - K\left(P_h - P_l\right) - K\left(P_h - P_s\right) - KP_h, \\
\frac{V_s}{\beta}\frac{dP_s}{dt} &= Q_h - Q_l - Q_1 + K\left(P_h - P_s\right) - K\left(P_s - P_l\right), \\
\frac{V_l}{\beta}\frac{dP_l}{dt} &= -Q_{lr} + Q_l + K\left(P_h - P_l\right) + K\left(P_s - P_l\right) - KP_l,
\end{aligned} \tag{67}$$

where

$$\begin{aligned}
Q_{dish} &= A_{sta}C_{sta}\sqrt{\frac{2}{\rho}\left(P_{dis} - P_h\right)}, \quad Q_{lr} = A_{sta}C_{sta}\sqrt{\frac{2}{\rho}\left(P_l - P_r\right)} \\
Q_h &= A_hC_{dh}\sqrt{\frac{2}{\rho}\left(P_h - P_s\right)}, \quad Q_l = A_lC_{dl}\sqrt{\frac{2}{\rho}\left(P_s - P_l\right)}.
\end{aligned} \tag{68}$$

As the reminder of the contents in Chapter 2, volumetric flow rate Q_1 is the volumetric flow rate into the two-way spool valve in Equation (18). Pressure P_s is the supply pressure provided by pressure wave generator, and it is the same supply pressure that feeds into the two-way spool valve. The rise and fall of supply pressure P_s will be

influence by high-pressure line volumetric flow rate Q_h, low-pressure line volumetric flow rate Q_l, the flow demanded by the two-way spool valve Q_1 and the leakage flow.

Volume V_h, V_l and V_s denote the high-pressure chamber volume, the low-pressure chamber volume and the supply volume between the pressure wave generator and the two-way spool valve respectively. Similar to the leakage from the pump piston chambers, it is very difficult to prove the leakage concerning the pressure wave generator is low Reynolds number flow. The linear leakage is used here as a crude approximation. In addition, all the linear leakage coefficients are assumed equal. The volume V_s will include the volume of the hose, which connect the pressure wave generator to the two-way spool valve. The area A_{sta} denotes the cross-sectional area of the orifices on the stator in Figure 19, which connect the variable axial-piston pump and reservoir to the pressure wave generator. These orifices are designed to have constant opening to the high-pressure chamber and the low-pressure chamber respectively.

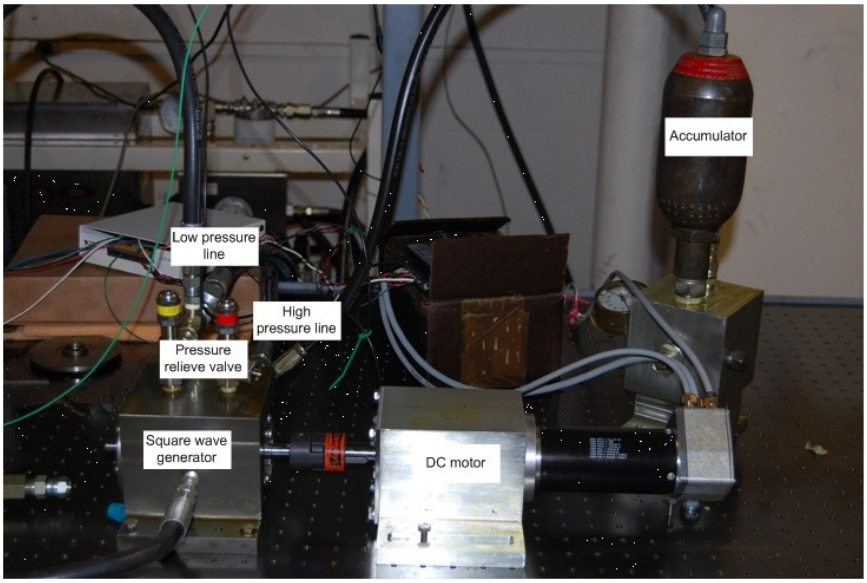

Figure 19 Pressure-wave generator within the hydraulic circuit

The cross sectional area A_h and A_l are two time-varying variables due to the rotational motion of the rotor. Typical orifice area changing patterns for the rotor design in Figure 18 are shown in Figure 20. Figure 20 has been nondimensionalized, so that unity means the orifice is fully open, while zero means the orifice is completely closed. The orifice area A_h first increase to the maximum opening and then drop to one-half of the maxim opening when extended groove enters. At last, the orifice area A_h is completely closed and the orifice area A_l begins another identical circle. This feature makes the system represented by Equation (67) a non-autonomous system, which depends on time explicitly. When the rotor is rotated, Equation (67) is the missing theoretical model for the square wave generator in reference [36] and [37].

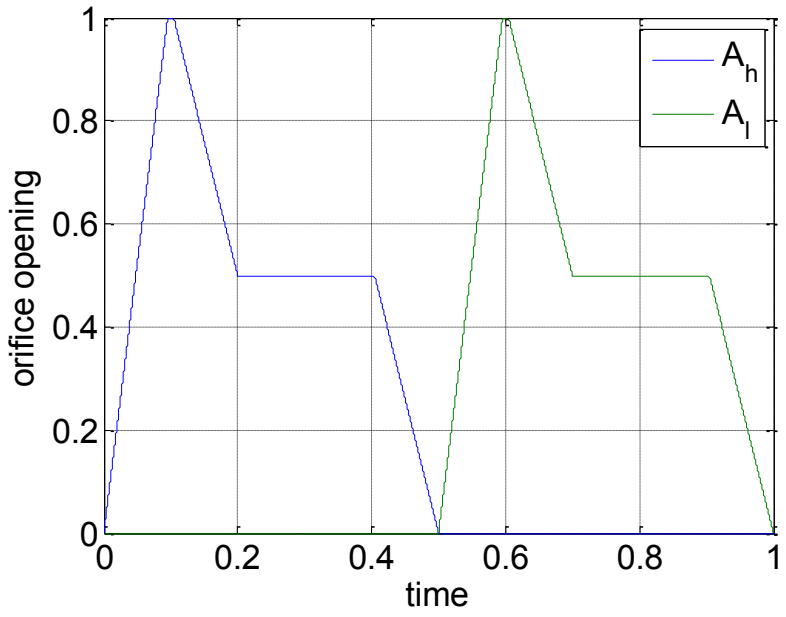

Figure 20 Time varying orifice in pressure wave generator

4.3.3 Nondimensionalization

By selecting the same scaling factor for pressure and time in Equation (54) and the following scaling factor for time-varying orifice area

$$A_h = A_{\max}\hat{A}_h, \quad A_l = A_{\max}\hat{A}_l, \tag{69}$$

where $A_{\max}$ is the maximum area that can connect the two pressure chambers to the two-way spool valve to the downstream, Equation (67) can be written in its nondimensional form

$$\begin{aligned}
\hat{\delta}_1\frac{d\hat{P}_h}{d\hat{t}} &= \hat{\delta}_2\sqrt{\hat{P}_{dis}-\hat{P}_h} - \hat{\delta}_3\hat{A}_h\sqrt{\hat{P}_h-\hat{P}_s} - \left(\hat{P}_h-\hat{P}_l\right) - \left(\hat{P}_h-\hat{P}_s\right) - \hat{P}_h,\\
\hat{\delta}_4\frac{d\hat{P}_s}{d\hat{t}} &= \hat{\delta}_3\hat{A}_h\sqrt{\hat{P}_h-\hat{P}_s} - \hat{\delta}_5\hat{A}_l\sqrt{\hat{P}_s-\hat{P}_l} - \hat{\delta}_6\sqrt{\hat{P}_s-\hat{P}_1} + \left(\hat{P}_h-\hat{P}_s\right) - \left(\hat{P}_s-\hat{P}_l\right),\\
\hat{\delta}_7\frac{d\hat{P}_l}{d\hat{t}} &= -\hat{\delta}_2\sqrt{\hat{P}_l-\hat{P}_r} + \hat{\delta}_5\hat{A}_l\sqrt{\hat{P}_s-\hat{P}_l} + \left(\hat{P}_h-\hat{P}_l\right) + \left(\hat{P}_s-\hat{P}_l\right) - \hat{P}_l,
\end{aligned} \tag{70}$$

where the delta family nondimensional groups are

$$\begin{aligned}
&\hat{\delta}_1 = \frac{V_h}{K\beta\tau}, \quad \hat{\delta}_2 = \frac{2C_{sta}A_{sta}}{K\sqrt{P_{s0}\rho}}, \quad \hat{\delta}_3 = \frac{2C_{dh}A_{\max}}{K\sqrt{P_{s0}\rho}}\\
&\hat{\delta}_4 = \frac{V_s}{K\beta\tau}, \quad \hat{\delta}_5 = \frac{2C_{dl}A_{\max}}{K\sqrt{P_{s0}\rho}}, \quad \hat{\delta}_6 = \frac{2C_{d1}A_1}{K\sqrt{P_{s0}\rho}}, \quad \hat{\delta}_7 = \frac{V_l}{K\beta\tau}
\end{aligned} \tag{71}$$

The performance of the square wave generator strongly depend on how well the high pressure P_h and low pressure P_l are kept at a constant level, and the amount of the leakage determined by coefficient K. When the linear leakage coefficient is larger, the nondimensional group $\hat{\delta}_4$ will be smaller. Thus the response of the square pressure wave generator to the pressure change in the upper stream will be slower. The selection of

characteristic time τ can change the size of nondimensional groups $\hat{\delta}_1$, $\hat{\delta}_4$ and $\hat{\delta}_1$. The smaller the characteristic time is the stronger the pressure transient term will be. Assuming the discharge coefficients $C_{dh} = C_{dl} = 0.62$ and linear leakage coefficient $K = 10^{-11} m^3 / Pa$, and the geometry parameters are given in Table 5. The corresponding delta family nondimensional group evaluated using the above data is given in Table 6. The values in Table 6 shows that the all the delta family nondimensional groups are greater than unity, which indicate the contribution of leakage. The largest nondimensional groups are related to volumetric flow Q_{dish}, Q_{lr}, Q_h and Q_l. This characteristic ensures that the variable axial-piston pump and the reservoir have the dominant influence over the pressure dynamics within the pressure wave generator. The influence of the two-way spool valve, which is indicated by nondimensional group $\hat{\delta}_6$, is the second largest. Therefore its influence on the pressure dynamics within the pressure wave generator is smaller than the variable axial-piston pump and the reservoir, but stronger than leakage and pressure transient effect. The pressure transient effect within the supply volume, which indicates by nondimensional group $\hat{\delta}_4$, is stronger than the pressure transient in the high-pressure chamber and the low-pressure chamber.

Table 5 Geometry parameters of the pressure wave generator

V_h	5.1022e-005 m^3	V_l	5.1022e-005 m^3
V_s	7.8540e-005 m^3	A_{sta}	2.8274e-005 m^2
$A_{\max}$	2.8274e-005 m^2		

Table 6 Delta family nondimensional groups $\tau = 1.5ms$

$\hat{\delta}_1$	2.8346	$\hat{\delta}_2$	83.8568	$\hat{\delta}_3$	83.8568
$\hat{\delta}_4$	4.3633	$\hat{\delta}_5$	83.8568	$\hat{\delta}_6$	25.6984
$\hat{\delta}_7$	2.8346				

4.3.4 Simulation results of the two-way valve subject to the excitation of the pressure wave generator

Assuming the discharge pressure P_{dis} and the reservoir pressure P_r are perfectly constant, and the two-way spool valve is not connected to the downstream of the pressure wave generator, the simulation result of the pressure wave generator can be shown in Figure 21. This response is very similar to the experimental result conducted by Kobata in [36], except for that the experimental measurement in [36] has the characteristic of overshoot. The model of the pressure wave generator may be questioned, because the lack of capability of capturing the second order response. However, it should be remembered that the variable axial-piston pump in the pressure generation system also contribute to the dynamics of the system. It is suspect that the action of the swash plate causes the second order response.

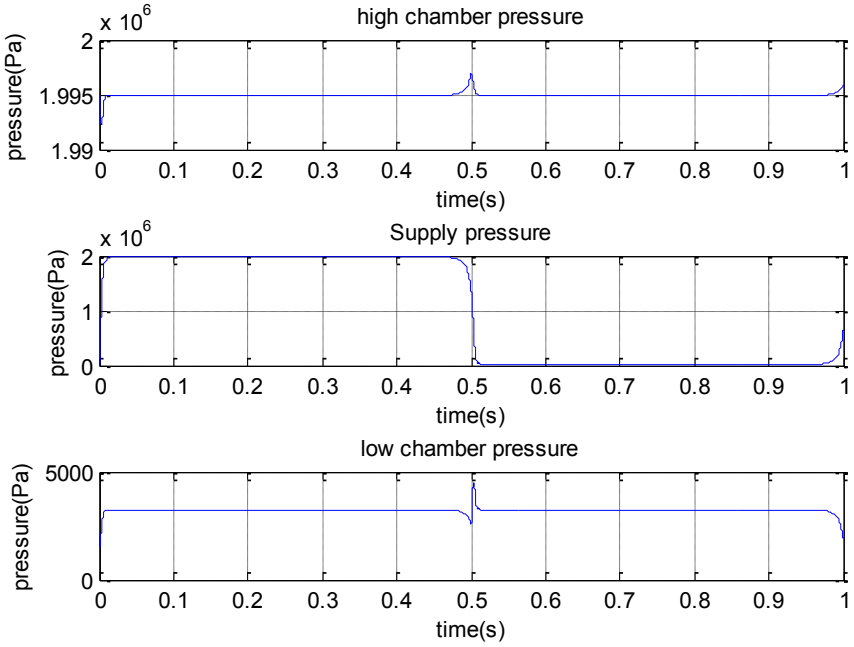

Figure 21 Response of the pressure wave generator with constant upper stream and downstream pressure

When the two-way spool valve described in Equation (19) is connected to the downstream of the pressure wave generator, the pressure dynamics is shown in Figure 22 and the corresponding flow forces are shown in Figure 23. In Figure 26 the maximum pressure rise rate is close to 500MPa/s, which will be proved by the experimental result shown in Figure 34 in the next chapter. It is predicted that the transient flow force that can be observed is only about $\pm$ 1N according to the theoretical model. However, this is not necessary true, because the steady state characteristic of the Bernoulli equation.

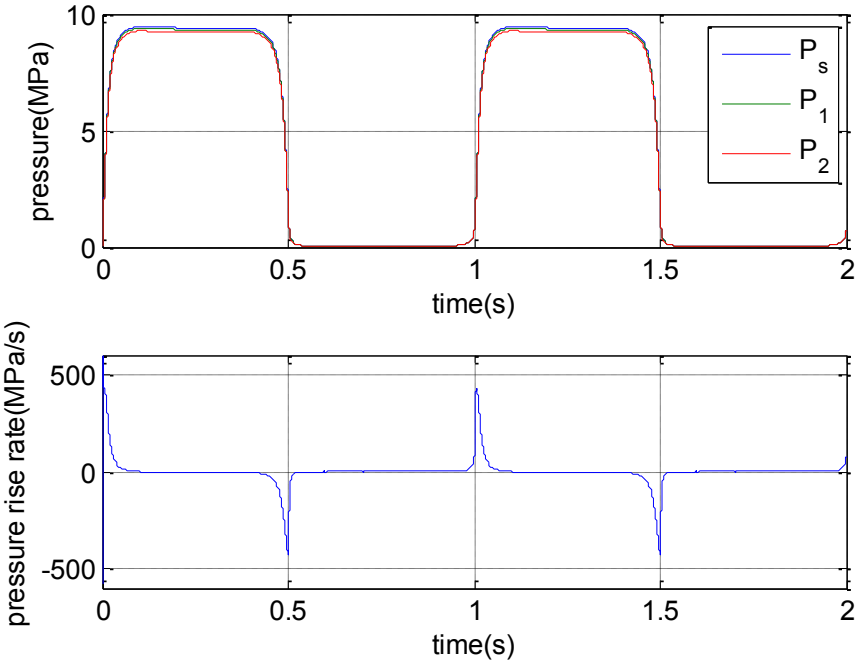

Figure 22 Response of system with a two-way valve in the downstream

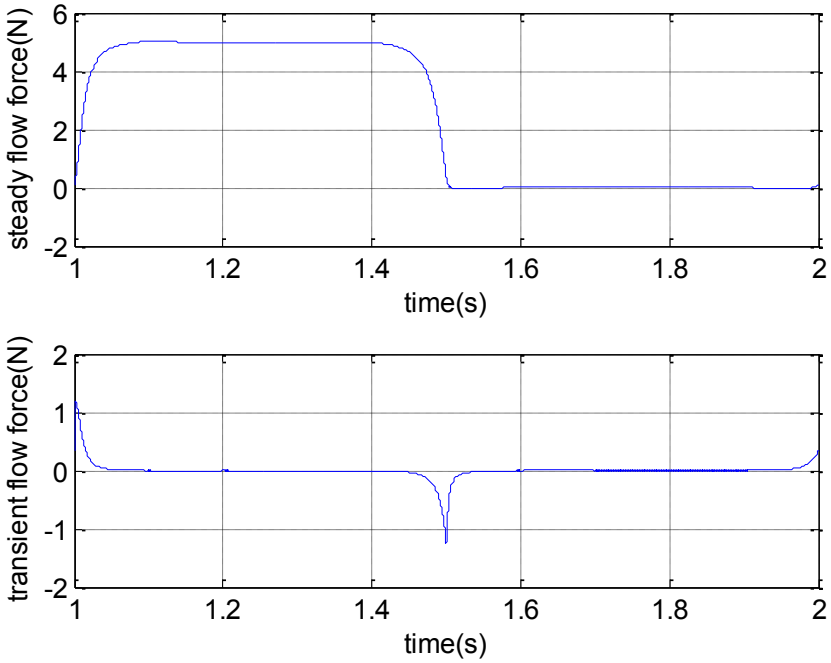

Figure 23 Simulated flow force

4.4 Accumulator

The accumulator is used to absorb pressure ripples from the axial piston pump. For a bladder type accumulator, the air in the bladder should be pressurized to the level near the operating pressure of the pump. As a result, when the pressure in the discharge line of the pump is perturbed around certain constant level, the sudden expansion and shrink of the bladder will attenuate the pressure ripple.

4.5 Summary

In this chapter, the structure of the pressure-wave generation system is introduced first. Three most important components of the pressure are described. The variable axial-piston pump and its control mechanism is shown to be able to stabilize the pressure around certain working condition and to be adaptive to the change in demanding volumetric flow rate. The bladder type accumulator is set to attenuate pressure ripples for certain working condition. Most importantly, a model is build for the rotary pressure wave generator. It is shown that it can produce a pressure wave, which is close to the previous experiments, and it is capable of making the transient flow force caused by pressure rise rate noticeable. However, it should be noticed that the mathematical model of the pressure wave generator does not include the dynamics of the pump, which can make the system to display the characteristic of overshoot. Furthermore, the simulated value of the transient flow force might not be accurate because the Bernoulli equation is essentially steady.

Chapter 5: Testing the Contribution of the Pressure Transient Effect Using a Valve with Extremely Small Leakage

5.1 General Experimental Steps

From the analysis in Chapter 2, it is known that the simplest way to estimate the flow force acting on a two-way spool valve is measuring the pressure at two ends of the piston and estimating the equivalent discharge coefficient across the valve body. The description involves with less error in the estimation of supply and return orifice discharge coefficient and the value of the jet angle. In Figure 24 a test valve housing and piston pare with clearance of about 10 μm is built to test the pressure transient effect. High pressure is supplied to the port on the top-right and the top-left port is connected to the reservoir. The two ports on the bottom of the picture will be used as sensor ports. In all the experiment of this Chapter, the return orifice will be restricted.

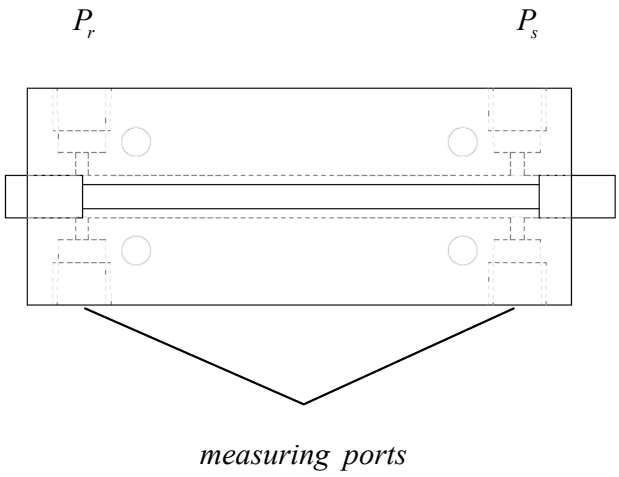

Figure 24 Valve configuration with two measuring ports

Due to the complexity of the flow force phenomenon, the structure of this chapter falls into the following steps:

1. Experimental proof of the sound wave phenomenon in the frequency domain;
2. Experimental proof of the pressure transient effect in the frequency domain;
3. Numerical computation of the pressure profile on the two ends of the piston and the calculation of pressure profile factor;
4. Estimate the equivalent discharge coefficient across the valve;
5. Calculate the difference between the averaged-measured flow force and the estimated steady flow force in time domain.

5.2 Transient Effect Concerning Sound Wave Phenomenon

Besides the pressure transient effect proposed in Chapter 2, the pressure wave can bouncing forwards and backwards and the flow force induced can be very oscillatory. It can be observed that the flow force in Figure 25 can vary between -10N to 30N without a pressure square wave generator in the circuit. The source of the sound wave in the valve can be the pressure ripple caused by the kinematics of the variable displacement axial piston pump because in Figure 26 and Figure 27 the signal of frequency 267Hz is identified and this value is very close to the 270 Hz piston passing frequency of the pump. The FFT or auto power spectral density of the measured flow force also shows that there are peaks around 30kHz, which is in the sound wave frequency range. With this kind flow-force variation, it becomes be very difficult to observe pressure transient effect proposed in Chapter 2. Therefore, the following methods may be employed to reduce the influence of sound wave phenomenon:

1. Filtering the measured signal by taking average of every 100 points and manually reduce the sampling rate from 100 kHz to 1 kHz. This reduced sample rate will enable to see the signal up to 500 Hz ;

2. Mitigating the wave by increase the energy loss at the wall and deliberately create a large pressure drop across the valve body.

The first method will be used in the current chapter because it does not require any geometry modification. The second method will be investigated in the next chapter.

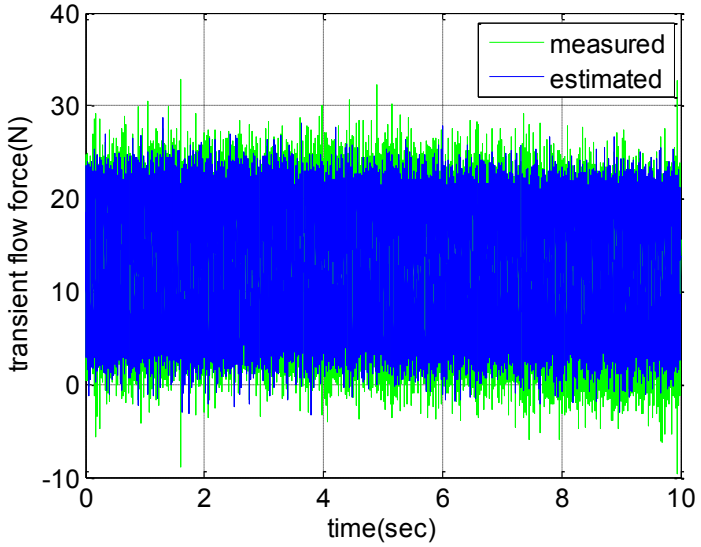

Figure 25 Strong oscillation within the measured flow force

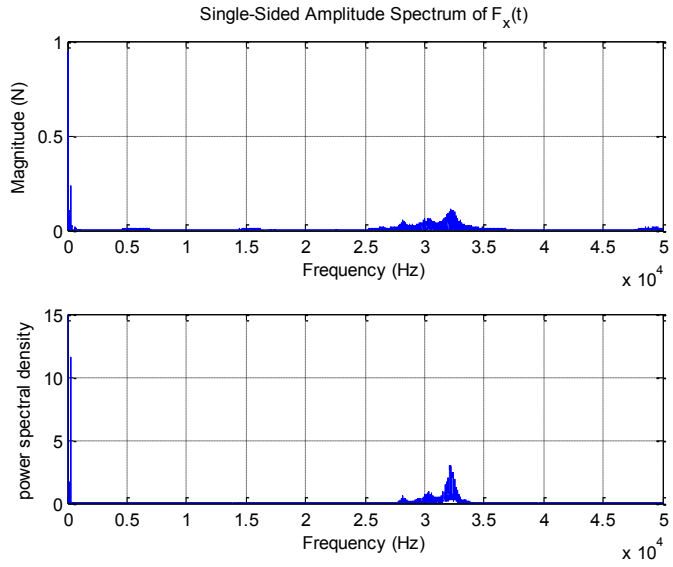

Figure 26 Broadband FFT and auto PSD of measured flow force

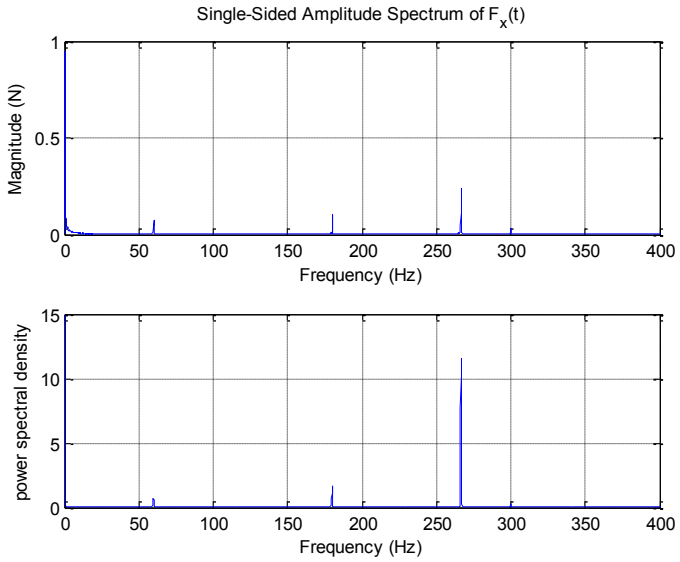

Figure 27 Narrow band FFT and auto PSD of measured flow force

5.3 Observing the Pressure Transient Effect in Frequency Domain

Although it is difficult to see the pressure transient effect clearly in the time domain, there is possibility to see its unique characteristic in the frequency domain. From the analysis in Chapter 2 the steady flow force can be represented by a function of pressure drop across the valve body. The function falls into a proportional function and a function of square root of pressure drop. For both proportional and square root relationship, the cross power spectral density (PSD) should only have one dominant peak at the zero frequency and the value of cross PSD will approach zero as the frequency increases. However the cross PSD in Figure 28 shows that there are peaks related to pump speed, pump piston passing frequency and sound wave phenomenon. As a result, it can be inferred that there is transient effect in the flow force. The transient effect between 30-400Hz in Figure 29 could be the transient effect proposed in Chapter 2 and the transient effect between 20-40kHz in Figure 30 is caused by sound wave phenomenon.

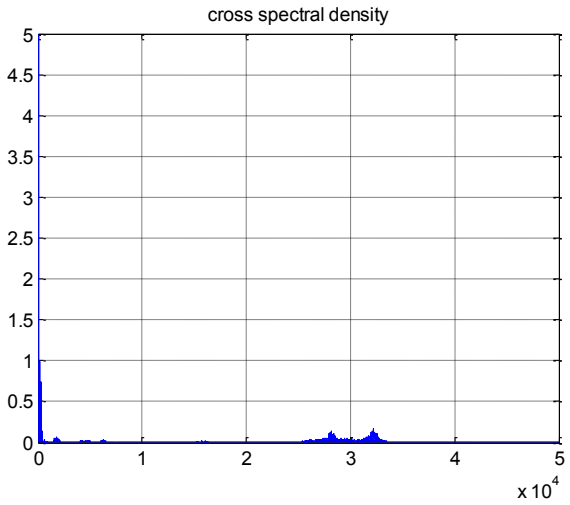

Figure 28 Cross PSD between pressure drop and measured flow force

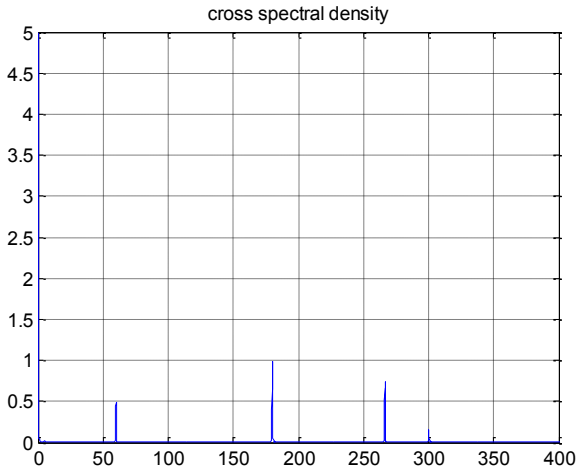

Figure 29 Cross PSD between pressure drop and measured flow force (low frequency)

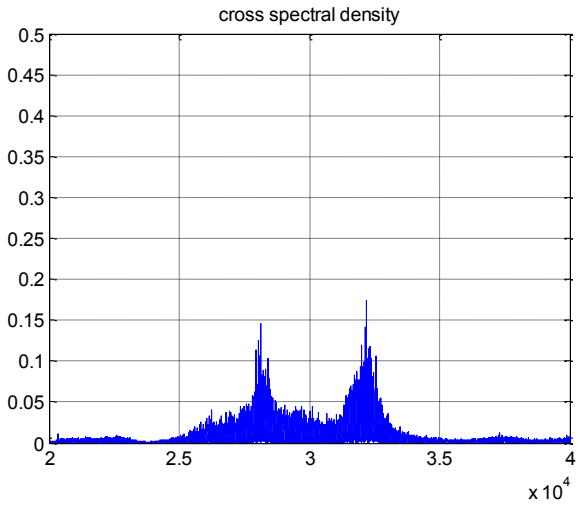

Figure 30 Cross PSD between pressure drop and measured flow force (high frequency)

Although the peak at the zero frequency is largest, it is not right to inferred that the relation between the two measured signal is mainly stationary. The power of the signal is represented by the area between the curve and the horizontal axis. Therefore the power falls between certain frequency range is presented in Table 7. It is known that the lower frequency signal only composes 8.092% of the total power, while the signal between 20-40kHz composes of 66.746%. The above characteristic shows that the sound wave phenomenon is dominant in the current experimental setup and indicate that it will be difficult to direct observe the pressure transient effect in time domain.

Table 7 Power distribution of the measured signal

Frequency range	Frequency percentage (%)	Power	Power percentage (%)	Power/ Frequency percentage ratio
0Hz-5Hz	0.01	16.8636	8.092	809.2
5.1Hz-50Hz	0.09	0.1569	0.075	0.8333
50.1Hz-500Hz	0.9	2.3117	1.109	1.232
500.1Hz-5000Hz	9	21.4856	10.310	1.146
5000.1Hz-50000Hz	90	167.5818	80.414	0.893
179.2Hz-180.8Hz	0.0032	0.5786	0.2776	86.75
265.5Hz-267.5Hz	0.002	0.4347	0.2086	104.3
20000Hz-40000Hz	40	139.0991	66.746	1.669
24000Hz-36000Hz	24	123.7534	59.383	2.474

5.4 Pressure Profile Factor Concerning the Pressure Distribution at the Two Ends of the Piston

In the analysis of Chapter 2 it is assumed that the pressure distribution at the two ends of the piston is uniform. However, in the trial steady state experiment, the estimated steady state flow force is still very far from the measured flow force, even when both pressure difference and viscous shear are taken into consideration. It is suspect that the reason is non-uniform distribution of the pressure on two ends of the piston. A trial CFD computation shows that the pressure distribution can be non-uniform in Figure 31. It

should be noticed that the pressure and vertical position are normalized in order to accommodate different pressure and dimension combination. Because of the Bernoulli effect, the fluid velocity in opposite side to the supply and return orifice will be comparative lower and the corresponding pressure will be higher. If our sensor is placed near those points, where the nondimensional vertical position is one, the actual average pressure difference will be larger than the measured value, because the pressure gradient in the vertical direction is much larger near the return orifice than near the supply orifice. In order to counter this assumption error, it is proposed to used the following pressure profile factor in the computation

$$C_{profile} = \frac{\Delta P_{averaged}}{\Delta P_{measured}}. \tag{72}$$

From the curve in Figure 31 the estimated $C_{profile}$ is 3.2. Because the CFD result is in two-dimensional world and the real measurement is taken in a three dimensional world, the actual profile factor can be different. Since there can hardly be a better way to accurately describe this phenomenon in a parametric way, the factor 3 will be used in this chapter. This nondimensional factor will later be proved accurate in steady state in this chapter even the two-dimensional CFD analysis does not match the actual three-dimensional structure in physical dimension. However, the validity of the pressure profile factor is very likely be not right in transient process.

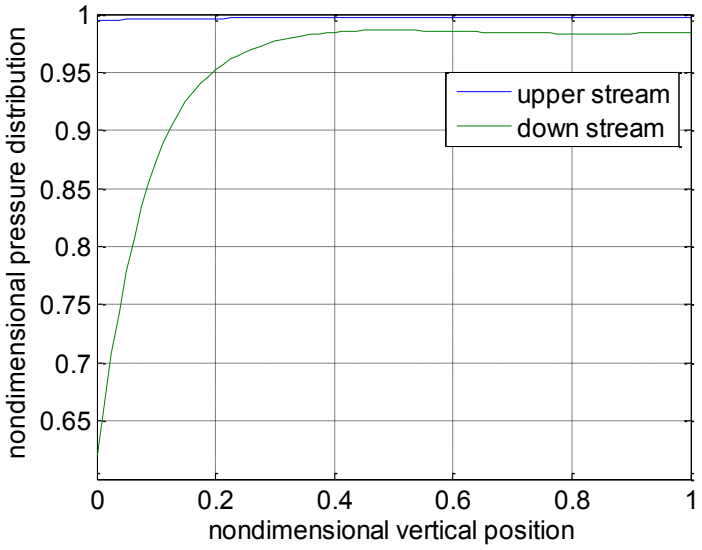

Figure 31 Pressure distribution at the two ends of the piston

The polynomial curve fitting for the two pressure profiles are

$$\begin{aligned}\hat{P}_{send} &= 0.3285\hat{y}^8 - 1.2787\hat{y}^7 - 2.0206\hat{y}^6 - 1.6786\hat{y}^5 + 0.7945\hat{y}^4 \\ &-0.2102\hat{y}^3 - 0.0185\hat{y}^2 + 0.0079\hat{y} + 0.9949, \\ \hat{P}_{rend} &= 3.1469\hat{y}^8 + 1.3415\hat{y}^7 - 39.9211\hat{y}^6 + 91.6662\hat{y}^5 - 98.2847\hat{y}^4 \\ &+59.1099\hat{y}^3 - 20.8218\hat{y}^2 + 4.1296\hat{y} + 0.6176,\end{aligned} \tag{73}$$

and are shown in Figure 32, where

$$\hat{P}_{send} = \frac{P_{send}}{\max\left(P_{send}\right)}, \hat{P}_{rend} = \frac{\hat{P}_{rend}}{\max\left(P_{send}\right)}, \hat{y} = \frac{y}{\max\left(y\right)}. \tag{74}$$

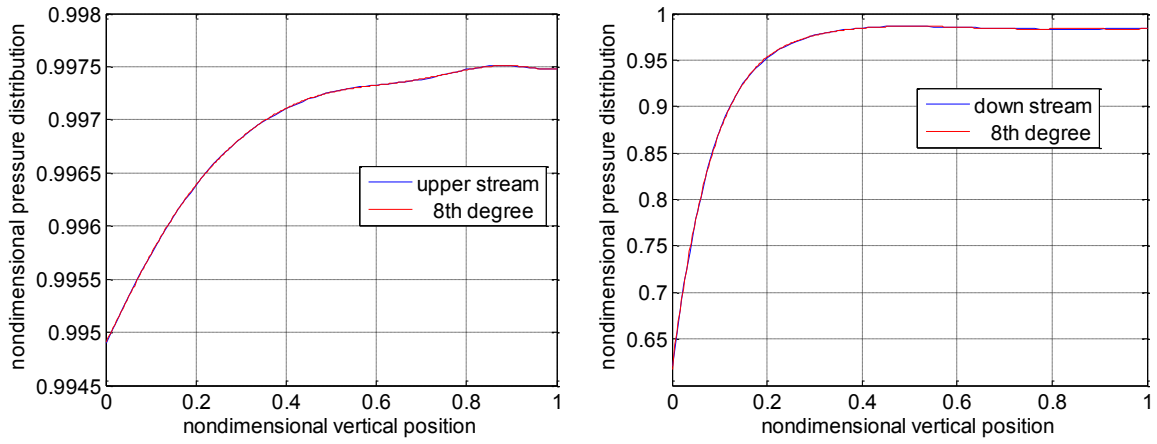

a) b)

Figure 32 Curve fitting for the pressure profile on the two ends of the piston

5.5 Observing the Pressure Transient Effect in Time Domain

After connecting the pressure square wave generator in the circuit, the flow force and pressure drop across the valve body are shown to be very oscillatory and their 100 point average is proved to be a good approximation that eliminate most of the sound wave phenomenon in Figure 33 with corresponding pressure rise rate in Figure 34.

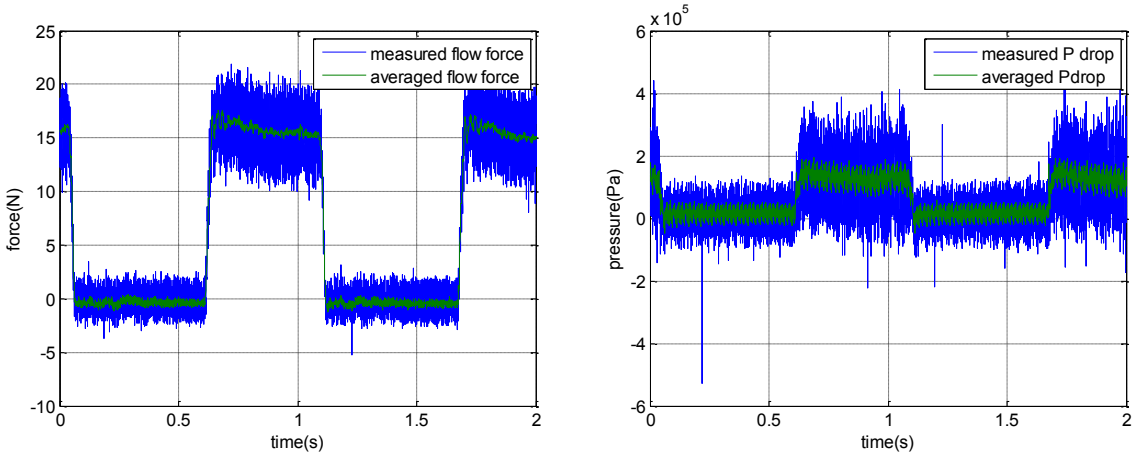

a) b)

Figure 33 Measured flow force, pressure drop and their average

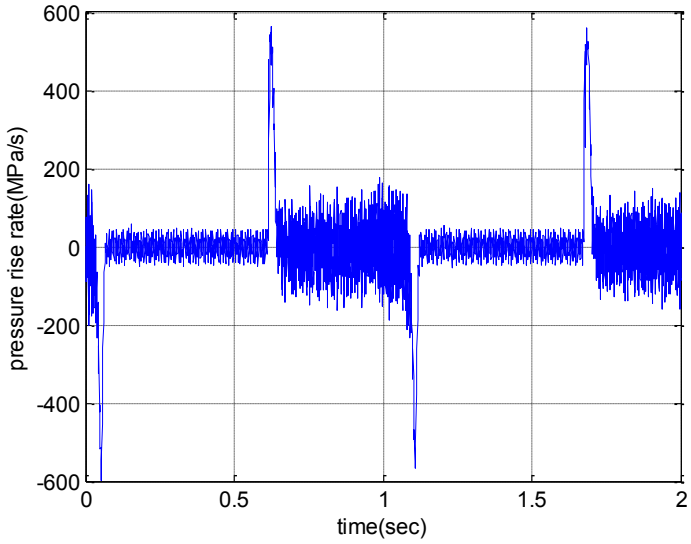

Figure 34 Computed pressure rise rate from the measured data

Considering the pressure profile factor, the estimated discharge coefficient C_{d2} is 0.3. The measured flow force and estimated flow force from measured pressure drop is shown in Figure 33 a). The corresponding difference between the two signals are given in Figure 35 and it is easy to observe that there are large spikes of flow force matching the position of sudden pressure rise and fall. When the fluid is accelerating, the direction of the flow force spike is positive while the decelerating fluid will induce a flow force spike in the negative direction. The magnitude of these pressure spikes is between 15-20N, which is almost the same as the theoretical steady flow force. Thus, it can be conclude that the pressure transient flow force can be very important, when the pressure rise rate is high.

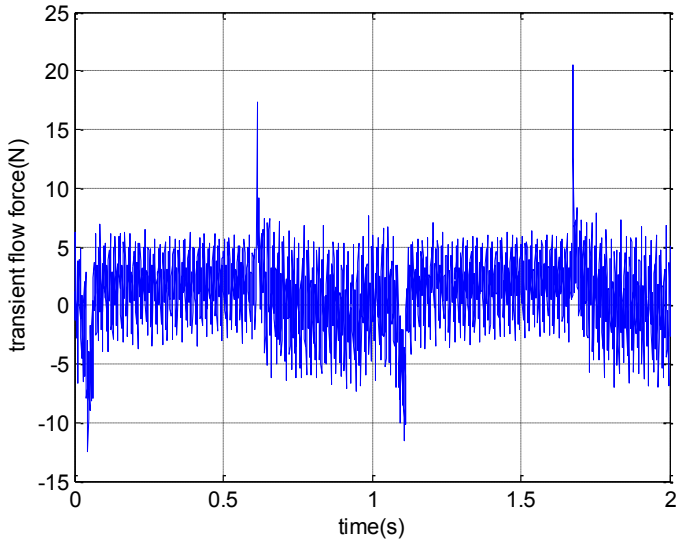

Figure 35 The difference between measurement and estimation

5.6 Summary

In this chapter, an experiment setup using only the measurement of the pressure drop across the valve body is built. It is first discovered in frequency domain that the sound wave phenomenon exist in the extremely high frequency and it can be the dominant phenomenon in the flow force. This discovery beyond the analytical result in Chapter 2 indicates that the high order other than the proposed pressure transient effect can exist. The steady state flow force measurement also implicitly indicates that the pressure drop across the valve body can be very un-uniform and this phenomenon is confirmed by CFD analysis. By introducing the 100-points average and a pressure profile factor it becomes possible to accurately estimate the steady flow force and finally the pressure transient effect is proved to be true by comparison between measured flow force and estimated flow force.

Although the 100-points average technique and the pressure profile factor can help in proving the pressure transient effect, it involves the manipulation of the acquired

data, which may cause some problem. In the next chapter, geometry modification will be used instead.

Chapter 6: Testing the Contribution of the Pressure Transient Effect Using a Valve with Large Leakage

6.1 General Experimental Steps

From the analysis in Chapter 2, it can be inferred that the pressure transient term can be observed in two ways: the equilibrium condition of the valve piston and the equilibrium condition of the fluid control volume. In the first way, the pressure transient term is the difference between the total flow force and the summation of the steady pressure difference term and viscous shear term. In the second way, the pressure transient term is the difference between total flow force and the summation of the steady viscous shear term and the momentum term. The experimental setup in Chapter 5 will require additional manipulation on the acquired data to compared the two theory. In this chapter, the following geometry modification is added to reduce the influence of sound wave phenomenon and non-uniform pressure profile at the two ends:

1. The pressure drop across the valve body is increased by longer valve body and a smaller bore diameter near the center;
2. The clearance between the piston and the bore is increased (0.05mm) to reduce the energy that can be reflected at the surface and reduce the pressure gradient in the vertical direction.

In Figure 36, the valve chamber length is twice the length of the valve in Chapter 5 and there is a step size of 1 mm near each end of the piston bore. Because of this additional step manufactured, the equilibrium condition of the fluid in the control volume requires additional pressure difference term related to these two annular area to be

satisfied. Even the additional pressure difference term can be computed from the measured pressure drop, it becomes difficult to match the two equilibrium condition, because the difficult to measure the pressure distribution on the step geometry. Therefore, the equilibrium condition for the valve piston is chosen in the current chapter as the major way to prove the existence of pressure transient effect, while the equilibrium condition of the fluid in the control volume is selected as a reference.

In order to test the pressure transient effect with velocity term excluded, the valve piston is fixed with respect to the valve housing in Figure 36. Multiple ports are machined on the valve housing to facilitate measuring the pressure at difference location of the valve piston chamber as well as changing the relative position of the supply line and return line. Because there are only two piezo-electric pressure sensors, the rest of the ports will be caped during the experiment. The experimental proof of the pressure transient effect will be conducted in the following steps:

1. Minimize the frictional force in experiment;
2. Prove that the in steady state flow the measured steady state pressure difference force matches the analytical solution in Chapter 2;
3. Experimentally estimate the discharge coefficients and prove that the viscous shear force matches the analytical solution in Chapter 2;
4. Measuring the flow force under the excitation of the pressure wave generator and subtract the estimated steady state flow force from the measured flow force to observe the pressure transient effect;
5. Test the pressure transient effect with different damping length and the same valve chamber length by changing the supply port position.

This chapter will be organized following these steps.

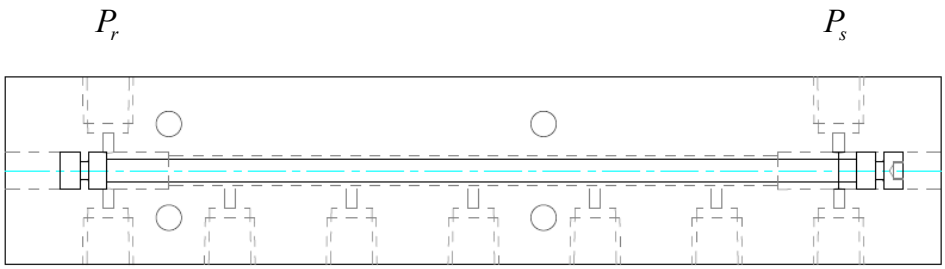

Figure 36 Valve configuration with multiple measuring port

6.2 Minimize Frictional Force

Before running in to the problem of how to verify the theoretical solution in Chapter 2, the size of friction f should be first estimated experimentally. If the magnitude of friction is too large compared with the flow force, the measurement will be overwhelmed by friction and it is difficult to tell whether the difference between the measurement and the theoretical steady flow force is the pressure transient effect. Therefore, it is necessary to minimize the frictional force. When there is no seal ring is installed on the valve piston, the static friction is about $\pm$ 1N in measurement. When a pair of seal rings is installed on two ends of the piston to eliminate leakage, the static friction is about $\pm$ 16N. Therefore, from the point of view to minimize frictional force, it is preferred to use the piston without a seal ring. To make sure that the additional leakage does not contaminate the measurement, the leakage flow is collected and the estimated flow force induced by the momentum of the leakage flow is in the order of 10^{-3} N. Thus, it can be conclude that eliminate the seal ring induced less unwanted force in the measurement. Any difference larger than $\pm$ 1N between the measured flow force and the theoretical steady flow force is contributed by the pressure transient effect.

6.3 Prove the Validity of Analytical Solution in Steady State Pressure Difference Force

It is proposed that the steady state flow force can be decomposed into the pressure difference term and viscous shear term in Chapter 2 Equation(1). This section will be devoted to prove this statement experimentally. In this step, the pressure square wave generator is removed from the circuit in Figure 15 temporary, and the two-way spool valve is directly connected to the high-pressure line. In addition, the two-way spool valve will be positioned, so that both supply orifice and return orifice will be fully open. These settings are selected in order to create a geometry, which is nearly symmetric, such that difference between the magnitudes of two jet angles is small. In addition the fully opened return orifice can make the pressure drop coefficients C_{fxms} and C_{fxmr} smaller than C_{fxp} as shown in Figure 6. Thus, the influence of the steady state momentum force caused by momentum flux across the valve is greatly reduced. The supply and return pressure then will be driven to steady state when certain amount of time such as 10 seconds has elapsed, and the measured steady state flow force is shown in Figure 37. In this picture, the measured flow force contains high frequency signal, which can be caused by pressure ripple from the pump, hose vibration and other un-modeled dynamics. Despite the high frequency perturbations and noise, the average value of the steady state flow force falls near 31N. According to the classic theory, when the valve geometry is nearly symmetric, the steady flow force caused by momentum change and should be very small. The measurement in Figure 37 simply proves that the classic theory cannot predict the correct magnitude of the steady flow force, because the important viscous shear term and pressure difference term is neglected. The conclusion about the recirculation land is also

problematic, because they do not account for the pressure difference term caused by the recirculation land.

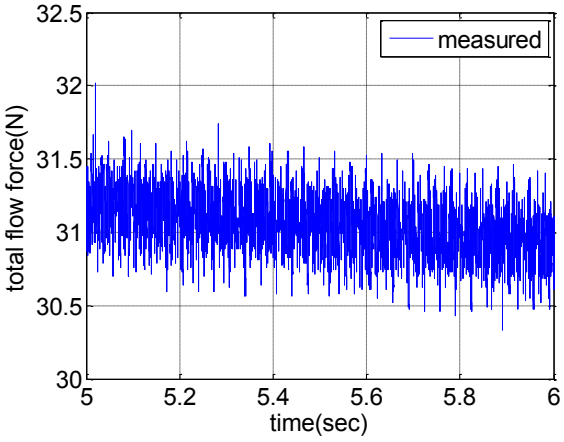

Figure 37 Measured steady state flow force

With all the settings including the controller of the variable axial-piston pump unchanged, the measured pressure from port number 1 to port number 7 is presented in Figure 38. The pressure drop across from port number 1 to port number 7 is nonlinear, but the pressure drop from port number 2 to port number 5 is very close to a linear function. This measurement partially confirms the steady CFD results in Figure 39.

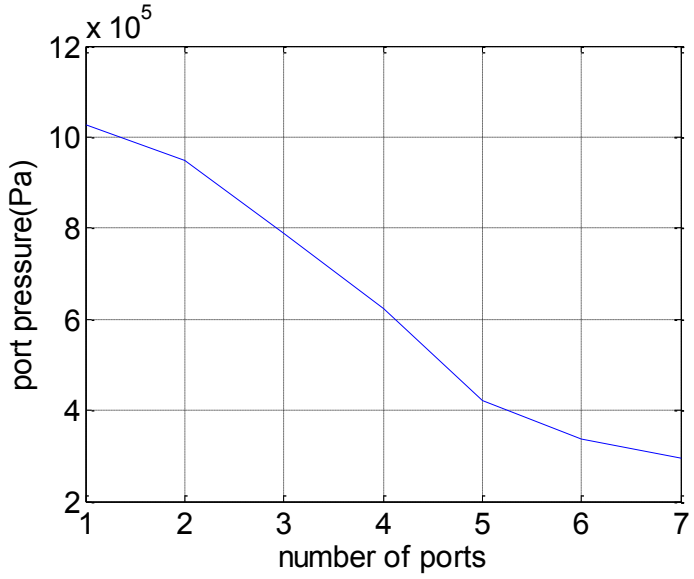

Figure 38 Measured pressure drop across valve body

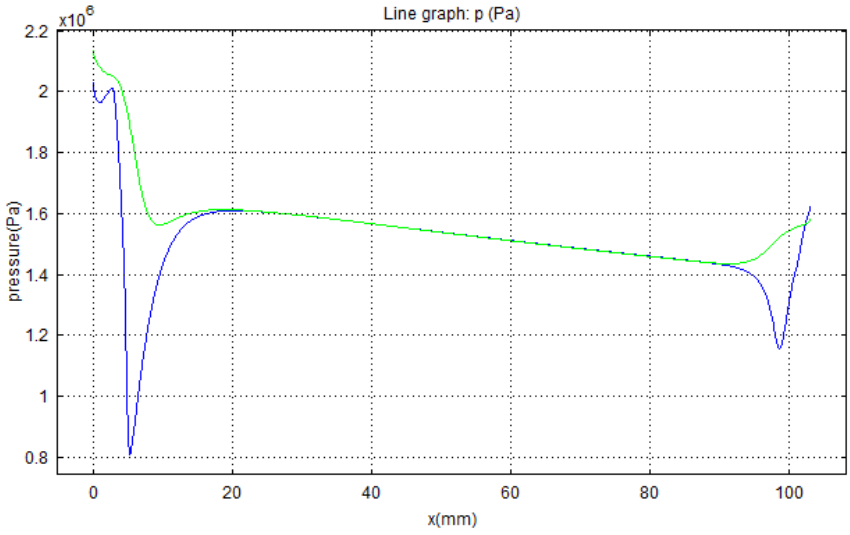

Figure 39 CFD results on the pressure drop across the valve body

The measured pressure drop from port number 1 to port number 7 is about 0.731MPa. Compared with the supply pressure, which is 1.19MPa, the pressure drop is about 61.43%. This large percentage indicates that the classic model, which does not account for the pressure drop across the valve piston chamber, might be not right in the current case of a very long valve piston chamber. It should be emphasized that the

experimental measurement does not show that the pressure drop across every valve piston chamber is important. For a valve with short valve piston chamber in Figure 40, the pressure drop across the valve piston chamber is very small compared with the pressure drop across the supply and return orifice.

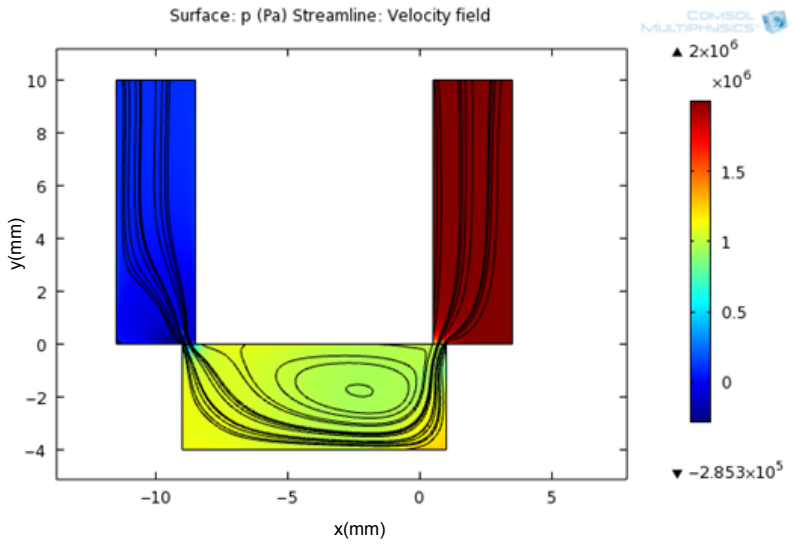

Figure 40 Pressure field with a short valve piston chamber and symmetric supply and return orifice

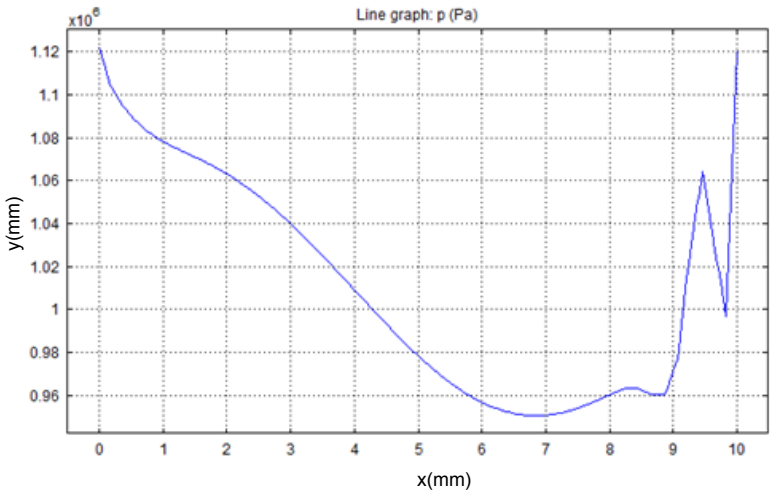

Figure 41 Pressure drop with a short valve piston chamber and symmetric supply and return orifice

As a result the pressure drop across the valve piston chamber should be modeled for the valve with long valve piston chamber. Assuming that the pressure on the cross section of the control volume is nearly uniform at the two ends of the piston, the estimated flow force caused by pressure difference can be calculated based on the following expression

$$F_{Pdiff} = A_v \left(P_{no1} - P_{no7} \right), \tag{75}$$

where P_{no1} and P_{no7} denotes the pressure in port No. 1 and port No.7 respectively. The corresponding estimated value for F_{Pdiff} is 36.05N from Figure 38. This estimated value is higher than the measured flow force, because part of the pressure difference caused force is canceled by viscous shear force as shown in Equation (1). In order to estimate the viscous shear force using Equation (39), discharge coefficient C_{d2} is required. Because the value of C_{d2} is temporarily unknown in this stage, it is impossible to estimate the viscous shear in this section. However, it can be conclude that the magnitude of the viscous shear on the valve piston is about 5N, which is 13.89% of the pressure difference caused force. This ratio is close to the ratio of $\hat{\lambda}_5 / \hat{\lambda}_4 = 11.26\%$ in Table 3. The error between them might be caused by the error in the estimation of surface roughness. It should be emphasize that the measured pressure drop does not satisfy the viscous laminar Hagen-Poiseuille equation

$$\Delta P = \frac{8 \mu Q L}{\pi D_h^4}. \tag{76}$$

The estimated pressure drop from Equation (76) is only 0.169MPa, which is much smaller than the measured value. Thus, it can be conclude that the Hagen-Poiseuille

equation cannot be used in this dissertation to estimate the pressure drop across the valve body. The major reason for the difference is mainly the low-Reynolds number characteristic of the Hagen-Poiseuille equation. When Reynolds number becomes larger, the fluid will be turbulent, leading to larger pressure drop than would be expected according to Hagen-Poiseuille equation. The surface roughness not accounted in the Hagen-Poiseuille equation also lower the threshold of the onset of turbulent flow. As a result, the fluid flow in the experiment is more likely to be turbulent flow, even when the Reynolds number is only several hundred.

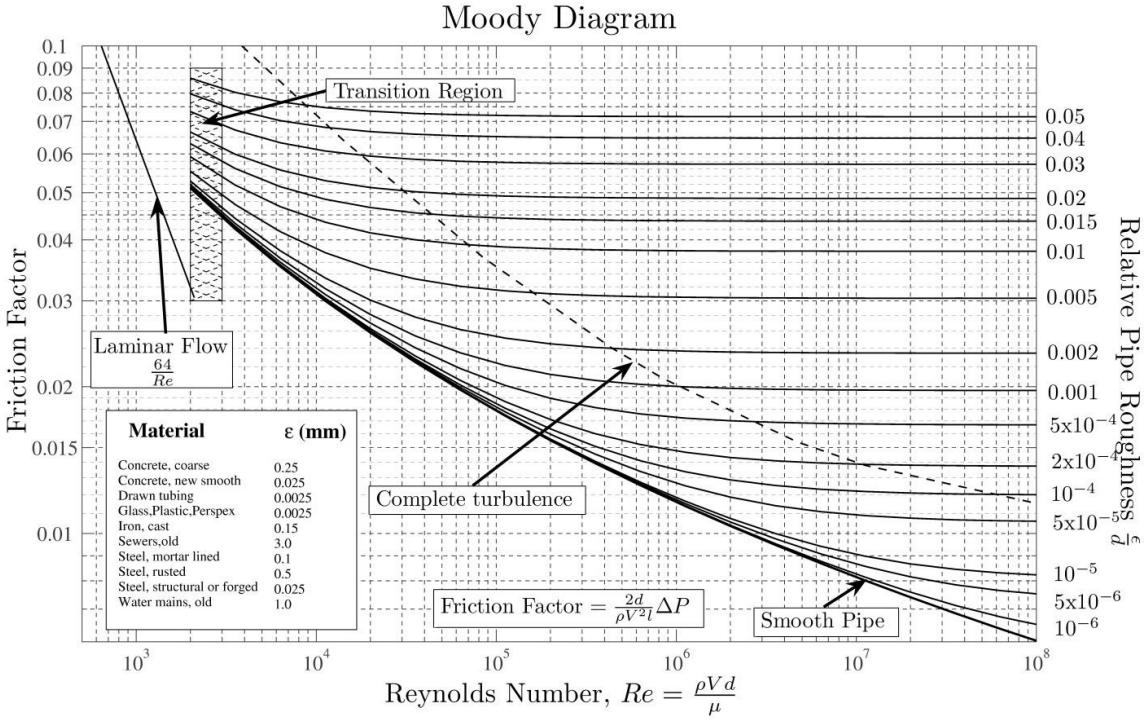

Figure 42 Moody diagram

The estimated Reynolds number is about 190.8 and from Moody diagram, the flow is still laminar. Thus, the frictional factor is about 0.34 based on $Frictional \quad factor = 64 / \mathrm{Re}$ and the corresponding pressure drop is about 0.367MPa. This

value is higher than the estimation from Hagen-Poiseuille equation, but lower than the experimental measurement. Noticing that the Moody diagram is used to describe pipe flow, which is different from the flow in the annular passage, the estimation will surely be different from the measurement.

6.4 Discharge Coefficient Estimation and the Validity of Steady State Viscous Shear Force

In the previous section, the validity of steady state flow force, especially the pressure difference term, has been proved. In this section, the discharge coefficients will be estimated experimentally and validity of Equation (38) concerning the viscous shear force will be investigated. In order to model the system more accurately, discharge coefficients for the supply orifice C_{d1} and return orifice C_{d3} should be estimated separately by measuring the volumetric flow rate and the pressure drop across the supply and return orifices with the pressure wave generator removed from the system that is being tested. When measuring the supply orifice, the flow meter is placed before the fluid enters the two-way valve, while measurement for the return orifice is taken by the flow meter placed after the fluid leaves the two-way valve. Table 8 shows the estimated discharge coefficient. The first two cases are for supply orifice with orifice fully open, the rest are for the return orifice which is only half open. For each of the estimation, six repetitive measurements are averaged to the get the final values in Table 8. The estimated discharge coefficients for supply orifice and return orifice are estimated to be 0.76 and 0.62 respectively. Therefore it can be inferred that the supply orifice causes less restriction that the return orifice. The discharge coefficient for the return orifice is very close to the classic value, because the tube is under contraction. The discharge coefficient for the

supply orifice is larger, because expansion cases less pressure loss than contraction. While measuring the discharge coefficient, it is noticed that the pressure to the downstream of the supply orifice can be larger than the pressure to the upper stream of the return orifice. This phenomenon again confirms the discovery in the previous section.

Table 8 Estimated discharge coefficients

Case	Pressure in the upstream (MPa)	Pressure in the downstream (MPa)	Volumetric flow rate($10^{-4} m^3 / s$)	Discharge coefficient
1	1.19	1.03	1.02	0.756
2	1.51	1.30	1.17	0.758
3	0.84	0.14	0.87	0.617
4	0.695	0.126	0.785	0.615

The discharge coefficient estimated from Equation (24) is about 0.1147. With the all three discharge coefficients estimated, the viscous shear force computed from Equation (39) is about 4.74N. This theoretical value is very close to the difference between the measured flow force the theoretical value for pressure difference force. Combined with the theoretical pressure difference force, the error between the theoretical steady flow force and the measured flow force is only 0.94%. This error can be contributed by the non-uniform pressure distribution on the cross-sectional area of the control volume and the error between the parabolic velocity profile and the real velocity profile.

6.5 Prove the Pressure Transient Effect

To prove the pressure transient effect in the flow force, the pressure wave generator should be connecting the variable axial-piston pump and two-way spool valve. When the variable axial-piston pump is turned on, the two-way spool valve will be excited by the pressure wave generated. In the experiment that will be conducted in the current section, the supply orifice is still uninfluenced by the valve displacement, while the return orifice area can be changed by valve displacement. In order to estimate the steady state flow force with higher accuracy, it is necessary to measure the circular orifice opening. Because the orifice opening is deep inside the National Pipe Thread (NPT) hole and the diameter is only 3 mm, it becomes impossible to use instruments such as caliper to measure the orifice opening. Therefore it is recommended to take picture of the valve opening as shown in Figure 43 and calculate the orifice area based on the magnified picture.

Figure 43 Real valve opening geometry

With two piezo-electric pressure sensors installed before and after the two-way valve, the upper stream supply pressure P_s and downstream return pressure P_r is measured. The total flow force is measured simultaneously using a piezo-electric force sensor. In a

trial experiment, the supply pressure P_s, the return pressure P_r, the estimated flow force and the measured flow force are shown in Figure 44. Estimation 1 is from the equilibrium condition of the valve piston, while estimation 2 is from the equilibrium condition of the fluid in the control volume. The second estimation cannot predict the correct steady state value because the measured pressure drop is not the pressure drop between the two step surfaces. The difference between the 1st estimated steady flow force and the measured flow force is shown in Figure 45. It is noticed that the signal in Figure 45 is subject to high frequency perturbation with the magnitude of 2 N. This variation can be contributed by pressure ripple, sound wave phenomenon, friction and sensor noise. Moreover, there are two spikes happen simultaneously with the existing rising and falling edge of the pressure wave. The magnitude of the pressure spike is more than 7 N, which is unable to be caused by the uncertainties within the system. Thus, these spikes prove the existence of the pressure transient effect. However, it should be noticed that only the direction of the transient flow force corresponding to the rising edge is right, while the direction of the transient flow force corresponding to the falling edge is opposite to the simulated theoretical prediction in Figure 23. The inconsistency between the theoretical pressure transient effect and the measured pressure transient effect may be contributed to the steady state feature of the orifice equation and the complexity of the fluid flow structure change that will be shown in the next Chapter.

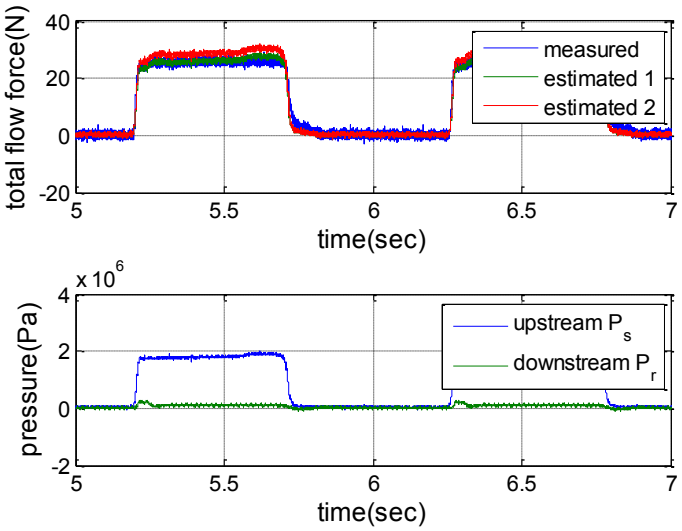

Figure 44 Response of the system in a trial test

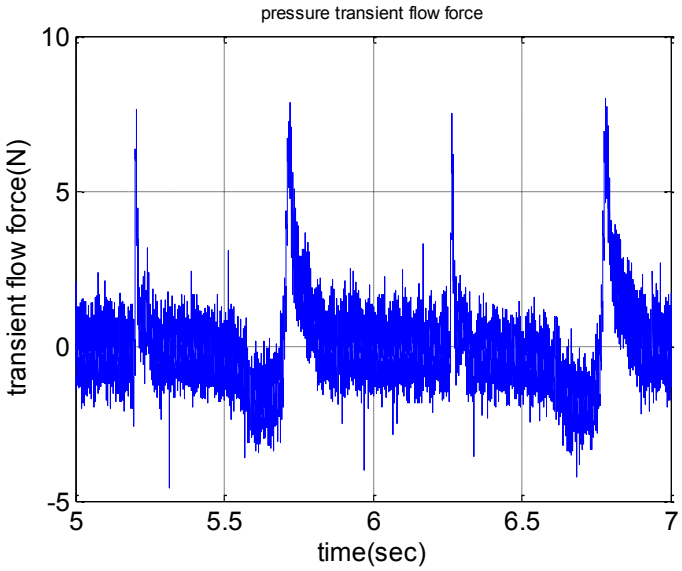

Figure 45 Pressure transient in the trial test

6.6 The Influence of Damping Length Over Pressure Transient Effect

In order to test the pressure transient effect with different damping length, the supply port is moved from the upper side to the lower side with seven ports. Then multiple tests are conducted, when the supply port is moved from port number 1 to port

number 6. Port number seven is avoided, because the definition of damping length is zero in this configuration. The responses of the system are shown in Figure 47. The difference between the measured flow forces and the estimated steady flow forces are shown in Figure 48.

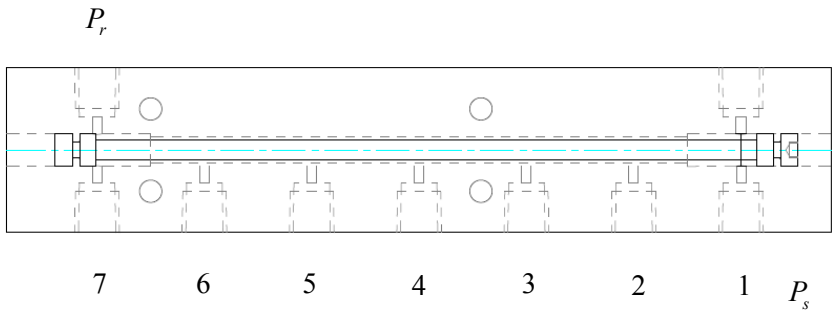

Figure 46 Valve configuration with changing supply port position

From Figure 47and Figure 48, it can be observed that the pressure transient spikes coincide with the falling edge of the pressure wave is wider than the pressure transient spikes coincide with the rising edge of the pressure wave in general. The pressure transient effect becomes stronger when the supply port and the return port are closer. In the fifth and sixth picture in Figure 47, the green curve shows the steady state results, which is related to the theoretical steady state results. According to this steady state solution, the flow force will increase when the pressure drop increases. However, the measured flow force drops during the rising edge of the pressure wave.

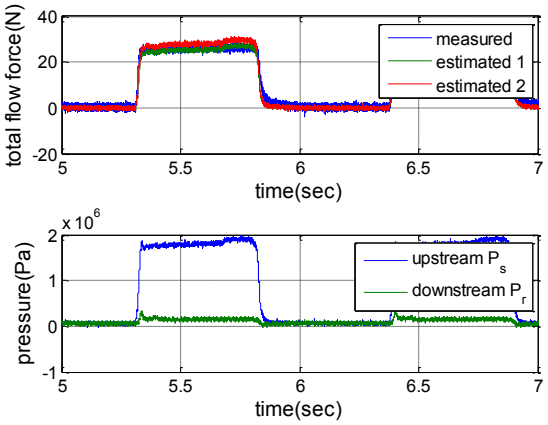

a) port number 1

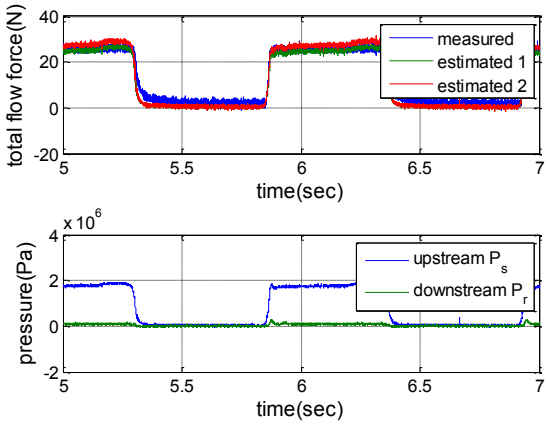

b) port number 2

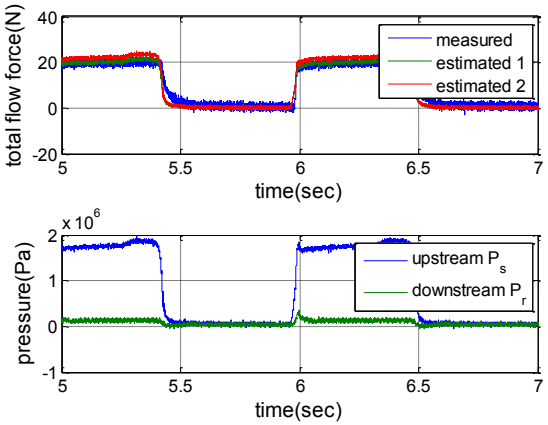

c) port number 3

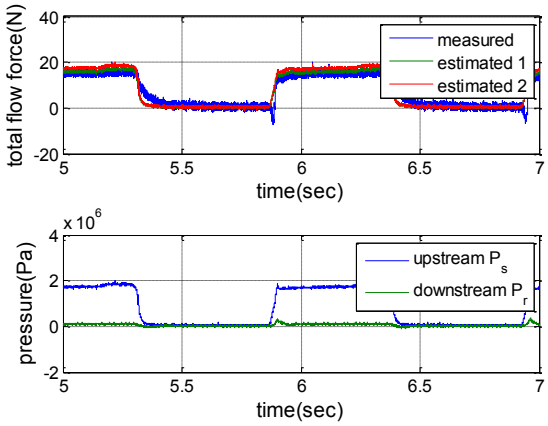

d) port number 4

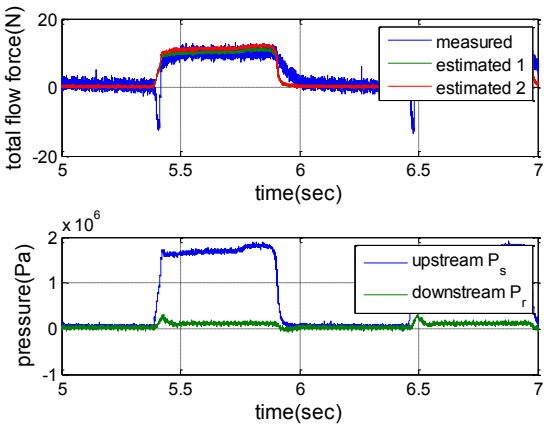

e) port number 5

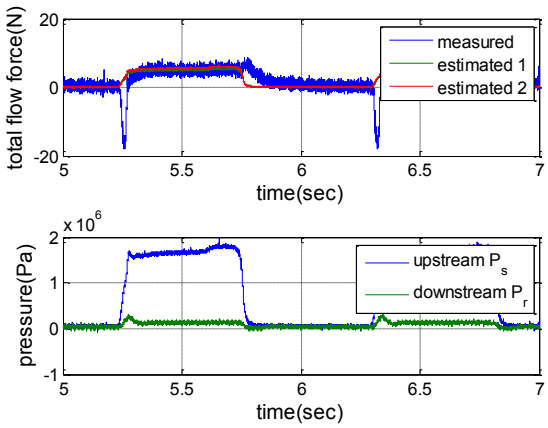

f) port number 6

Figure 47 Response of system with different damping length

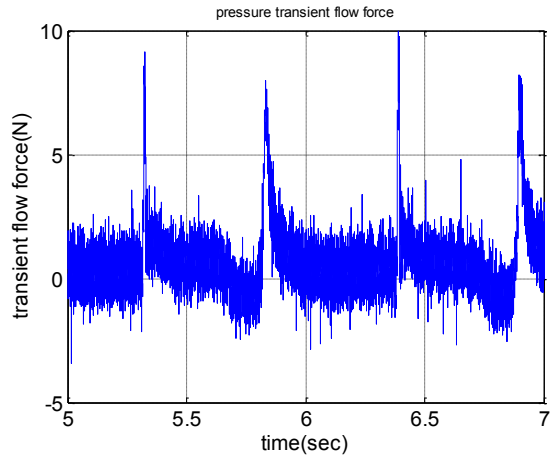

a) port number 1

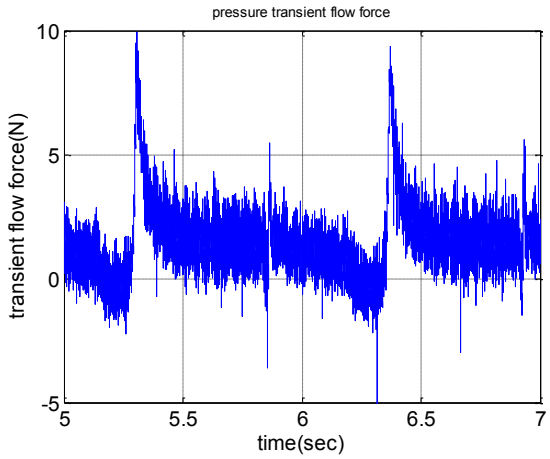

b) port number 2

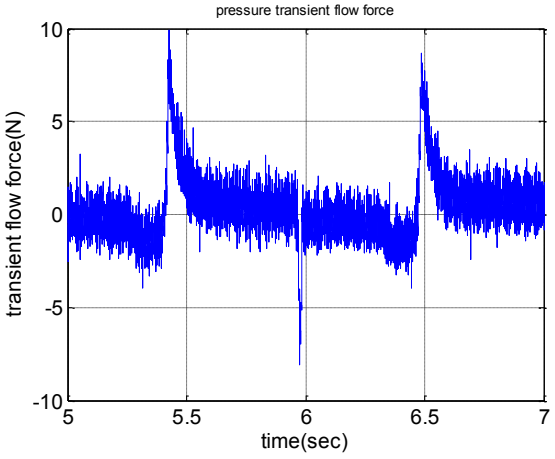

c) port number 3

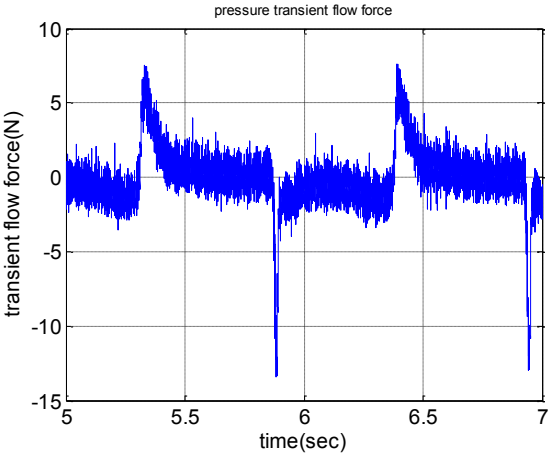

d) port number 4

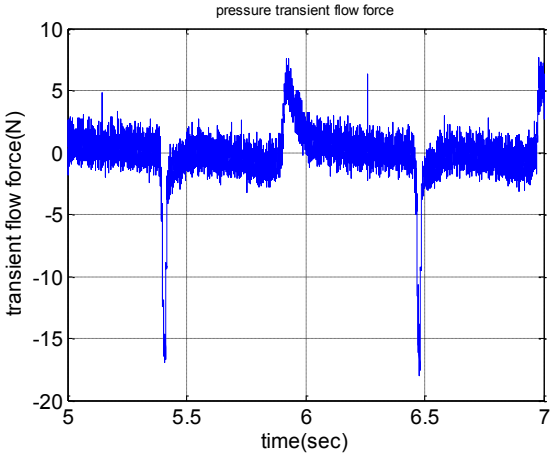

e) port number 5

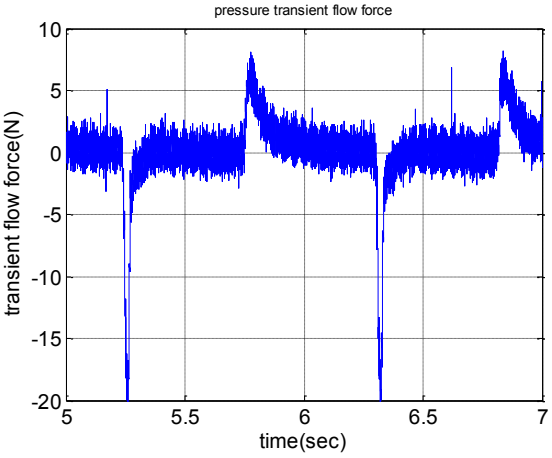

f) port number 6

Figure 48 Pressure transient effect with different damping length

It seems that the theoretical pressure transient effect fails to predict the change of direction of the pressure transient flow force. The reason might be the incapability of taking the momentum of the fluid between the supply orifice and the right end of the piston into consideration. When the supply pressure suddenly changes, the fluid between the supply orifice and the return orifice will be moving. However, the classic theory is assuming the fluid in this section to be stationary.

6.7 Summary

In the current chapter the steady state theoretical flow force is first validate by experiment by measuring pressure on two-ends of the valve piston and estimating the discharge coefficients. Then existence of pressure transient effect is proved by showing the difference between measured flow force and theoretical steady flow force. However, the direction of the transient flow force corresponding to the falling edge does not match the predicted direction based on the one-dimensional momentum conservation in Chapter 2. In addition the magnitude of the pressure transient flow force is much larger than the estimation in Chapter 4.

Furthermore, the influence of damping length L is tested experimentally. It can be observed from the measured pressure transient effect that the pressure transient flow force will not decrease, when the damping length L decreases. The reason for the above inconsistency between the theoretical pressure transient effect and the measured pressure transient effect can be contributed by the complexity of the unsteady flow field in the valve chamber.

Chapter 7 Preliminary Transient Computational Fluid Dynamics Results

It is suspected that the difference between the analytical transient flow force and the measured transient flow force is caused by the complexity of the flow field within the valve. This chapter will be devoted in investigation the geometry of the flow field within the valve and its evolution with respect to time.

7.1 Valve with Damping Length Close to Valve Chamber Length

Because of the limitation of the computer that will be used in this research, the original three-dimensional turbulent flow is reduced to a two-dimensional turbulent flow and the length of the valve chamber is reduced to emphasize the influence of the orifice instead of the pipe flow. The fluid will flow from the inlet on the right-hand side to the outlet on the left-hand side. The inlet boundary pressure is assumed to rise from zero to 2 MPa in 10 ms. Then the evolution of flow field within the valve is shown in Figure 49. At the beginning of the process, the fluid flow is laminar, because the pressure difference between inlet and outlet is relative low and the Reynolds number is low. As a result, the flow field in the first picture in Figure 49 shows streamlines close to the shape of the valve chamber. As the pressure increases, some of the streamlines are detached from the valve housing, and a vortex is born and grows. Finally, when the time elapse reaches infinity the vortex disappears.

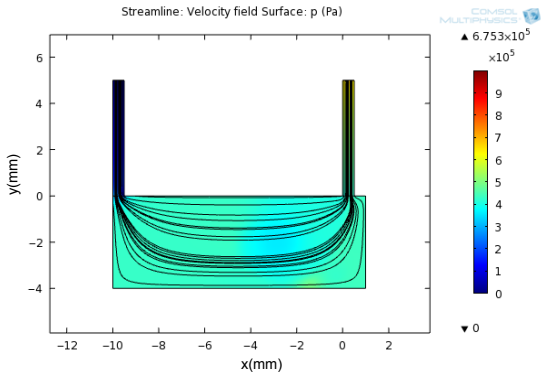

a) t=0.001s

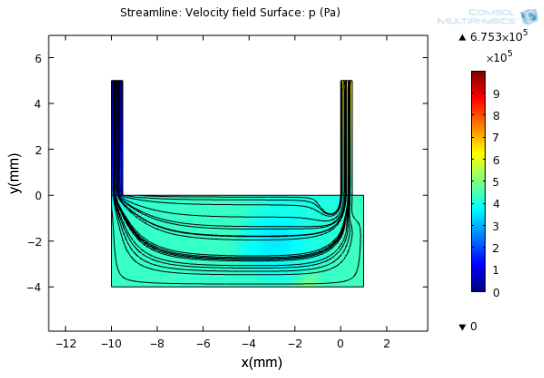

b) t=0.002s

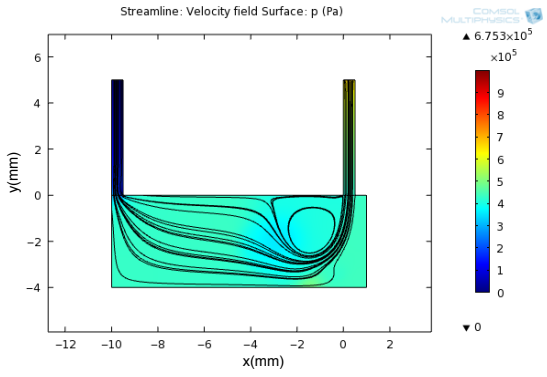

c) t=0.003s

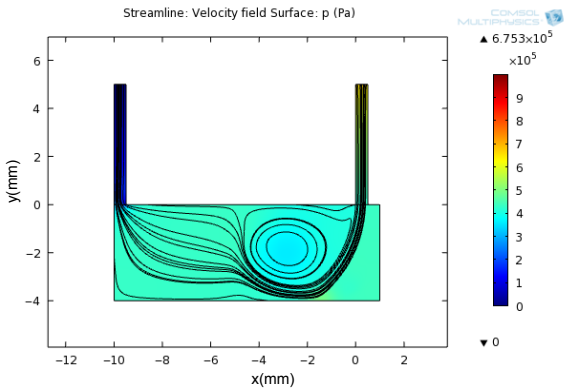

d) t=0.0039s

Box intended blank

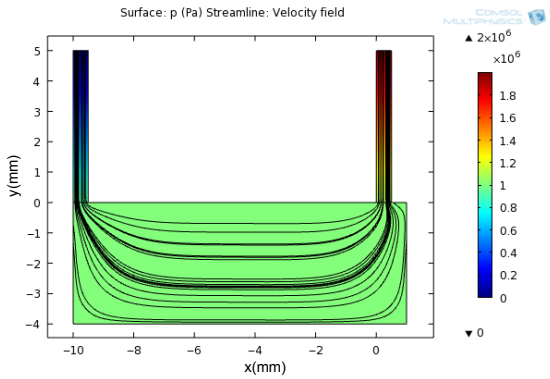

e) t=∞

Figure 49 Flow fields evolution for valve with damping length close to valve chamber length

The flow force in this case can be computed from numerical integration of pressure distributed on the right end and left end of the valve chamber or modeled to be proportional to the pressure difference between inlet boundary pressure and outlet

boundary pressure. They are compared in Figure 50 and the value based on numerical integration is larger than the proportional model.

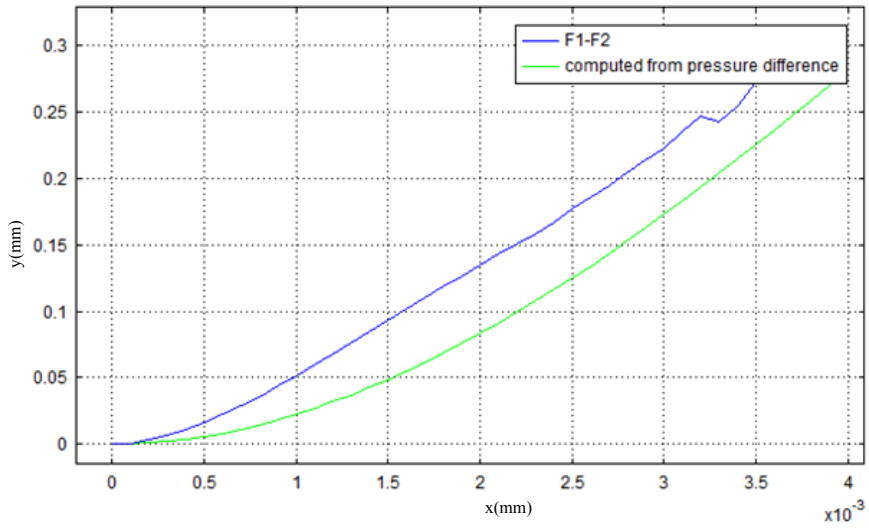

Figure 50 Integrated flow force and flow force calculated from pressure difference between inlet boundary pressure and outlet boundary pressure for valve with damping length close to valve chamber length

The flow field structure can be significantly influence by the geometry of the valve. When the valve piston is longer and the damping length increase accordingly with it, the flow field structure can be shown in Figure 51. As the damping length and valve chamber length increases the structure of the vortices becomes even more complex in the transient stage. However, when time elapse goes to infinity some of the vortices diminish and only one of them is preserved near the inlet.

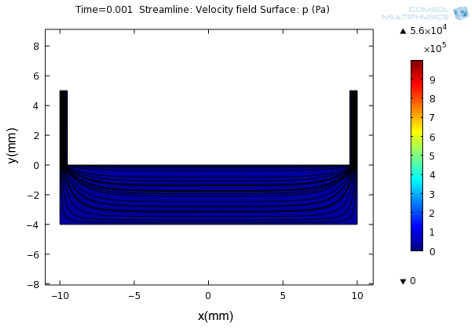

a)t=0.001s

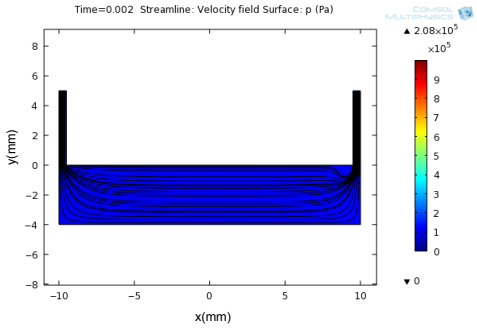

b)t=0.002s

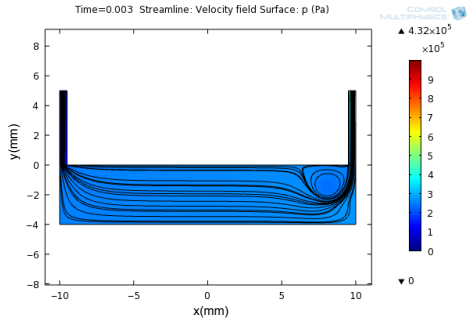

c)t=0.003s

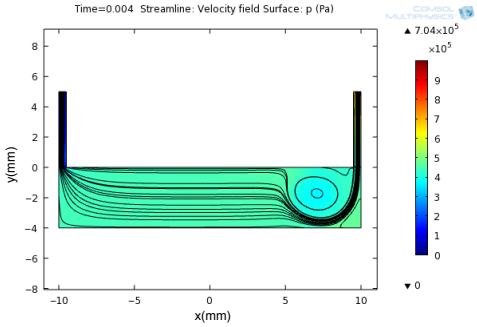

d)t=0.004s

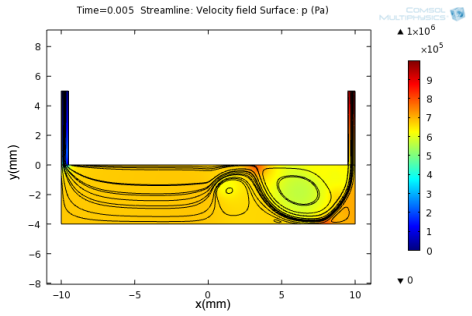

e)t=0.005s

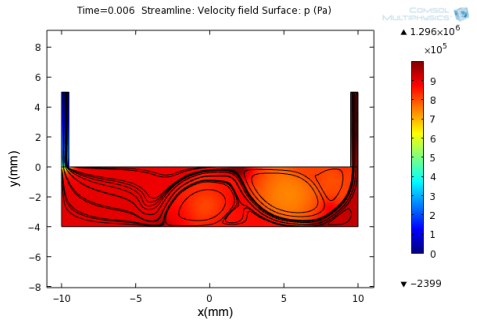

f)t=0.006s

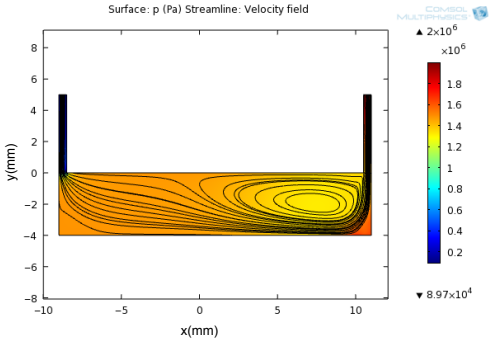

f)t=∞

Figure 51 Flow fields evolution for valve with damping length close to valve chamber length (longer valve piston)

The integrated flow force in Figure 52 is still larger than the linear proportional simplified model. The difference is larger because there is more fluid in the valve piston chamber.

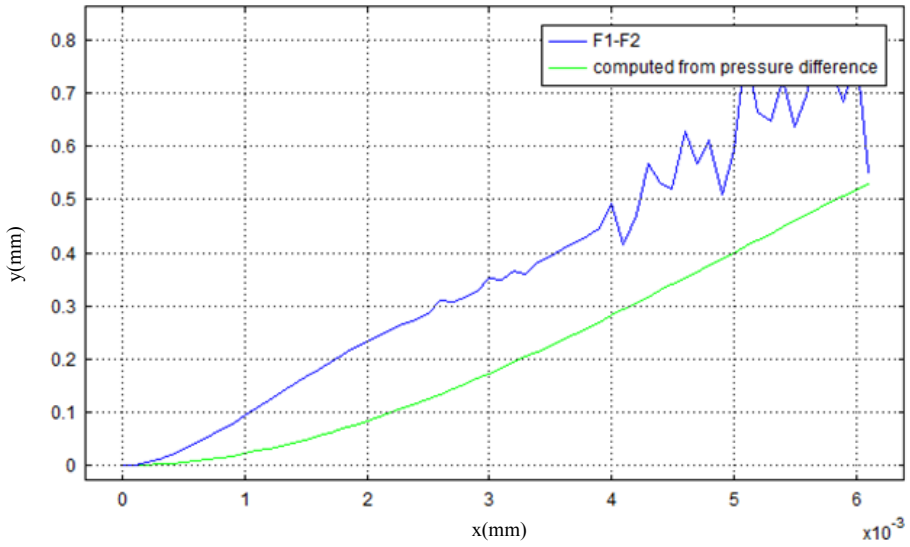

Figure 52 Integrated flow force and flow force calculated from pressure difference between inlet boundary pressure and outlet boundary pressure for valve with damping length close to valve chamber length (longer valve piston)

7.2 Valve with Damping Length Shorter than Valve Chamber Length

The flow field evolution for valve with damping length shorter than valve chamber length is even more complex. It can be observed from Figure 53 that at time t=0.002, two vortices are born on the left-hand side and right-hand side of the inlet respectively. The one on the left expands and is moving toward the outlet on the left. The one on the right grows and then gradually separate into three adjacent vortices in steady state.

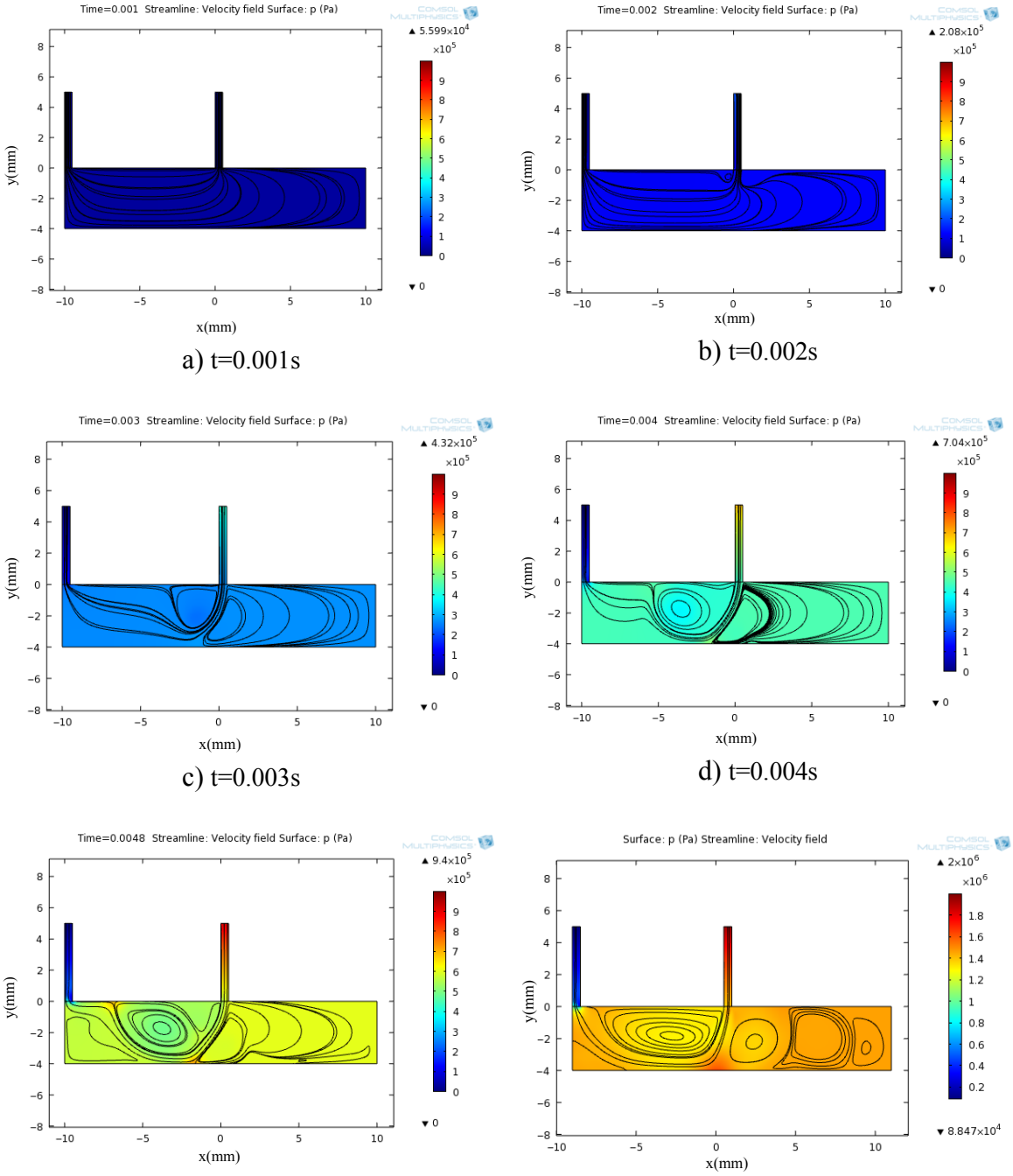

a) t=0.001s b) t=0.002s

c) t=0.003s d) t=0.004s

e) t=0.0048s f) t=∞

Figure 53 Flow fields evolution for valve with damping length shorter than valve chamber length

Similar to the results in Figure 50, the force computed from numerical integration and proportional model for the valve with damping length shorter than valve chamber length is shown in Figure 54. In this picture, the integration result is larger than value

computed from the proportional model. There is no significant change between the integrated value and the proportional model, mainly because the damping lengths are the same. However, The direction of the pressure transient flow force is not reversed as in the experiment. This might be the lack of ability to model leakage flow in the CFD model.

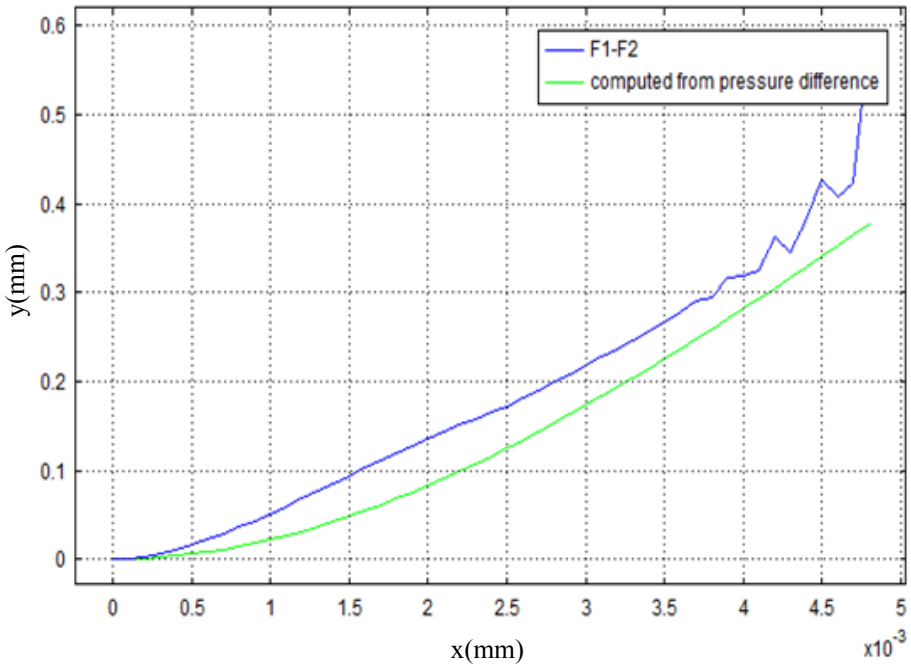

Figure 54 Integrated flow force and flow force calculated from pressure difference between inlet boundary pressure and outlet boundary pressure for valve with damping length shorter than valve chamber length

7.3 Summary

From the numerical solution presented in this chapter, it can be concluded in general that the flow field under the pressure transient is divided into multiple regions, because of the birth and evolution of vortices within the valve chamber. Thus it is not proper to model the inertial effect of the fluid in the control volume as a single chunk of fluid. This might be one of the main reasons for the inconsistency between theoretical pressure transient flow force and the measured pressure transient flow force.

In addition, the comparison between first two cases computed in this chapter shows that two different steady flow structures exist for the cases with valve damping length close to valve chamber length. The reason for this difference can be the length of the valve piston. The comparison between the second and the third case shows that different flow structures exist for the same valve piston length with different valve damping length. In the first two cases with valve damping length close to valve chamber length, some of the vortices will be born grow and then disappear in steady state. However, in the third case the vortices are born and finally preserved in steady state. It can be inferred that the damping length and valve chamber length both have influences on the flow structure.

Chapter 8 Conclusions

8.1 Conclusions

The primary objective of this research is to prove the existence of the pressure transient effect experimentally. In order to have the pressure transient effect observable, it is necessary to know the accurate steady state flow force and to generate a proper excitation pressure wave. In pursuing the primary objectives the following conclusions are obtained

- The total flow force can be decomposed into the pressure difference induced force and viscous shear force acting on the valve piston shaft in equilibrium condition of the valve piston or decomposed into the viscous shear force acting on the valve housing and the momentum induced flow force in the equilibrium condition of the fluid in the control volume.
- The classic orifice equation can be made more computational efficient by correcting the discontinuity around the origin using a polynomial function.
- The pressure drop across the valve chamber for fully developed turbulent flow can be equivalently modeled by an orifice equation. The equivalent discharge coefficient automatically takes the wall friction and Reynolds number into consideration.
- The steady state pressure difference induced force can be computed based on a three-orifice valve pressure dynamics model, which takes the pressure drop across the valve chamber into consideration.

- Three pressure drop coefficients are derived to calculate the contribution of supply orifice, return orifice and valve chamber in the total pressure drop.
- The steady state viscous shear force acting on the valve piston shaft and valve housing can be computed using a parabolic velocity profile approximation in an annular flow passage. And the parabolic velocity profile approximation should match the volumetric flow rate across the valve body.
- The steady state viscous shear force can be influenced by the surface roughness, as a result the theoretical solution is only accurate on the contact area with good surface finish.
- The momentum induced flow force can be decomposed into a transient term and multiple steady state term. Among the steady state term, the contribution of leakage flow is proved not important.
- Two jet angles are assigned to the supply orifice and return orifice respectively. This characteristic enables the description of canceling effect between the steady state flow force induced by the fluid flow through the supply orifice and return orifice.
- Although the two descriptions about the total flow force in Equation (48) are equivalent in steady state, it is not possible for them to be equivalent in transient state. They are not possible to include both transient effect caused by fluid compressibility and transient effect caused by fluid inertial.
- Nondimensional analysis for the steady flow force decomposed in the equilibrium condition of the valve piston equilibrium condition shows that the pressure

difference induced flow force is much larger than the viscous shear force acting on the valve piston shaft.

- Nondimensional analysis for the steady flow force decomposed in the equilibrium condition of the valve-piston equilibrium condition shows that the pressure transient effect caused by compressibility can be increased by increasing damping length L.
- Nondimensional analysis for the flow force decomposed in the equilibrium condition of the fluid in the control volume shows that the transient flow force is the largest one with the viscous shear force acting on the valve housing the second largest. In addition, the steady state flow force caused by the fluid flow through the supply and return orifice are canceling each other, and the net contribution of the steady momentum caused flow force is small.
- Nondimensional analysis for the flow force decomposed in the equilibrium condition of the fluid in the control volume shows that pressure transient effect caused by fluid inertial within the control volume can be increased by increasing damping length L.
- The linearization of the steady flow force in the equilibrium condition of the valve piston shows that the linearized steady flow force has a pressure term and a displacement term.
- The linearization of the flow force with a fixing valve piston in the equilibrium condition of the fluid in the control volume shows that the linearized flow force has a pressure term, a displacement term and a pressure transient term.

- Experimental measurement shows that sound wave phenomenon can be a dominant influence although it is not in the analytical flow force model.
- Experimental measurement shows that the pressure on the two ends of the piston is not uniformly distributed and it is confirmed by CFD analysis.
- One hundred point average technique and the pressure profile factor can be introduced to prove the pressure transient effect by process the acquired data.
- The pressure transient effect is proved on a valve piston pair which has the same geometry characteristic as the model in the analysis.
- Geometry modification of longer valve, stepped valve housing and large clearance is proved to be effective in reducing sound wave phenomenon and non-uniform pressure profile on the two ends.
- Experimental measurements confirm that the model for the steady state pressure difference induced flow force and steady state viscous shear force is accurate.
- Experimental measurements prove the existence of pressure transient effect. And the pressure transient effect locates around the rising and falling edge of the pressure wave.
- Measured pressure transient flow force differs from the theoretical pressure transient flow force in magnitude. Sometimes even the direction of the transient flow force could be opposite.
- CFD analysis shows that it is not proper to model the inertial of the fluid as a chunk of mass moving in one direction, because the flow transient field will be divided into different reigns by vortices.

- Two different flow structures exist for all three cases computed in Chapter 7. In the first case, the vortex will born, grow and then diminish in steady state. In the second case multiple vortices will born, but some of them will diminish in steady state. In the third case, the all vortices born will still be preserved in steady state.
- It can be inferred that both damping length and valve chamber length can influence the flow field structure with in the two-way valve.

8.2 Recommendation for Future Work

It is recommended that measurement of the pressure drop across the valve body should be made directly on the valve piston surface instead of on the sidewall of the valve housing. Experimental works concerning the pressure distribution on the valve piston will also be very useful. It is proposed that a specially made pressure sensor should be made to measure the average pressure on a annular area.

Perhaps a Particles velocimetry technology can be applied to visualize the flow field in the valve piston chamber. To achieve this goal several obstacles must be overcome. First, it is necessary to find a way to make a transparent valve housing and piston good tolerance and surface finish. Second, reflecting particles are required to be small enough to pass the filter.

Artificial neural networks can be used to identify the transient flow force dynamics by finding the proper neural network to produce the response, which can approximate the input-output relationship between pressure and flow force.

References

[1] Manring, N. D., "Modeling spool-valve flow forces," Proceedings of IMECE2004: 2004 ASME International Mechanical Engineering Congress and RD&D Expo, Anaheim, CA, USA, November, 2004, pp-13-19

[2] Nakada, T., Ikebe, Y., "Measurement of the unsteady axial flow force on a spool valve," Proceedings of the IFAC Symposium- Pneumatic and Hydraulic Compenents and Instruments in Automatic Control, Warsaw, Poland. IFAC, May 1980, pp-193-198

[3] Boswirth, L., "A model for valve taking non steady flow into account: part I." Proceedings of Purdue International Compressor conference, Lafayette, IN, USA, 1984, pp-227-241

[4] Boswirth, L., "A model for valve taking non steady flow into account: part II." Proceedings of Purdue International Compressor conference, Lafayette, IN, USA, 1984, pp-235-241

[5] Boswirth, L., "Non steady flow in valves," Proceedings of Purdue International Compressor conference, Lafayette, IN, 1990, pp-664-673

[6] Shi, W., S. Li, S. Ge, "New technique for steady flow force compensation in spool valves," Proceedings of the Institution of Mechanical Engineers, Part E: Journal of Process Mechanical Engineering, 204(E1), 1990, pp-7-14

[7] Johnston, D. N., K.A. Edge, N. D. Vaughan, "Experimental investigation of flow and force Characteristics of hydraulic poppet and disk valves," Proceedings of the Institution of Mechanical Engineers. Part A, Journal of power and energy, 205(3), 1991, pp-161-171

[8] Urata, E., C. Yamashina, "Influence of flow force on the flapper of a water hydraulic servovalve," JSME International Journal. Series B, Fluids and Thermal Engineering, 41(2), pp-278-285, 1998

[9] Urata, E., Y. Nakao, "Study of a flapper nozzle system for a water hydrualic servovalve," JSME International Journal. SeriesB, 41(2), 270-277, 1998

[10] Ruan, J., R. Burton, P. Ukrainetz, "An investigation into the characteristics of a two dimensional 2D Flow Control Valve," Transactions of the ASME, 124, pp-214-220, Mar. 2002

[11] Krishnaswamy, K., Perry Y. Li, "On using unstable electrohydraulic valves for control," Journal of Dynamic Systems, Measurement, and Control, Vol 124, pp-183-190, Mar. 2002

[12] Yuan, Q., Perry Y. Li,"Using steady flow force for unstable valve design: modeling and experiments," Journal of Dynamic Systems, Measurement, and Control, 127, pp-451-462, Sept. 2005

[13] Yuan, Q., Perry Y. Li,"An Experimental Study on the Use of Unstable Electrohydraulic Valves for Control,"Proceedings of the American Control Conference, Anchorage, pp-4943-4848, May. 2002

[14] Wang, T., G. Peng, T. Kagawa, "Design of pressure control system including flow force of pneumatic servo valves," Journal of Beijing Institute of Technoloty, English Language Issue, 27(12), pp-1081-1084, 2007

[15] Wang, T., M. Cai, K, Kawashima, et al. "Modeling of a nozzle-flapper type pneumatic servo valve including the influence of flow force," International Journal of fluid Power, 6(3), pp-33-43, 2005

[16] Herakovic, N., "Flow-force analysis in a hydraulic sliding spool-valve," Strojarstvo, 49(3), pp-117-126, 2007

[17] Ikeo, S., M. Hanya, "Flow force acting on two-way-cartridge valve," Bulletin of JSME, 29(255),2938-2945, 1986

[18] Hayase, T. P., Cheng, S. Hayashi, "Numerical analysis of transient flow through a pipe orifice (1st Report, Time Constant for Settling Flow)", Transactions of the Japan Society of Mechanical Engineers, Part B, 59(560), pp-1023-1029, 1993

[19] Hayase, T. P., Cheng, S. Hayashi, "Numerical analysis of transient flow through a pipe orifice (2nd Report, Step Response from Initial Steady Flow)", Transactions of the Japan Society of Mechanical Engineers, Part B, 60(560), pp-78-84, 1994

[20] Hayase, T. P., Cheng, S. Hayashi, "Numerical analysis of transient flow through a pipe orifice," JSME international Journal, 38(2), pp-157-163, 1995

[21] Hayase, T. P., Cheng, S. Hayashi, "Numerical analysis of transient flow through spool valve," Transaction of the Japan Society of Mechanical Engineers. B61(584), pp-1382-1388, 1995

[22] Sanada, K., C. Richards, D.K. Longmore, D. N. Johnston, "A Finite element model of hydraulic pipelines using an optimized interlacing grid system," Proceedings of institution of Mechanical Engineers, Part I: Journal of Systems and Control Engineering, 207(14), pp-213-222, 1993

[23] Taylor, S. E. M., D. N. Johnston, D.K. Longmore, "Modelling of transient flow in hydraulic piplines," Proceedings of the Institution of Mechanical Engineers, Part 1: Journal of Systems and Control Engineering, 211(6), pp-447-455,1997

[24] Borghi, M, M. Milani, R. Paoluzzi, "Transient flow force estimation on the pilot stage of a hydraulic valve," Proceedings of the ASME-IMECE FPST-Fluid Power Systems & Technology, 5, 1998, 157-162

[25] Wang, L., Y. Chen, Y. Lu, "Numerical study on the axial flow force of a spool valve, FPST-Fluid Power Systems and Technology," Vol 5, pp-177-183, 1998

[26] Renn, J. Wu, "Analysis of Compensation of the flow force in a 4/3 oil hydraulic directional solenoid valve," Journal of the Chinese Society of Mechanical Engineers, 21(2), pp-209-215,2000

[27] Kondoh, Y., H. Suzuki, M. Itoh, "Analysis of flow force acting on a spool valve (1st report, non-uniformity of flow pattern and momentum flux in the azimuthal direction)," Kikai Gakkai Ronbunshu B, 65(639), pp3577-3585,1999

[28] Kondoh, Y., H. Suzuki, M. Itoh, "Analysis of flow force acting on a spool valve (2nd report, lateral flow force caused my main flow)," Nihon Kikai Gakkai Ronbunshu B, 68(667), pp-680-688, 2000

[29] Kondoh, Y., H. Suzuki, M. Itoh, "Analysis of flow force acting on a spool valve (3rd report,influence of valve dimentions on lateral flow force)," Nihon Kikai Gakkai Ronbunshu B, 68(675), pp-2951-2959, 2000

[30] Ji, H., X. Fu, H. Yang, "Study on the steady flow force of non-circular opening spool valve," Chinese Journal of Mechanical Engineering, 39(6), pp-13-17, June 2003

[31] Zhou, S., B. Xu, H. Yang, "Flow force compensation of high speed on/off valve," Chinese Journal of Mechanical Engineering, Vol 42 Supp., pp-5-8, 2006

[32] Dempster, W., C.K. Lee, J. Deans, "Prediction of the flow and force characteristics of safety relief valves," Proceedings of PVP 2006-ICPVT-11 ASME Pressure Vessels and Piping Division Conference, pp-93-99, 2006

[33] Zhao, L. Q. Chen, Q. Long, "Visualization analysis of the flow field in a moving spool valve," Transaction of the Chinese Society of Agricultural Machinery, 39(11), pp-142-155, 2008

[34] Vescovo, G.D., Antonio Lippolis, "Three-dimensional analysis of flow forces on directional control valves," International Journal of fluid Power, 4(2),pp-15-24, 2003

[35] Stankevic, V., C. Simkevicius, "Use of a shock tube in investigations of silicon micromachined piezoresistive pressure sensors," Sensors and Actuation 86, pp-58-65, 2000

[36] Kobata, T., Ooiwa, A., "Square-wave pressure generator using a novel rotating valve," Metrologia, 1999, 36, pp-637-640, 1986

[37] Kobata, T., Ooiwa, A., "Method of evaluating frequency characteristics of pressure transducers using newly developed dynamic pressure generator," Sensors and Actuators, 2000, 79, pp-97-101

[38] Wang, S. H., T.T. Tsung, L.L. Han, The measurement and analysis of pressure square wave generator, Journal of Physics: Conference Series 48, pp-616-619, 2006

[39] Wang, S.H., T.T. Tsung, L.L. Han, "Hydraulic square-wave generator with a specific rotating valve," Measurement 42, pp- 672-677, 2009

[40] Kitagawa, T., T. Takenaka, Y. Kato, "Study on the high pressure generation by means of oil hammer: 1st report, fundamental properties of repeated high pressure generator," Buletin of JSME, 27(234), pp-2779-2786, 1984

[41] Kitagawa, T., T. Takenaka, Y. Kato, "Study on the high pressure generation by means of oil hammer: 2nd report, application to pressure intensifier and lateral pressure cutting," Bulletin of JSME, 27(229), pp-1472-1478, 1984

[42] Ouyang, X. P., H. Y. Yang, H. Y. Hao, Bng Xu, "Simulation of the piezoelectric high-speed on/off valve", Chinese Science Bulletin, 53(17), pp-2706-2711, Sept. 2008

[43] Kira, A., Daisuke Takaenoki, Hideki Hamashima, et al. al, "Optical observation of extremely high impulsive pressure generator using collosion of high velocity metal jets," Material Science Forum Explosion: Shock Wave and Hypervelocity Phenomena in Materials, 456, pp-265-270, 2004

[44] Zhou, M., Y. Tian, Z. Yang, et al, "Control of a new type of direct drive piezo electric servo valve," Proceedings of the 2004 IEEE International Conference on Robotics and Biomimetics, pp-795-798, Aug. 2004

[45] Xu, X . P., R. T. Burton, C. M. Sargent, "Experimental identification of a flow orifice using a neural network and the conjugate gradient method," Journal of Dynamic Systems, Measurement and Control, 118(2), pp-272-277, 1996

[46] Watton, J., Y. Xue, "Simulation of fluid power circuits using artificial network models: Part 1: slection of component models," Proceedings of the Institution of Mechanical Engineers, Part 1: Journal of Systems and Control Engineering, 211(6), pp-417-428, 1997

[47] Xue, Y., J. Watton, "Simulation of fluid power circuits using artificial network models: Part 2: circuit simulation," Proceedings of the Institution of Mechanical Engineers, Part 1: Journal of Systems and Control Engineering, 211(6), pp-429-437, 1997

[48] Xue, Y., J Watton, Dynamics modeling of fluid power systems applying a global error descent algorithm to a self-organizing radial basis function network, Mechatronics, 8, pp-727-745, 1998

[49] Cao, M., K.W. Wang, L. Devries et.al, "Steady state hydraulic valve fluid field estimator based on non-dimensional artificial neural network," Journal of Computing and Information Science in Engineering, 4(3), pp-257-270, Sept. 2004

[50] Aman, R., H. Handroos, T. Eskola, "Computationally efficient two-regime flow orifice model for real time simulation", Simulation Modlling Practice and Theory, 16, pp-945-961, 2008

[51] De Martino, G., Fontana, N., Giugni, M., "Transient flow caused by air expulsion through an orifice", Journal of Hydraulic Engineering, 134(9), pp-1395-1399, Sept. 2008

[52] Manring, N, Hydraulic control systems, Wiley, April 15, 2005

[53] Merritt, H. E.. Hydraulic Control System. John Wiley and Sons, 1967

[54] Oberg, E., D. J. Franklin, L. H. Holbrook, H. H. Ryffel, Machinery's Hanbook, 27th Edition, Industrial Press Inc, New York, 2004

Appendix

Kistler Model 603B1 Pressure Transducer, acceleration-sompensated, 15000 psi, high frequency response

Kistler Model 9212 Load Cell, 5000lbs

Kistler Model 5010B1 Dual Model Laboratory Charge Amplifier, Frequency measurement up to 180 kHz

Kistler Model 5073A411 Industrial Charge Amplifier, 4 Channel

AW flow meter JVM-60CG: 1731.5 impulse/Gallon

Maxon Motor EC-60, brushless, 400W

Maxon Planetary Gearhead GP 81 A, 20-120Nm

Maxon motor control 4-Q-EC Amplifier DEC 70/10

Dada acquisition card: NI PCI-7831R RSeries Multifunction Rio with Virtex-II 1MGate FPGA, analog inputs sampling rates up to 200kHz, analog outputs update rate up to 1MHz

VITA

Shusen Zhang was born in Yangzhou China in year 1983. He is now the Ph. D candidate with Mechanical & Aerospace Engineering in University of Missouri-Columbia. His primary interest is in modeling and control of dynamic systems. Earlier he received his undergraduate and master's degree in Nanjing University of Aeronautics and Astronautic in 2006 and 2008 respectively.